AD/A-001 387

DYNAMIC ANALYSIS OF A BUILDING AND BUILDING ELEMENTS

STANFORD RESEARCH INSTITUTE

PREPARED FOR

DEFENSE CIVIL PREPAREDNESS AGENCY

APRIL 1974

UNCLASSIFIED

SECURITY CLASSIFICATION OF THIS PAGE (When Data Entered)

AD/A-001387

REPORT DOCUMENTATION PAGE

READ INSTRUCTIONS BEFORE COMPLETING FORM

1. REPORT NUMBER	2. GOVT ACCESSION NO.	3. RECIPIENT'S CATALOG NUMBER
(none)		

4. TITLE (and Subtitle)

DYNAMIC ANALYSIS OF A BUILDING AND BUILDING ELEMENTS

5. TYPE OF REPORT & PERIOD COVERED

Technical Report

6. PERFORMING ORG. REPORT NUMBER

7. AUTHOR(s)

C. K. Wiehle

8. CONTRACT OR GRANT NUMBER(s)

DAHC20-71-C-0292

9. PERFORMING ORGANIZATION NAME AND ADDRESS

Stanford Research Institute
Facilities and Housing Research Dept.
Menlo Park, California 94025

10. PROGRAM ELEMENT, PROJECT, TASK AREA & WORK UNIT NUMBERS

DCPA Work Unit 1154I

11. CONTROLLING OFFICE NAME AND ADDRESS

Defense Civil Preparedness Agency
Washington, D.C. 20301

12. REPORT DATE

April 1974

13. NO. OF PAGES

131

14. MONITORING AGENCY NAME & ADDRESS (if diff. from Controlling Office)

15. SECURITY CLASS. (of this report)

UNCLASSIFIED

15a. DECLASSIFICATION/DOWNGRADING SCHEDULE

16. DISTRIBUTION STATEMENT (of this report)

Approved for public release; distribution unlimited.

17. DISTRIBUTION STATEMENT (of the abstract entered in Block 20, if different from report)

18. SUPPLEMENTARY NOTES

PRICES SUBJECT TO CHANGE

19. KEY WORDS (Continue on reverse side if necessary and identify by block number)

Restrained reinforced concrete slabs
Wood-joist floor systems
Dynamic analysis
Blast
Frames

20. ABSTRACT (Continue on reverse side if necessary and identify by block number)

The objective of the overall research program is to develop an evaluation procedure applicable to existing NSS-type structures and private homes. Past efforts have been concerned with examining exterior walls, window glass, steel frame connections, applications to actual buildings, and reinforced concrete floor systems. This report presents modifications to the mathematical model previously developed for reinforced concrete floor slabs to include the effect of longitudinal restraint on slab resistance. Also included in the report are

DD FORM 1 JAN 73 1473

EDITION OF 1 NOV 65 IS OBSOLETE

UNCLASSIFIED

SECURITY CLASSIFICATION OF THIS PAGE (When Data Entered)

19. KEY WORDS (Continued)

20 ABSTRACT (Continued)

the development of the resistance function for predicting the collapse of wood-joist floor systems, and the dynamic inelastic analysis of an eight-story steel-frame office building.

STANFORD RESEARCH INSTITUTE
Menlo Park, California 94025 · U S A

Technical Report *April 1974*

DYNAMIC ANALYSIS OF A BUILDING AND BUILDING ELEMENTS

By: C. K. WIEHLE
Facilities and Housing Research

Prepared for:

DEFENSE CIVIL PREPAREDNESS AGENCY
WASHINGTON, D.C. 20301

CONTRACT DAHC20-71-C-0292
DCPA Work Unit 1154I

SRI Project 1219-2

DCPA REVIEW NOTICE

ABSTRACT

The objective of the overall research program is to develop an evaluation procedure applicable to existing NSS-type structures and private homes. Past efforts have been concerned with examining exterior walls, window glass, steel frame connections, applications to actual buildings, and reinforced concrete floor systems. This report presents modifications to the mathematical model previously developed for reinforced concrete floor slabs to include the effect of longitudinal restraint on slab resistance. Also included in the report are the development of the resistance function for predicting the collapse of wood-joist floor systems, and the dynamic inelastic analysis of an eight-story steel-frame office building.

CONTENTS

ILLUSTRATIONS

TABLES

SUMMARY

Introduction

The objective of this investigation was to develop an evaluation procedure for determining the blast protection afforded by existing NSS-type structures and private residences. The approach adopted was to formulate a procedure for examining the dynamic response of a structure over a range of incident overpressure levels to determine the pressure at which collapse of the various elements occurs.

Background

Past efforts in this program have examined exterior walls, window glass, steel-frame connections, applications of the procedures to actual NSS buildings, and reinforced concrete floor systems. The report summarizes the three phases of the research effort conducted during the current contract period. First, are the modifications to the previously developed analytical expressions for reinforced concrete floor systems to include the effect of longitudinal edge restraint on the resistance of the slab. (An appendix presents the correlations between the analytical predictions and published experimental data on the response of longitudinally restrained slabs.) Second, the report contains the development of the resistance function used to predict the dynamic response and collapse of wood-joist floor systems. Third, a number of elastic and inelastic analyses were performed to determine the response of an eight-story, steel-frame office building subjected to nuclear air blast. The results of the frame analyses, together with an estimate of the collapse strength of the building, are presented in the report.

Discussion

Longitudinally Restrained Reinforced Concrete Slabs

Since there was a need to determine the blast strength of floor systems for actual NFSS buildings, the previous effort was concerned primarily with the development of interim analytical procedures for predicting the dynamic response and collapse of various types of reinforced concrete floor systems over basement areas. During the current study, it was possible to modify the resistance function for floors by including the effect of longitudinal edge restraint on the slab resistance. Compressive membrane forces, which occur in slabs that are restrained from outward movement at their edges, can be a controlling factor in determining the magnitude of the slab resistance; therefore, its inclusion in the mathematical model enhances the ability to make realistic collapse predictions for blast-loaded flocrs in existing buildings. It was also possible to make comparisons between analytical predictions and various published experimental data on the static and dynamic response of restrained slabs. The results of the analytical and experimental correlations, presented in the report, justify the use of the compressive membrane mode for predicting the collapse of floor systems in existing structures that are longitudinally restrained at the edges.

Wood-Joist Floor Systems

One of the goals of this research program has been to examine the blast strength of private residences. In previous studies, analytical procedures were developed for predicting the collapse of exterior walls of typical residences, and the analytical predictions were verified by comparison with results of nuclear weapon field experiments. Because of the possibility of using home basements for blast shelters during emergencies, the development of a method to predict the collapse of

wood-joist floors was initiated during the current research study. A literature search of the pertinent publications indicated that wood-joist floor systems are complex structural systems that are not readily amenable to precise theoretical analysis because of the wide variation in the mechanical properties of wood, and the variability in construction methods and details.

The resistance function developed for wood-joist floors consists of elastic and inelastic phases. The elastic phase is limited by the bending strength of the weakest joist (first break), which is limited by a defect resulting from the largest permissible knot for the grade and species of wood used in the joists. The inelastic phase, which results from the nonlinear behavior of wood in compression above the proportional limit, is limited by the theoretical ultimate strength of a clear wood specimen. The failure criterion is developed in the form of a truncated normal probability function.

Dynamic Analysis of North Carolina National Bank Building

A continuing concern in evaluating the collapse overpressure of existing buildings has been the relative blast strength of the exterior walls and frames of multistory buildings. It is often assumed for the analysis of blast-loaded frame buildings that the exterior walls can be considered as frangible, and therefore, that the wall loading transferred to the frame can be approximated by an impulse loading. However, for many of the actual buildings analyzed, the strength of the exterior walls under blast loading was sufficiently high to make it doubtful that the frame could survive at the overpressure level required to collapse the walls. Therefore, in this phase of existing computer program for analyzing the elastic and inelastic dynamic response of two-dimensional structural frames was used to analyze the frame of an eight-story steel-frame bank and office building. This building was selected for study because

a previous analysis had indicated that the exterior walls had an incident collapse overpressure of 15.7 psi, and the building could therefore be considered as strong-walled.

A series of elastic and plastic analyses were performed to determine the dynamic response of the frame of the building to various blast overpressure levels. Even though the computer program used could not predict frame collapse, the results of the analyses indicated that the frame would probably collapse between 3- and 4-psi incident overpressure level. For the case examined, the blast resistance of the building frame was predicted to be much less than that of the exterior walls, which is an important consideration in predicting either the magnitude of building damage or the number of casualties that might occur in buildings subjected to nuclear air blast.

I INTRODUCTION

Under contract to the Defense Civil Preparedness Agency, Stanford Research Institute is developing a procedure for the evaluation of existing structures subjected to nuclear air blast. The objective of the overall program is to develop an evaluation procedure applicable to existing NSS-type structures and private homes. The purpose of this phase of the research was to improve the prediction techniques for reinforced concrete floor systems, develop analytical procedures for dynamically-loaded wood-joist floor systems, and make a preliminary examination of the response of multistory buildings to nuclear blast loading.

Background

Past efforts in this program have been concerned with examining exterior walls (Ref. 1), window glass (Ref. 2), steel-frame connections (Ref. 3), two-way action walls (Ref. 4), applications to NSS buildings (Refs. 5 and 6), and reinforced concrete floor systems (Ref. 7).

Even though the primary interest since the inception of this program has been in the behavior and collapse of the building system, the complexity of an overall building evaluation procedure necessitated the establishment of a ranking of structural elements. It is apparent that the collapse of the exterior walls of most buildings is important to the casualties produced. This is especially true for large multistory buildings where the collapse of the exterior and interior walls could result in a large number of casualties as a result of ejection from the building, even if the floors and frame remained intact. Also, for a load-bearing-wall building, where the exterior walls are the primary structural member,

the collapse of the exterior walls can precipitate a catastrophic collapse of the entire building. Since one of the primary uses of a building evaluation procedure is to provide input for predicting the survival of people located in buildings subjected to nuclear air blast, the initial research effort was directed toward development of a method for determining the response and collapse of exterior wall elements. The three basic types of exterior walls considered were unreinforced concrete or masonry unit walls without arching, unreinforced concrete or masonry unit walls with arching, and reinforced concrete walls. With minor modification, the analytical procedures for exterior walls also apply to interior partitions of similar construction.

As noted in Ref. 7, there was a need to develop interim procedures for predicting the collapse of floors over basement areas in existing NSS buildings. Therefore, mathematical models for the behavior of reinforced concrete floor systems were formulated, based on readily available technical information. During the current research effort it was possible to modify the previously developed analytical expressions to include the effect of longitudinal edge restraint on the resistance of reinforced concrete slabs. Compressive membrane forces occur in concrete slabs that are restrained from outward movement at the edges as a result of adjacent floor panels, or such other restraints as heavy spandrel beams. Since compressive membrane forces can be a controlling factor in determining the magnitude of slab resistance, its inclusion in the floor prediction schemes enhances the ability to make realistic collapse predictions for floors in existing buildings.

Although collapse predictions have been made for blast-loaded wood-joist floors on an individual basis in this program, the procedure was not systematized. During the current effort, a large body of analytical and experimental information on wood and wood-joist floors was reviewed

and a resistance function developed for modelling the complex structural behavior of wood-joist floors.

A continuing concern in this program has been the relative strength of the exterior walls and frames of multistory buildings. To investigate the relative strength of the walls and frame would require a comprehensive computer program that included the inelastic response of the frame under dynamic loading, as well as realistic frame collapse mechanisms. Since no such program could be developed during this study, an available computer program for analyzing the elastic and inelastic dynamic response of two-dimensional structural frames (Ref. 8) was used to estimate the blast strength of an eight-story steel-frame office building. Although the frame program does not include frame collapse mechanisms, the results of the analyses provided considerable insight into the relative collapse strengths of the exterior walls and frame of a typical multistory building.

The analytical method used in the research study has been to establish the resistance function for each structural element of interest by considering the approximate response mode, and by assuming that the element is subjected to a uniformly distributed static load. To analyze the dynamic response and collapse of the member, it is transformed into an equivalent single-degree-of-freedom system by the use of transformation factors for the load, resistance, and mass. The equation of motion is then solved on a computer using a numerical integration procedure. Although established analytical procedures have been used wherever possible, it has been necessary to modify and adapt current procedures as well as develop new procedures for specific use. Relatively simplified analytical models have been used for wall and floor element analysis to prevent the evaluation of a structure from becoming unwieldly as a result of excessive computation.

As discussed in Ref. 4, the analysis of actual building elements subjected to nuclear air blast requires the assumption of values for many of the physical properties of the structure that are unknown and cannot be measured without an unwarranted amount of effort. Similarly, assumptions are also required in the determination of the parameters defining the load acting on the building element. Since precise values cannot usually be specified for many of the parameters that influence the collapse of actual structures, a probabilistic approach was formulated to provide a more realistic method for evaluating existing structures subjected to air blast loading.

Report Organization

Section II gives the mathematical expressions developed for modifying the resistance functions for reinforced concrete slabs to include the effect of longitudinal edge restraint. The correlation of the analytical predictions with experimental data on the response of longitudinally restrained slabs is included in the Appendix. The development of the resistance function for predicting the behavior of wood-joist floor systems is presented in Section III. The results of the elastic and inelastic analyses of the dynamic response of the multistory office building is given in Section IV.

Acknowledgements

The author gratefully acknowledges the assistance and guidance of G. N. Sisson and M. A. Pachuta of the Defense Civil Preparedness Agency during the conduct of this program. Also acknowledged is the contribution of Dr. J. L. Bockholt, consultant to SRI, to this effort, especially in the area of longitudinally restrained slabs.

II LONGITUDINALLY RESTRAINED REINFORCED CONCRETE SLABS

Introduction

Interim analytical procedures for calculating the resistance function for reinforced concrete slabs is presented in Ref. 7. In that study, the yield-line theory was used to predict the ultimate flexural strength of the slab. For slabs with continuous reinforcement, a tensile membrane mode was also included in the resistance function, but such refinements as compressive membrane action in slabs with restrained edges were not included in the interim techniques.

However, several investigators (e.g., Refs. 9, 10, 11, and 12) have found that the yield-line theory grossly underestimates the strength of slabs with longitudinal edge restraint, such as that provided by surrounding floor panels, or by heavy spandrel beams or walls. When a slab with edge restraint deflects under load, significant compressive membrane forces are induced in the slab that result in ultimate moments at the yield lines considerably higher than when the forces are not present. Since the ultimate strength predicted by the yield-line theory is too conservative for longitudinally restrained slabs, the resistance function for reinforced concrete slabs presented in Ref. 7 has been modified to include the compressive membrane mode. The analytical procedure developed in this report for calculating the resistance function of longitudinally restrained slabs was based primarily on the investigations presented in Refs. 9 and 10.

As shown on Figure 1, the resistance function for longitudinally restrained slabs consists of three phases:

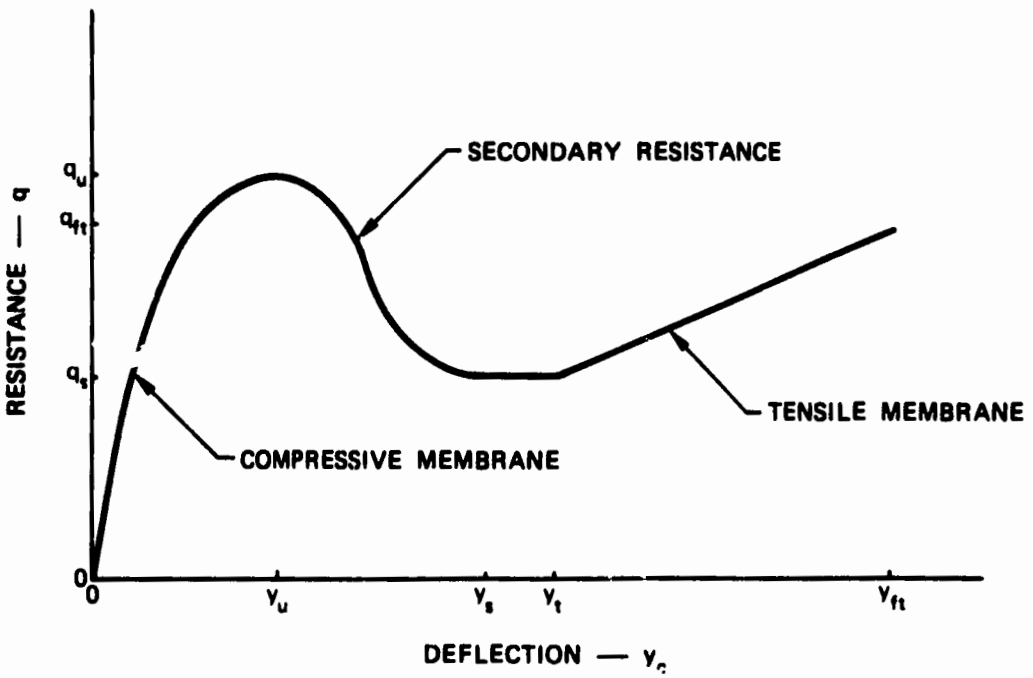

FIGURE 1 RESISTANCE FUNCTION FOR LONGITUDINALLY RESTRAINED REINFORCED CONCRETE SLAB

- Compressive membrane resistance
- Secondary resistance
- Tensile membrane resistance.

The development of the analytical expressions for determining the slab resistance for each of these phases is presented in the following subsections. The analytical methods used for predicting the ultimate flexural strength for the compressive membrane resistance phase are based primarily on the investigations summarized in Refs. 9 and 10. The methods used for determining the slab resistance during the secondary and tensile membrane resistance phases are based on the expressions previously developed in this program (Ref. 7).

Compressive Membrane Resistance

The ultimate resistance during the compressive membrane phase is determined by assuming the slab to fail along the yield lines shown in Figure 2. The value of β, defining the location of the yield lines, is determined from the following equation, previously given in Ref. 7:

$$\beta = \frac{1}{2} \frac{M_{u2}}{M_{u1}} \frac{\gamma_2}{\gamma_1} \left(\frac{L_s}{L_l}\right)^2 \left[\sqrt{\left(\frac{\gamma_2}{\gamma_1}\right)^2 + 3 \frac{M_{u1}}{M_{u2}} \left(\frac{L_s}{L_l}\right)^2} - \frac{\gamma_2}{\gamma_1}\right] \tag{1}$$

where

$$\gamma_1 = 2\sqrt{1 + M_{u3}/M_{u1}} \tag{1a}$$

$$\gamma_2 = 2\sqrt{1 + M_{u4}/M_{u2}} \quad . \tag{1b}$$

Each segment of the pattern is assumed to rotate as a plane surface.

For a slab with edges restrained against longitudinal movement, both thrust and moment act on sections along the yield lines. These thrust forces significantly increase the moment resistance of the slab cross

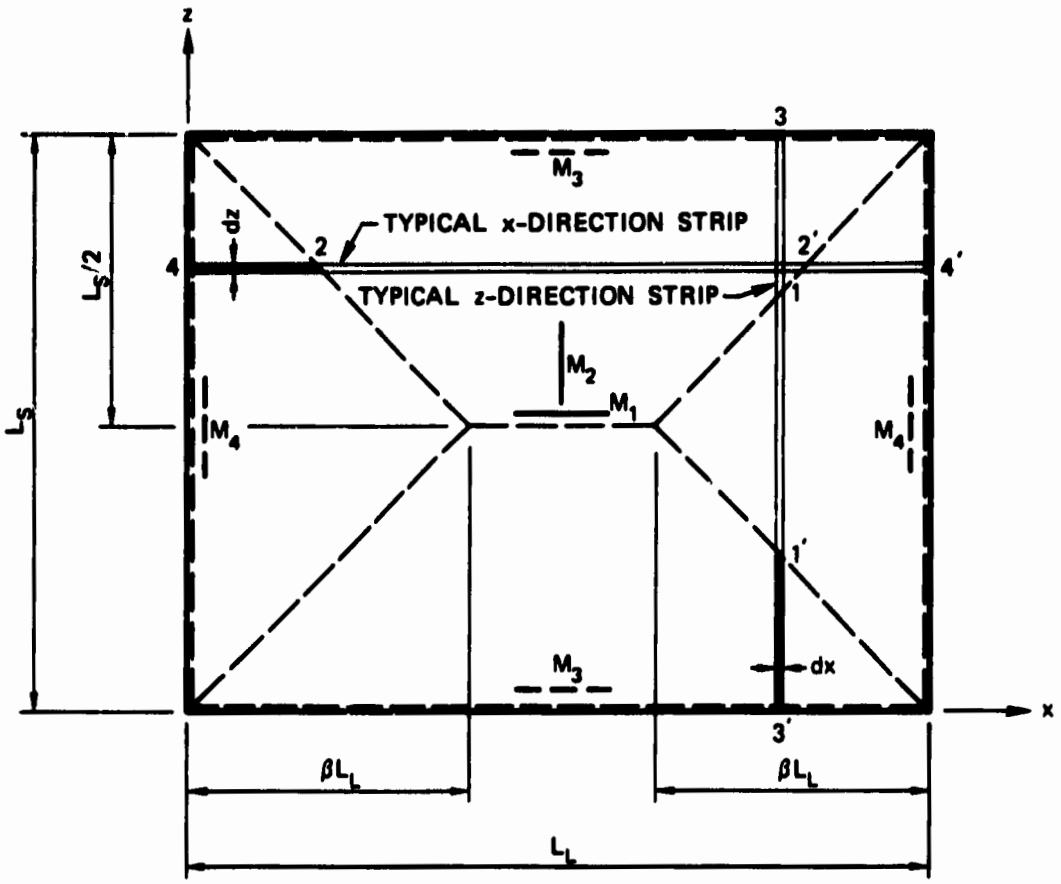

NOTE: Moment key lines indicate the moment capacity per unit length perpindicular to these lines.

Positive Moment

Negative Moment

FIGURE 2 ASSUMED COLLAPSE MECHANISM FOR LONGITUDINALLY RESTRAINED REINFORCED CONCRETE SLAB

section. This increase is determined by using the moment equations developed previously in Appendix A of Ref. 1. In this study, however, the moments are related to the mid-thickness of the slab rather than to the centroid of the tensile reinforcement. This is done since, as subsequently shown, the thrust forces are also assumed to act at the mid-thickness of the slab.

The magnitude of the thrust induced in the longitudinally restrained slab when the collapse mechanism forms is determined by assuming the slab to be composed of strips oriented in the x and z directions, as shown in Figure 3. A strip in either direction has the same thickness as the slab and contains only the reinforcement steel in that direction. The yield sections are perpendicular to the direction of the strip, with the torsional moments on these sections assumed to be zero. The static load resistance can now be expressed as the sum of the load carried by each of the individual strips.

Consider a typical strip 4-2-2′-4′ in the x-direction, with plastic hinges just formed at 4, 2, 2′, and 4′, as shown in Figure 4. The forces acting on portion 4-2 at this stage of behavior are shown in Figure 5. In addition to the yield-line moments, compressive membrane forces are induced by longitudinal restraint at the ends of the strip. Considering the equilibrium of these horizontal forces,

$$N_{u2} = N_{u4} = N_{ux} \quad . \tag{2}$$

The subscript u refers to the ultimate stage of behavior (initial crushing of the extreme fiber of the concrete at each hinge section).

The strain at the extreme fiber of the concrete is assumed to be equal to ϵ_u, the crushing strain of the concrete. Assuming the crushing strain is reached simultaneously at sections 2 and 4, the thrust at

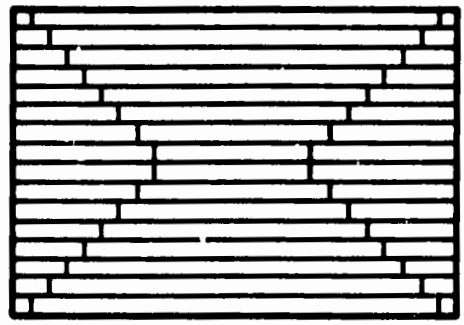

x-DIRECTION STRIPS

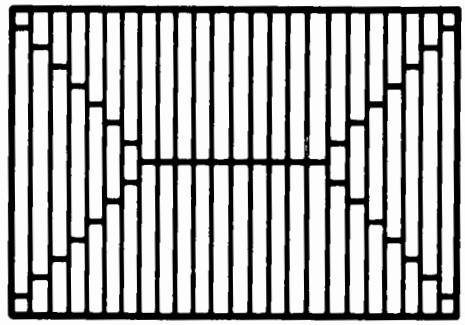

z-DIRECTION STRIPS

FIGURE 3 SYSTEM OF EQUIVALENT SLAB STRIPS

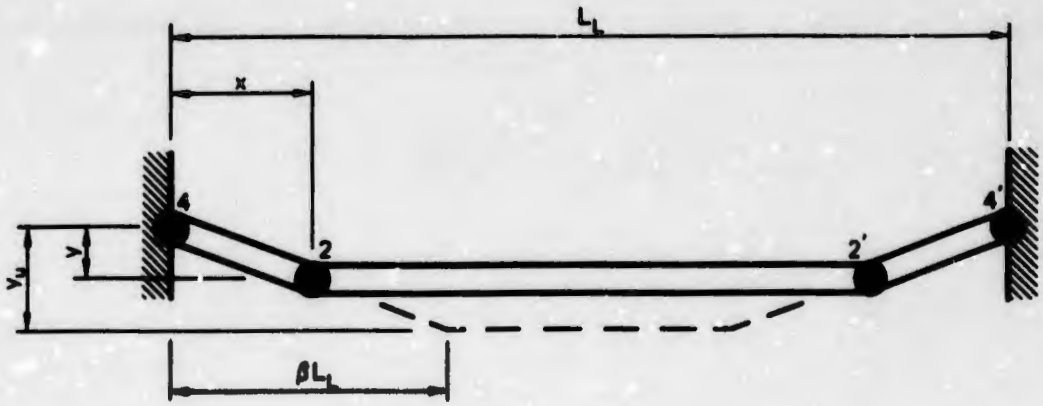

FIGURE 4 COLLAPSE MECHANISM OF A TYPICAL STRIP IN x-DIRECTION

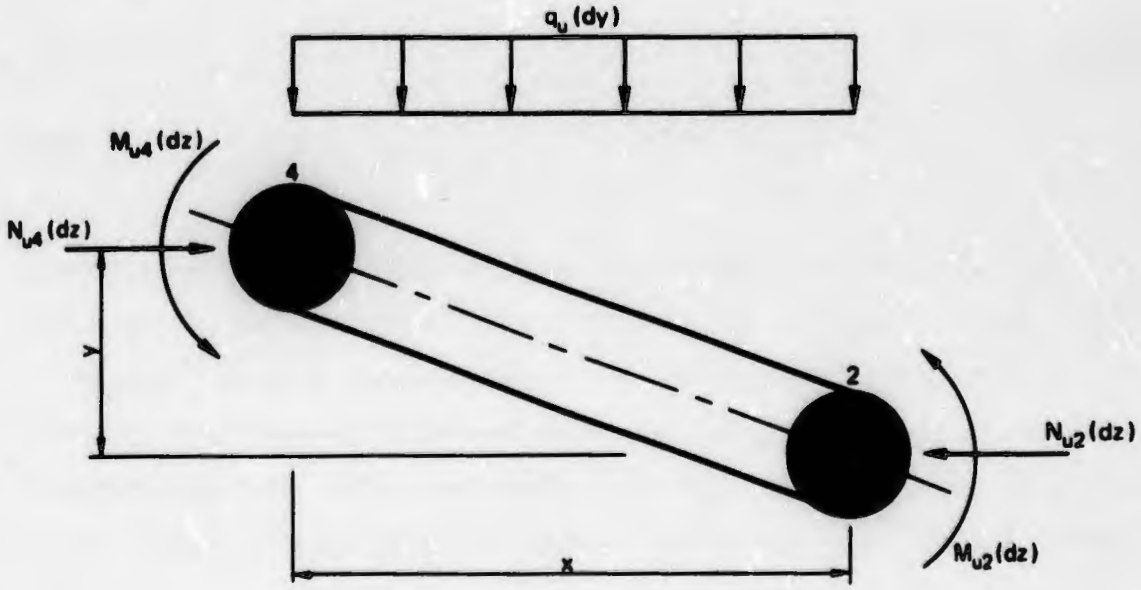

FIGURE 5 INTERNAL FORCES AT YIELD SECTIONS OF STRIP 4-2

section 2 in Figure 6 required to initiate crushing of the concrete is given by

$$N_{u2} = k_1 k_u d_2 f''_c - p_2 d_2 f_{s2} + p'_2 d_2 f'_{s2}$$

or

$$N_{u2} = f''_c \left(k_1 k_u d_2 - \bar{r}_2 \right) \tag{3}$$

where

$$\bar{r}_2 = \left(\frac{p_2 f_{s2} - p'_2 f'_{s2}}{f''_c} \right) d_2 \quad . \tag{3a}$$

Similarly, the thrust at section 4 (Figure 7) required to initiate crushing of the concrete is

$$N_{u4} = f''_c \left(k_1 k_u d_4 - \bar{r}_4 \right) \tag{4}$$

where

$$\bar{r}_4 = \left(\frac{p_4 f_{s4} - p'_4 f'_{s4}}{f''_c} \right) d_4 \quad . \tag{4a}$$

An enlarged view of the strip, relating the depths to the neutral axis, $k_u d_2$ and $k_u d_4$, to the geometry of the strip at a deflection y, is shown in Figure 8. The effect of partial restraint against in-plane movement at the supports is taken into account by assuming the support lines at 4 and 4′ to move outward a distance $s_x L_\ell / 2$. This longitudinal movement increases the original distance between supports from L_ℓ to $(1 + s_x) L_\ell$.

The slab also shortens axially due to the effects of the compressive membrane force. The total axial strain, ϵ_a, will have a constant value along the length of the strip, since the membrane force is constant.

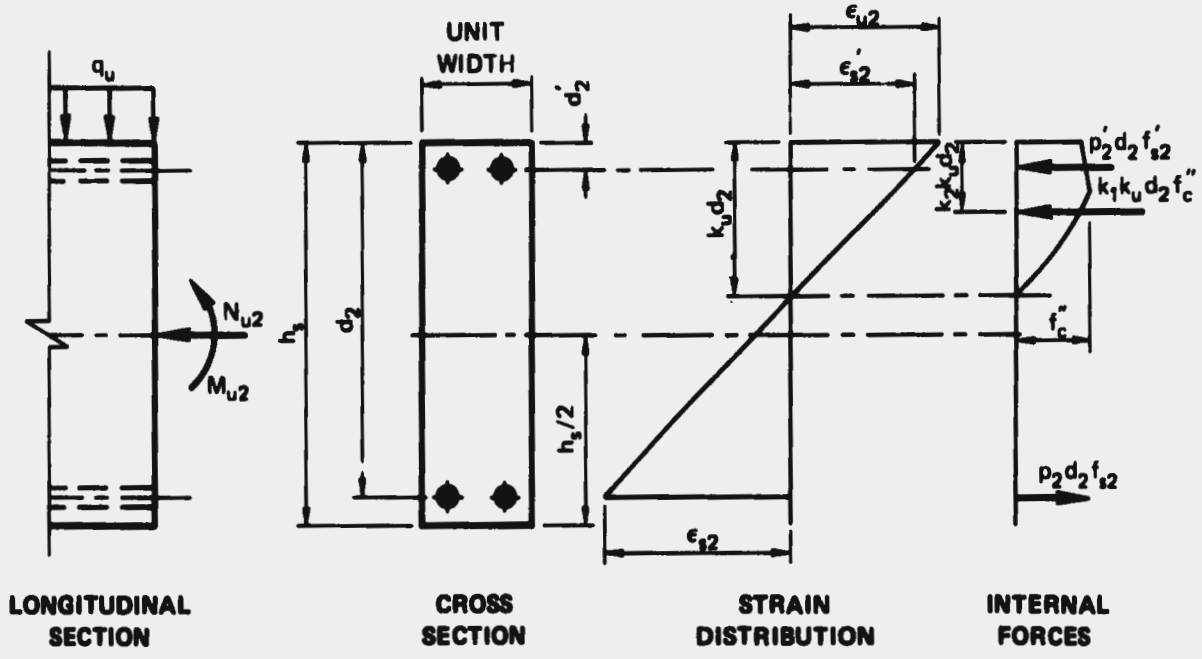

FIGURE 6 CONDITIONS AT SECTION 2 OF STRIP 4-2

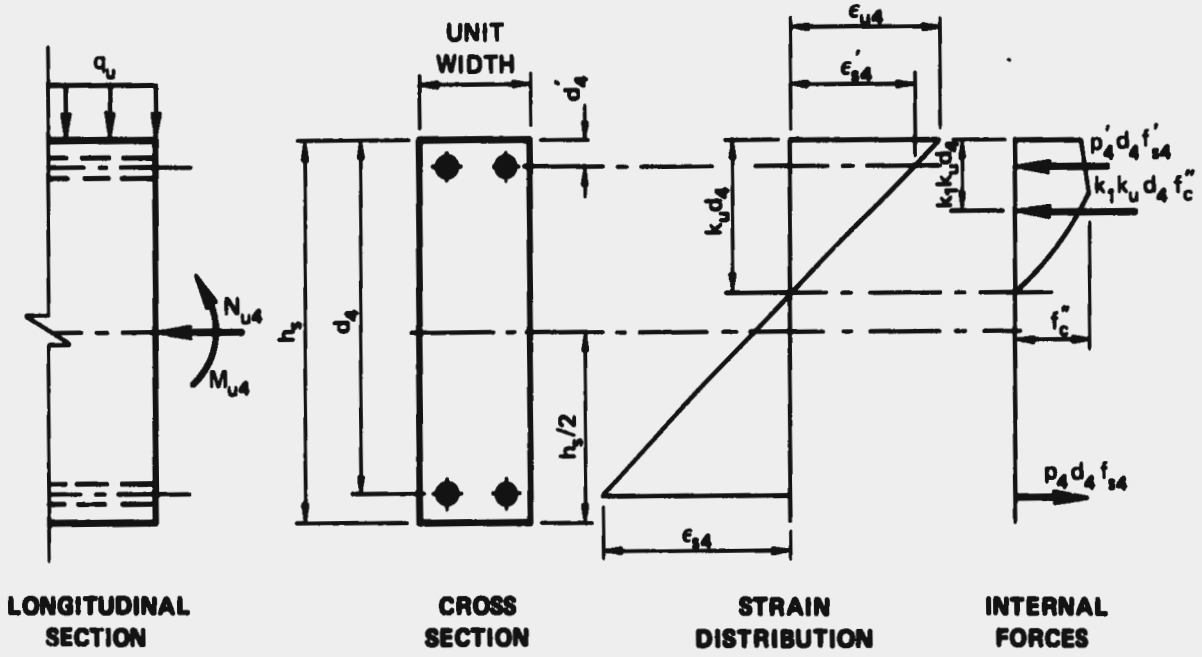

FIGURE 7 CONDITIONS AT SECTION 4 OF STRIP 4-2

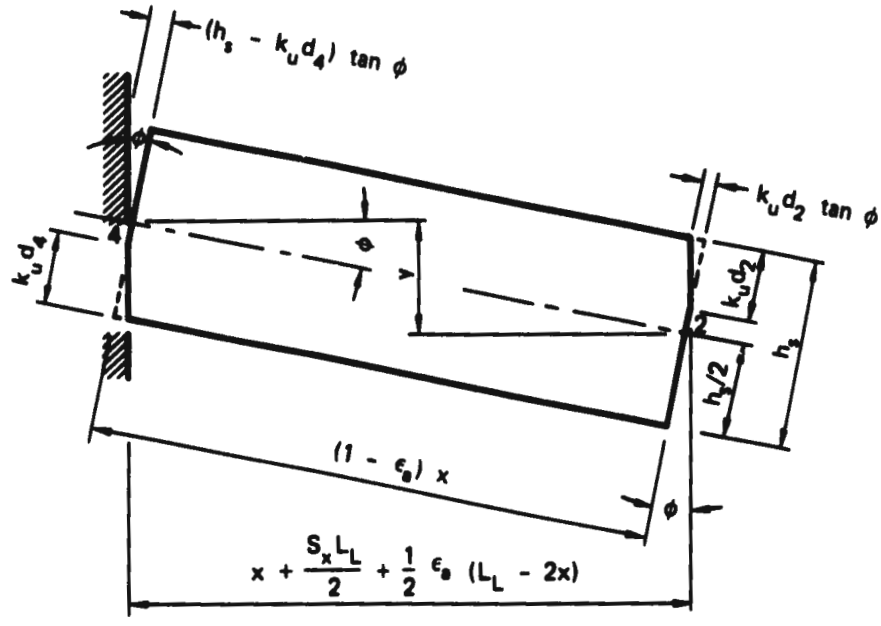

FIGURE 8 GEOMETRIC RESTRAINTS FOR STRIP 4-2

Because of ϵ_a, the shortening of the middle portion 2-2′ of the strip will be $\epsilon_a(L_L - 2x)$ and, because of symmetry, the ends of the portion 2-2′ will approach the center of the strip by $0.5\ \epsilon_a(L_L - 2x)$. Also, due to ϵ_a, the lengths of portions 4-2 and 4′-2′ will decrease to $(1 - \epsilon_a)x$. The distance between points 4 and 2 (Figure 8) is given by

$$\left[x + \frac{s_x L_L}{2} + 0.5\ \epsilon_a (L_L - 2x)\right]\sec \varphi = (1 - \epsilon_a)x + (h_s - k_u d_4)\tan \varphi - k_u d_2 \tan \varphi$$

or

$$h_s - k_u d_2 - k_u d_4 = \frac{1}{\sin \varphi}\left[\left(2 \sin^2 \frac{\varphi}{2}\right)x + \epsilon_a\left(x \cos \varphi + \frac{L_L}{2} - x\right) + \frac{s_x L_x}{2}\right] \quad . \tag{5}$$

Since φ is small (thus $\sin \varphi \cong 2 \sin \frac{\varphi}{2} \cong \frac{y}{x}$ and $\cos \varphi \cong 1$), Eq. 5 reduces to

$$h_s - k_u d_2 - k_u d_4 = \frac{y}{2} + \frac{xL_L}{2y}(\epsilon_a + s_x) \tag{6}$$

Therefore,

$$k_u d_2 + k_u d_4 = h_s - \frac{y}{2} - \frac{xL_L s_x'}{2y} \tag{7}$$

where

$$s_x' = s_x + \epsilon_a \quad . \tag{7a}$$

From the geometry of the deflected shape, shown in Figure 4,

$$y = y_u \left(\frac{x}{\beta L_l}\right) \qquad x \leq \beta L_l \quad . \tag{8}$$

Substituting Eq. 8 in Eq. 7 yields

$$k_u d_2 + k_u d_4 = h_s - \left(\frac{x}{2\beta L_l}\right) y_u - \frac{\beta s_x' L_l^2}{2y_u} \quad . \tag{9}$$

Substituting Eqs. 3 and 4 into Eq. 2 yields

$$k_1 k_u d_2 - \bar{r}_2 = k_1 k_u d_4 - \bar{r}_4$$

or

$$k_u d_2 - k_u d_4 = \frac{1}{k_1} (\bar{r}_2 - \bar{r}_4) \quad . \tag{10}$$

Solving Eqs. 9 and 10 simultaneously yields the following two expressions for the depths to the neutral axis

$$k_u d_2 = \frac{1}{2}\left\{\left[h_s - \left(\frac{x}{2\beta L_l}\right) y_u - \frac{\beta s_x' L_l^2}{2y_u}\right] + \frac{1}{k_1} (\bar{r}_2 - \bar{r}_4)\right\} \tag{11}$$

$$k_u d_4 = \frac{1}{2}\left\{\left[h_s - \left(\frac{x}{2\beta L_l}\right) y_u - \frac{\beta s_x' L_l^2}{2y_u}\right] + \frac{1}{k_1} (\bar{r}_4 - \bar{r}_2)\right\} \quad . \tag{12}$$

Examination of these equations shows that the effect of s_x' is to reduce the depths to the neutral axis at the yield sections.

Substituting Eq. 11 into Eq. 4, and noting from Eq. 2 that $N_{ux} = N_{u4}$, the thrust developed at the ends of the strip is

$$N_{ux} = \frac{f_c''}{2}\left\{\left[h_s - \left(\frac{x}{2\beta L_l}\right) y_u - \frac{\beta s_x' L_l^2}{2y_u}\right] k_1 - \bar{r}_2 - \bar{r}_4\right\} \quad . \tag{13}$$

To evaluate N_{ux} from Eq. 13, it is necessary to know the values of $\bar{r}_2$ and $\bar{r}_4$. These depend upon the steel stresses f_{s2}, f_{s2}', f_{s4}, and f_{s4}'.

The values of these stresses in turn depend on the value of the balanced thrust for the cross sections 4 and 2.

The balanced thrust is the thrust that causes yielding of the tension steel and crushing of the concrete to occur simultaneously. Its value is dependent on the properties of the cross section. For any thrust less than the balanced thrust, N_b, the tension steel is yielding ($f_s = f_y$) when crushing of the concrete occurs. It is also assumed that the compression steel is yielding ($f_s' = f_y$) when crushing occurs, as will generally be the case. Referring to Figures 6 and 7, the positions of the neutral axis at each hinge section for a balanced thrust are

$$k_{ub} d_2 = \left[\frac{\epsilon_u}{\epsilon_u + (f_y/E_s)}\right] d_2 \tag{14}$$

$$k_{ub} d_4 = \left[\frac{\epsilon_u}{\epsilon_u + (f_y/E_s)}\right] d_4 \quad . \tag{15}$$

The subscript b refers to the balanced condition.

Substituting Eqs. 14 and 15 into Eqs. 3 and 4, respectively, the balanced thrusts are given by

$$N_{b2} = f_c'' k_1 \left[\frac{\epsilon_u}{\epsilon_u + (f_y/E_s)}\right] d_2 - f_c'' r_2 \tag{16}$$

$$N_{b4} = f_c'' k_1 \left[\frac{\epsilon_u}{\epsilon_u + (f_y/E_s)}\right] d_4 - f_c'' r_4 \quad , \tag{17}$$

where

$$r_2 = d_2 (p_2 - p_2') \frac{f_y}{f_c''} \tag{16a}$$

$$r_4 = d_4 (p_4 - p_4') \frac{f_y}{f_c''} \quad . \tag{17a}$$

For the case of a tension failure at both ends of strip 4-2, the thrust at initial crushing of the concrete is found from Eq. 13 to be

$$N_{ux} = \frac{f''_c}{2}\left\{\left[h_s - \left(\frac{x}{2\beta L_l}\right)y_u - \frac{\beta s'_x L_l^2}{2y_u}\right]k_1 - r_2 - r_4\right\} \qquad (18)$$

provided

$$\left.\begin{aligned} N_{ux} &\leq N_{b2} \\ N_{ux} &\leq N_{b4} \end{aligned}\right\} \quad . \qquad (18a)$$

Next, considering a typical strip 3-1-1′-3′ in the z-direction (see Figures 2 and 3), the strips are similar to those in the x-direction, except that the strips are of length L_s, rather than L_l. Also, across the central portion of the slab only two segments exist instead of the three segments across the diagonals. An enlarged view of the diagonal portion of segment 3-1 is shown in Figure 9. Comparing this with Figure 8, the geometry is seen to be the same except for the change in notation from x, L_l, 4, and 2 for the x-direction strips to z, L_s, 3, and 1 for the z-direction strips. The corresponding equations for the z-direction strips can thus be obtained by merely interchanging the notation. From Eq. 7,

$$k_u d_1 + k_u d_3 = h_s - \frac{y}{2} - \frac{zL_s s'_z}{2y} \qquad (19)$$

where

$$s'_z = s_z + \epsilon_a \quad . \qquad (19a)$$

From the geometry of the deflected shape,

$$y = y_u\left(\frac{z}{L_s/2}\right) \qquad 0 \leq z \leq \frac{L_s}{2} \quad . \qquad (20)$$

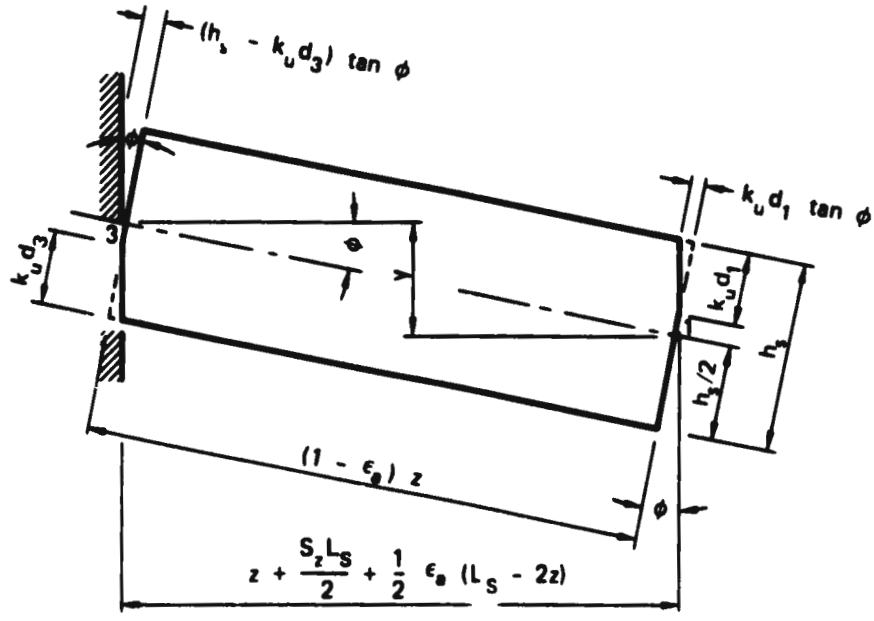

FIGURE 9 GEOMETRIC RESTRAINTS FOR STRIP 3-1

This equation is the same as Eq. 8 if $\beta = 1/2$. Substituting this value, along with the previous notation changes, in Eqs. 11 and 12, the depths to the neutral axis are given by

$$k_u d_1 = \frac{1}{2}\left\{\left[h_s - \left(\frac{z}{L_s}\right)y_u - \frac{s_z' L_s^2}{4y_u}\right] + \frac{1}{k_1}(\bar{r}_1 - \bar{r}_3)\right\} \tag{21}$$

$$k_u d_3 = \frac{1}{2}\left\{\left[h_s - \left(\frac{z}{L_s}\right)y_u - \frac{s_z' L_s^2}{4y_u}\right] + \frac{1}{k_1}(\bar{r}_3 - \bar{r}_1)\right\} . \tag{22}$$

The values of $\bar{r}_1$ and $\bar{r}_3$ depend on the value of the balanced thrust for the cross sections at 1 and 3. From Eqs. 16 and 17, the balanced thrusts are given by

$$N_{b1} = f_c'' k_1 \left[\frac{\epsilon_u}{\epsilon_u + (f_y/E_s)}\right] d_1 - f_c'' r_1 \tag{23}$$

$$N_{b3} = f_c'' k_1 \left[\frac{\epsilon_u}{\epsilon_u + (f_y/E_s)}\right] d_3 - f_c'' r_3 \tag{24}$$

where

$$r_1 = d_1 (p_1 - p_1') \frac{f_y}{f_c''} \tag{23a}$$

$$r_3 = d_3 (p_3 - p_3') \frac{f_y}{f_c''} . \tag{24a}$$

For the case of a tension failure at both ends of strip 3-1, the thrust at initial crushing of the concrete is found from Eq. 18 to be

$$N_{uz} = \frac{f_c''}{2}\left\{\left[h_s - \left(\frac{z}{L_s}\right)y_u - \frac{s_z' L_s^2}{4y_u}\right]k_1 - r_1 - r_3\right\} \tag{25}$$

provided

$$\left.\begin{aligned} N_{uz} &\leq N_{b1} \\ N_{uz} &\leq N_{b3} \end{aligned}\right\} . \tag{25a}$$

Ultimate Deflection

The ultimate deflection, y_u, is the central deflection of the slab at initial formation of the flexural collapse mechanism. In other words, y_u is the deflection required to develop the crushing strain, ϵ_u, along the hinge lines. For the general case of a rectangular slab, this value will be different for the x-direction and z-direction strips due to the difference in the length of these strips. Only for the special case of a square slab will y_u be the same. Since the short direction strips usually provide the greatest portion of the slab resistance, the approach taken in this study is to use the value of y_u for the z-direction (short direction) strips, except for the cases subsequently noted. This value is calculated as follows.

From the geometry of the z-direction strip 3-1 shown in Figure 9,

$$\tan \varphi = \frac{\epsilon_u (z/2)}{k_u d_3} \cong \frac{y}{z + s_z L_s/2 + \epsilon_a (L_s - 2z)/2} \quad .$$

Solving for y, and noting that at $z = L_s/2$, $y = y_u$, obtain the following equation for y_u,

$$y_u = \frac{\epsilon_u L_s^2}{8 k_u d_3} (1 + s_z) \quad . \tag{26}$$

Substituting the value of $k_u d_3$ from Eq. 22, with $z = L_s/2$, into Eq. 26, and rearranging, the following quadratic equation is obtained,

$$y_u^2 - 2\left[h_s + \frac{1}{k_1} (\bar{r}_3 - \bar{r}_1)\right] y_u + \frac{L_s^2}{2} \left[\epsilon_u (1 + s_z) + s_z'\right] = 0 \quad .$$

For $N_{uz} \leq N_{b1}$ and $N_{uz} \leq N_{b3}$ (tension failure at both ends) this can be rewritten as

$$y_u^2 - 2\left[h_s + \frac{1}{k_1}(r_3 - r_1)\right]y_u + \frac{L_s^2}{2}\left[\epsilon_u(1 + s_z) + s_z'\right] = 0 \quad . \tag{27}$$

Solving for y_u, the central deflection required to crush the concrete along the hinge lines for the z-direction strips is

$$y_u = \left[h_s + \frac{1}{k_1}(r_3 - r_1)\right] - \sqrt{\left[h_s + \frac{1}{k}(r_3 - r_1)\right]^2 - \frac{L_s^2}{2}\left[\epsilon_u(1 + s_z) + s_z'\right]} \tag{28}$$

where r_1 and r_3 are given by Eqs. 23a and 24a.

Equation 28 shows that y_u depends on (1) the properties of the cross section at the ends of the strip; (2) the crushing strain of the concrete; (3) the span and thickness of the slab; (4) the amount of longitudinal movement at the supports; (5) the axial stiffness of the slab; (6) the depth to the tension steel relative to the slab thickness; and (7) the ratio of f_y to f_c''.

For certain combinations of these slab properties, the quantity under the radical in Eq. 28 may be negative. This indicates insufficient longitudinal restraint in the z-direction to develop crushing strain along the hinge lines, thus resulting in an imaginary value for y_u. In this case the corresponding ultimate deflection for the x-direction (long direction) strip is calculated.

Following the same procedure as for the z-direction strips, the central deflection required to crush the concrete along the hinge lines for the x-direction strips is

$$y_u = \left[h_s + \frac{1}{k_1}(r_4 - r_c)\right] - \sqrt{\left[h_s + \frac{1}{k_1}(r_4 - r_2)\right]^2 - \beta L_t^2\left[\epsilon_u(2\beta + s_x - 2\beta\epsilon_a + \epsilon_a) + s_x'\right]} \quad (29)$$

where r_4 and r_2 are given by Eqs. 16a and 17a.

If the value of y_u from Eq. 29 is also imaginary, the longitudinal restraint in both directions is insufficient to develop the crushing strain along the yield lines. For such cases the compressive membrane forces are insignificant, and the slab resistance is calculated using the yield-line theory previously outlined in Ref. 7.

Equations 28 and 29 do not apply if the ultimate thrust, N_u, is greater than the balanced thrust, N_b. However, since an exact solution for such cases would require a complicated iterative procedure to solve for f_s and f_s' along the yield lines, Eqs. 28 and 29 were also used for those slabs where $N_u > N_b$. For such cases, the slabs have limited rotational capacity along the hinge lines, thus introducing the possibility of a brittle collapse mechanism that can precipitate a premature shear failure. As noted previously, this situation was not considered in this study due to the lack of information regarding the increase in shear strength due to the presence of compressive membrane forces.

Examining Eqs. 28 and 29 in more detail, it can be noted that y_u reaches a limiting value when the quantity under the radical equals zero. In other words, the compressive membrane forces induced in the slab reach a maximum value regardless of the span/thickness ratio. According to Eqs. 28 and 29 the upper bound for y_u is $h_s + (r_3 - r_1)/k_1$ for the z-direction strips and $h_s + (r_4 - r_2)/k_1$ for the x-direction strips. These upper bounds correspond to large values of the span/thickness ratio.

However, examination of test values from Refs. 9, 10, 11, and 12 indicate a limiting value of y_u much less than the slab thickness. Reference 10 suggests an empirical value for the limiting ultimate deflection of

$$y_u \leq 0.42\, h_s \quad . \tag{30}$$

This upper bound was also used in this study.

Ultimate Flexural Resistance

The ultimate flexural resistance can now be determined by means of the work-energy method. The work done can be found by multiplying the resisting moment per unit length normal to the axis of rotation by the angle of rotation for each of the x-direction and z-direction strips, and summing for all the strips.

The sum of the moments on the x-direction strips are

$$M_{u2}\ (dz) + M_{u4}\ (dz) - N_{ux}y\ (dz)$$

while the angle of rotation is

$$\theta_x = \frac{y_u}{\beta L_4} \quad .$$

The work done for the x-direction strips is thus given by

$$W_x = \left[M_{u2} + M_{u4} - N_{ux}y\right]\left(\frac{y_u}{\beta L_4}\right)dz \tag{31}$$

where, from Eq. 8,

$$y = y_u \left(\frac{x}{\beta L_4}\right) \qquad 0 \leq x \leq \beta L_4 \quad . \tag{8}$$

The corresponding work done for the z-direction strips is

$$W_z = \left[M_{u1} + M_{u3} - N_{u2}y\right]\left(\frac{y_u}{L_s/2}\right)dx \tag{32}$$

where, from Eq. 19,

$$y = y_u\left(\frac{z}{L_s/2}\right) \qquad 0 \le z \le \frac{L_s}{2} \quad . \tag{19}$$

The energy input for a uniform load, q, can be determined by multiplying the total load acting on the strip by the deflection at the center of gravity of the strip. Thus, the energy input for the x-direction strips is

$$E_x = \left[q_u(dz)x\right]\frac{y}{2} = \frac{q_u y_u}{2\beta L_\ell}x^2dz \tag{33}$$

where

$$x = z\left(\frac{\beta L_\ell}{L_s/2}\right) = 2\beta\left(\frac{L_\ell}{L_s}\right)z \qquad 0 \le z \le \frac{L_s}{2} \quad . \tag{34}$$

Similarly, the energy input for the z-direction strips is

$$E_z = \left[q_u(dx)z\right]\frac{y}{2} = \frac{q_u y_u}{L_s}z^2dx \tag{35}$$

where

$$z = x\left(\frac{L_s/2}{\beta L_\ell}\right) = \frac{1}{2\beta}\left(\frac{L_s}{L_\ell}\right)x \qquad 0 \le x < \beta L_\ell \tag{36a}$$

$$z = \frac{L_s}{2} \qquad \beta L_\ell \le x \le \frac{L_\ell}{2} \quad . \tag{36b}$$

The total work done by the x-direction and z-direction strips is obtained by integrating over the total area of the slab. Thus,

$$W_T = 2\int_0^{L_S} W_x + 2\int_0^{L_L} W_z \quad ,$$

which, by substituting Eqs. 31 and 32, becomes

$$W_T = 2\int_0^{L_S} [M_{u2} + M_{u4} - N_{ux}y]\left(\frac{y_u}{\beta L_L}\right)dz + 2\int_0^{L_L} [M_{u1} + M_{u3} - N_{uz}y]\left(\frac{y_u}{L_S/2}\right)dx \quad . \qquad (37)$$

Substituting the expressions for N_{ux} and N_{uz} (Eqs. 18 and 25), y (Eqs. 8 and 19), and x and z (Eqs. 34, 36a, and 36b) into Eq. 37, and integrating yields the following equation for W_T,

$$W_T = 4\left(\frac{y_u}{\beta L_L}\right)\left[\int_0^{L_S/2} M_{u2}\,dz + \int_0^{L_S/2} M_{u4}\,dz\right]$$

$$+ 8\left(\frac{y_u}{L_S}\right)\left[\int_0^{\beta L_L} M_{u1}\,dx + \int_0^{\beta L_L} M_{u3}\,dx + \int_{\beta L_L}^{L_L/2} M_{u1}\,dx + \int_{\beta L_L}^{L_L/2} M_{u3}\,dx\right]$$

$$- \frac{y_u^2 L_S}{\beta L_L}\left(\frac{f_c''}{2}\right)\left[\left(h_s - \frac{y_u}{3} - \frac{s_x'\beta L_L^2}{2y_u}\right)k_1 - (r_2 + r_4)\right]$$

$$- \frac{4y_u^2\beta L_L}{L_S}\left(\frac{f_c''}{2}\right)\left[\left(h_s - \frac{y_u}{3} - \frac{s_z'L_S^2}{4y_u}\right)k_1 - (r_1 + r_3)\right]$$

$$- \frac{4y_u^2(1 - 2\beta)L_L}{L_S}\left(\frac{f_c''}{2}\right)\left[\left(h_s - \frac{y_u}{2} - \frac{s_z'L_S^2}{4y_u}\right)k_1 - (r_1 + r_3)\right] . \tag{38}$$

Since M_{u2}, M_{u4}, M_{u1}, and M_{u3} are nonlinear, the first four integrals are awkward to evaluate. A simple expression that may be used to approximate these integrals is

$$\int_0^{L_S/2} M_{u2}\,dz = (\bar{M}_{u2})\frac{L_S}{2} \tag{39a}$$

$$\int_0^{L_S/2} M_{u4}\,dz = (\bar{M}_{u4})\frac{L_S}{2} \tag{39b}$$

$$\int_0^{\beta L_l} M_{u1}\,dx = (\bar{M}_{u1})\,\beta L_l \tag{39c}$$

$$\int_0^{\beta L_l} M_{u3}\,dx = (\bar{M}_{u3})\,\beta L_l \tag{39d}$$

where

$\bar{M}_{u2}$ = the ultimate moment resistance about midthickness of sections along the diagonal produced by the average thrust acting across the span, $[N_{ux}(0) + N_{ux}(\beta L_l)]/2$.

$\bar{M}_{u4}$ = the ultimate moment resistance about midthickness of sections along the edge produced by the average thrust acting across the span, $[N_{ux}(0) + N_{ux}(\beta L_l)]/2$.

$\bar{M}_{u1}$ = the ultimate moment resistance about midthickness of sections along the diagonal produced by the average thrust acting across the span, $[N_{uz}(0) + N_{uz}(L_s/2)]/2$.

$\bar{M}_{u3}$ = the ultimate moment resistance about midthickness of sections along the edge produced by the average thrust acting across the span, $[N_{uz}(0) + N_{uz}(L_s/2)]/2$.

The fifth and sixth integrals can be easily evaluated, since M_{u3} and M_{u4} are constant across the center yield line. Thus,

$$\int_{\beta L_l}^{L_l/2} M_{u1}\,dz = \left(\frac{1}{2} - \beta\right) L_l M_{u1}(\beta L_l) \tag{39e}$$

$$\int_{\beta L_l}^{L_l/2} M_{u3}\,dz = \left(\frac{1}{2} - \beta\right) L_l M_{u3}(\beta L_l) \tag{39f}$$

where

$M_{u1}(\beta L_L)$ = the ultimate moment resistance along the center produced by the thrust $N_{uz}(L_S/2)$

$M_{u3}(\beta L_L)$ = the ultimate moment resistance along the edge produced by the thrust $N_{uz}(L_S/2)$.

The last three terms of Eq. 38 can also be expressed in terms of the thrust by noting from Eqs. 17 and 24 that

$$N_{uz}\left(\frac{L_S}{2}\right) = \frac{f_c''}{2}\left[\left(h_s - \frac{y_u}{2} - \frac{s_z' L_S^2}{4y_u}\right) k_1 - (r_1 + r_3)\right] \tag{39g}$$

$$\frac{1}{3}\left[N_{uz}(0) + 2N_{uz}\left(\frac{L_S}{2}\right)\right] = \frac{f_c''}{2}\left[\left(h_s - \frac{y_u}{3} - \frac{s_z' L_S^2}{4y_u}\right) k_1 - (r_1 + r_3)\right] \tag{39h}$$

$$\frac{1}{3}\left[N_{ux}(0) + 2N_{ux}(\beta L_L)\right] = \frac{f_c''}{2}\left[\left(h_s - \frac{y_u}{3} - \frac{s_x' \beta L_L^2}{4y_u}\right) k_1 - (r_2 + r_4)\right] . \tag{39i}$$

Substituting Eqs. 39a through 39i in Eq. 38 yields the following expression for W_T,

$$\begin{aligned} W_T = {} & \frac{2y_u L_S}{\beta L_L}\left\{\bar{M}_{u2} + \bar{M}_{u4} - \frac{y_u}{6}\left[N_{ux}(0) + 2N_{ux}(\beta L_L)\right]\right\} \\ & + \frac{8y_u \beta L_L}{L_S}\left\{\bar{M}_{u1} + \bar{M}_{u3} - \frac{y_u}{6}\left[N_{uz}(0) + 2N_{uz}\left(\frac{L_S}{2}\right)\right]\right\} \\ & + \frac{4y_u(1 - 2\beta)L_L}{L_S}\left\{M_{u1}(\beta L_L) + M_{u3}(\beta L_L) - y_u N_{uz}\left(\frac{L_S}{2}\right)\right\} . \end{aligned} \tag{40}$$

The total energy input can be determined by integrating the energy input for the individual x-direction and z-direction strips over the entire area of the slab. Thus,

$$E_T = 2\int_0^{L_S} E_x + 2\int_0^{L_L} E_z \quad ,$$

which, by substituting Eqs. 33 and 35, becomes

$$E_T = 2\int_0^{L_S} \frac{q_u y_u}{2\beta L_L} x^2 dz + 2\int_0^{L_L} \frac{q_u y_u}{L_S} z^2 dx \quad .$$

Substituting the expressions for x and z from Eqs. 34, 36a, and 36b, and integrating, the total energy input is expressed by

$$E_T = \frac{q_u y_u L_S L_L}{6} (3 - 2\beta) \quad . \tag{41}$$

Equating the total work done (Eq. 40) to the total energy input (Eq. 41), and solving for the slab resistance, yields

$$q_u = \frac{12}{L_S^2(3 - 2\beta)} \left[\frac{1}{\beta} \left(\frac{L_S}{L_L} \right)^2 \left\{ \bar{M}_{u2} + \bar{M}_{u4} - \frac{y_u}{6} \left[N_{ux}(0) + 2N_{ux}(\beta L_L) \right] \right\} \right.$$

$$+ 4\beta \left\{ \bar{M}_{u1} + \bar{M}_{u3} - \frac{y_u}{6} \left[N_{uz}(0) + 2N_{uz}\left(\frac{L_S}{2}\right) \right] \right\}$$

$$\left. + 2(1 - 2\beta) \left\{ M_{u1}(\beta L_L) + M_{uz}(\beta L_L) - y_u N_{uz}\left(\frac{L_S}{2}\right) \right\} \right] \quad . \tag{42}$$

The coordinates of the point defining the ultimate flexural resistance are now defined by Eq. 28, 29, or 30 for y_u and by Eq. 42 for q_u. Reference 10 found that the resistance for values less than q_u can be approximated by the expression

$$q = q_u \left[1 - \left(1 - \frac{y_e}{y_u} \right)^{1.8} \right]^{\frac{1}{1.8}} \qquad y_e \leq y_u \quad . \tag{43}$$

This equation, which assumes a vertical tangent at (0,0) and a horizontal tangent at (q_u, y_u), was determined by a best fit of the experimental results from static tests of square slabs longitudinally restrained on all edges. In this study, this expression is also assumed to apply to rectangular slabs and to slabs with partially restrained edges.

Secondary Resistance

After the resistance reaches its ultimate value, there is a decrease in the resistance as the deflection increases. Tests show that the resistance reaches a minimum value approximately equal to the value obtained using yield-line theory (not considering membrane forces). This equivalence is reasonable to expect, since the minimum resistance should correspond to a change of membrane forces from compression to tension in the central region of the slab. The secondary resistance can thus be determined from Eq. 42 by setting N_{ux} and N_{uz} equal to zero, resulting in the following equation for q_s,

$$q_s = \frac{12}{L_S^2(3 - 2\beta)} \left[\frac{1}{\beta} \left(\frac{L_S}{L_L} \right)^2 (M_{u2} + M_{u4}) + 2(M_{u1} + M_{u3}) \right] \quad , \qquad (44)$$

where M_{u2}, M_{u4}, M_{u1}, and M_{u3} are the resisting moments for a zero thrust and β is determined from Eq. 1.

Expressions previously given in Ref. 7 for the tensile membrane behavior of slabs are used to determine the deflection at the intersection of the tensile membrane resistance and secondary resistance. These expressions, which were based primarily on the development presented in Ref. 13, assume the reinforcing steel to act as a plastic membrane. Additional assumptions, all of which are conservative, include:

(1) The concrete has cracked throughout its depth, hence is incapable of carrying any load.

(2) All the reinforcing steel has yielded.

(3) No strain-hardening of the reinforcing steel occurs.

The resulting expression for the tensile membrane resistance is

$$q = k_t' \frac{A_{ts} f_{dy}}{L_s^2} y_c \quad , \tag{45}$$

where

$$k_t' = 1.5\, k_t = \frac{1.5\,\pi^3}{4 \sum_{n=1,3,5}^{\infty} \frac{1}{n^3} (-1)^{\frac{n-1}{2}} \left[1 - \operatorname{sech}\left(\frac{n\pi L_L}{2L_S}\sqrt{\frac{A_{ts}}{A_{tL}}}\right)\right]} \quad . \tag{46}$$

A_{ts} is the area (per unit width) of the reinforcing steel (both top and bottom bars) continuous along the short span of the slab. Similarly, A_{tL} is the area (per unit width) of the reinforcing steel continuous along the long span of the slab. Values of the factor k_t are plotted in Figure 10 for $A_{ts}/A_{tL} \geq 1$. The 1.5 factor was included to reflect the approximately 50 percent increase in test values of the tensile membrane strength over the calculated values.

Setting $q = q_s$ in Eq. 45 and solving for the center deflection at the intersection of the secondary resistance and tensile membrane resistance,

$$y_t = \frac{q_s L_s^2}{k_t' A_{ts} f_{dy}} \quad . \tag{47}$$

In general, the secondary deflection is taken to be the same as the intersection of the secondary resistance and the tensile membrane resistance, or

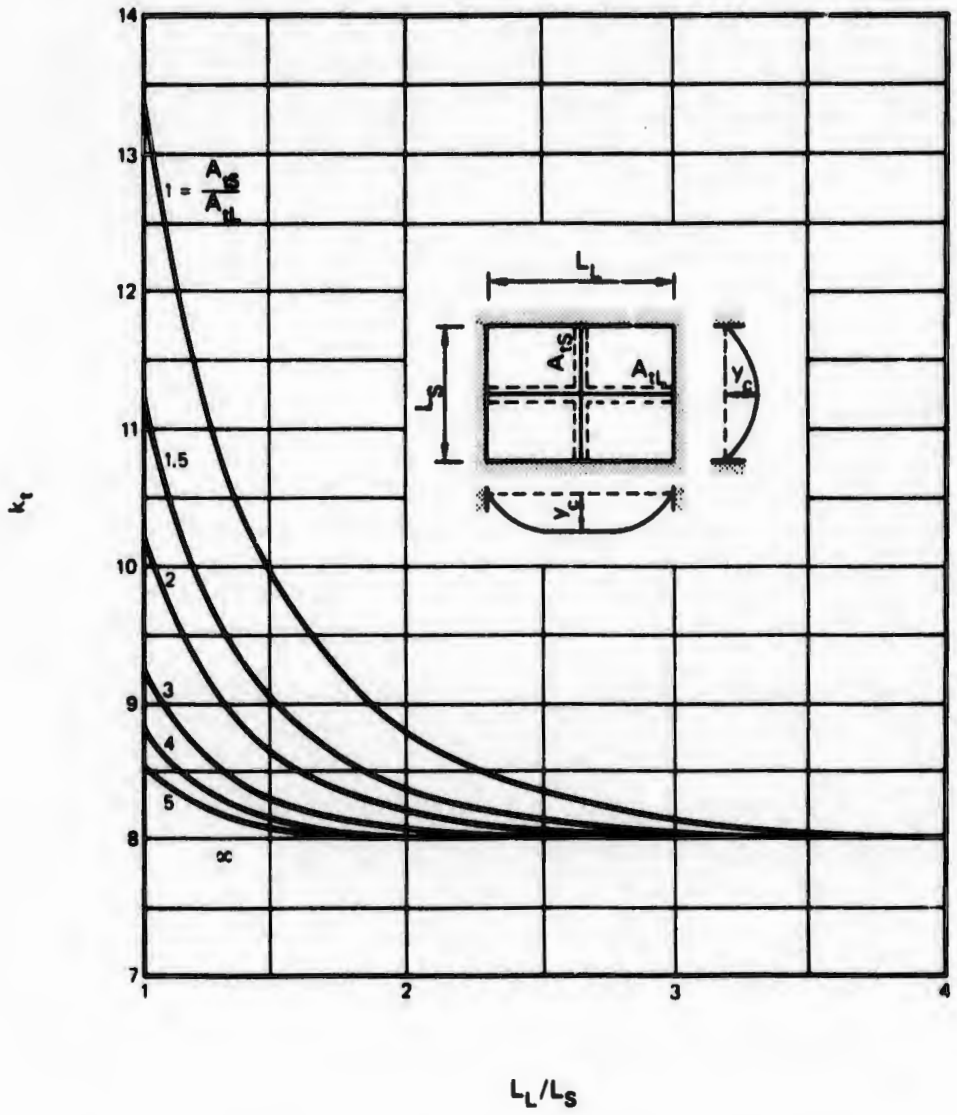

SOURCE: Reference 13.

FIGURE 10 COEFFICIENTS FOR TENSILE MEMBRANE RESISTANCE IN TWO-WAY ACTION SLABS

$$y_s = y_t = \frac{q_s L_s^2}{k_t' A_{ts} f_{dy}} \quad . \tag{48}$$

Examination of test results indicate that for certain slabs, primarily those with low tensile membrane resistance, the value given by Eq. 48 is much larger than the actual secondary deflection. Based on a study of test results, an upper bound of

$$y_s \leq 3\, y_u \quad . \tag{49}$$

is placed on the secondary deflection.

The coordinates of the point defining the secondary resistance are now defined by Eq. 44 for q_s and by Eq. 48 or 49 for y_s. In Ref. 10 resistance for values between y_u and y_s was approximated by the expression

$$q = \frac{q_u}{2}\left\{1 + \left(\frac{q_s}{q_u}\right) + \left[1 - \left(\frac{q_s}{q_u}\right)\right] \cos\left[\frac{\pi(y_c - y_u)}{y_s - y_u}\right]\right\} \quad . \tag{50}$$

This expression was also used in this study to describe the resistance-deflection behavior for this region.

For the special case of a slab with no reinforcement, the secondary resistance is zero. For this case the secondary deflection is defined to be equal to the slab thickness,

$$y_s = h_s \quad . \tag{51}$$

The resistance for values between q_u and q_s is still given by Eq. 50.

Tensile Membrane Resistance and Collapse

After the deflection y_t is reached, the tensile membrane region begins to grow outward towards the supports. Cracks begin to penetrate the entire depth of the concrete, and yielding of the reinforcement

spreads throughout the slab. The top and bottom reinforcement acts as a tensile membrane, causing the slab resistance to increase with the center deflection, as shown by Eq. 42. This continues until the reinforcement ruptures. Reference 13 reported that a safe maximum value for the central deflection is 0.10 of the short span. Examination of test results indicates that a more realistic value for collapse of the slab is approximately 0.15 of the short span. Thus, for the present study, the failure deflection is taken as

$$y_{ft} = 0.15\ L_s \quad . \tag{52}$$

For slabs unrestrained in the short direction, Eq. 52 does not apply. For these cases, the failure deflection is taken as 0.15 of the long span,

$$y_{ft} = 0.15\ L_l \quad . \tag{53}$$

Summary

The resistance function for reinforced concrete slabs with longitudinal edge restraint, as previously illustrated in Figure 1, with the corresponding equations is summarized as follows.

Compressive Membrane Resistance ($0 \leq y_c \leq y_u$)

$$q = q_u\left[1 - \left(1 - \frac{y_c}{y_u}\right)^{1.8}\right]^{\frac{1}{1.8}} \tag{43}$$

q_u —— Eq. 42

y_u —— Eq. 28, Eq. 29, or Eq. 30

Secondary Resistance ($y_u \leq y_o \leq y_s$)

$$q = \frac{q_u}{2}\left\{1 + \left(\frac{q_s}{q_u}\right) + \left[1 - \left(\frac{q_s}{q_u}\right)\right]\cos\left[\frac{\pi(y_o - y_u)}{y_s - y_u}\right]\right\} \tag{50}$$

q_s — Eq. 44

y_s — Eq. 48, Eq. 49, or Eq. 51

Tensile Membrane Resistance ($y_t \leq y_o \leq y_{ft}$)

$$q = k_t' \frac{A_{ts} f_{dy}}{L_s^2} y_o \tag{45}$$

k_t' — Eq. 46

y_{ft} — Eq. 52 or Eq. 53

After development of the resistance function for longitudinally restrained reinforced concrete slabs, the computer programs prepared under the previous study (Ref. 7) were modified accordingly. This required transforming the slab into an equivalent single-degree-of-freedom dynamic system by the use of transformation factors for the load, resistance, and mass. The equation of motion is solved on a computer using numerical integration procedures. Analytical predictions of the static and dynamic response of restrained slabs were then generated for comparison with various published experimental data. The results of the analytical and experimental correlations are presented in the Appendix. In general, the correlations justify the use of the compressive membrane mode for predicting the collapse of floor systems in existing structures that are longitudinally restrained at the edges, such as the interior panels of a multibay floor system.

III WOOD-JOIST FLOOR SYSTEMS

Introduction

Wood-joist floor systems are complex structural systems that are not readily amenable to precise theoretical analysis because of the wide variability in the mechanical properties of wood, even within the same species and grade, and the variability in construction methods and details. Even though it is known that the finish flooring and subflooring contribute to the strength and stiffness of floor systems, design codes invariably specify maximum stresses and deflections for the design of the joists to resist the total floor load without regard to other factors. The allowable stress specified in the design codes are quite low, since 95 percent of the individual load-carrying members in a given lumber grade can safely support the design load (Ref. 14). For example, Ref. 15 specifies an allowable unit stress in the extreme fiber in bending of 2050 psi for the highest grade Douglas fir, coast region joist and plank stress-graded lumber, whereas Ref. 16 indicates a modulus of rupture in excess of 12,000 psi for small wood beam specimens in static bending tests of the same species.

As noted in various research publications, design codes do not take into account the effect of the interaction between individual members of a completed floor system, and the specifying of relatively low allowable stresses for joist design is equivalent to requiring floor system design to be based on the weakest link. On the other hand, the available test information shows that the strength of a floor system, beyond that of the weakest joist, is largely dependent on the interaction effects between floor elements. For example, the finish and subflooring both contribute

to the strength and stiffness of the joist through composite or T-beam action. However, the primary effect of the flooring is a result of its contribution to load sharing between individual joists. The wood industry's concept of load sharing has been described in Ref. 14 as being a reduction in the effective variability between individual joists when they are grouped into a structural system, an increase in the effective strength provided by the mutual constraint resulting from joining members into an indeterminate structure, and an increase in the effective strength by the local reinforcement of defects by adjacent members.

Although design procedures do not permit assigning a value to load sharing, as mentioned, the enhancement of the floor system strength as a result of the interacting effects among the various elements in a wood-joist floor system has been conclusively demonstrated in many tests of actual floors (e.g., Refs. 17 through 22). The intent of this discussion is not to judge the merits of any code requirements, but merely to point out that for predicting the collapse of wood-joist floors, it is necessary to include effects that are not treated directly in any design procedure.

The development of a realistic resistance function to represent the response of a wood-joist floor system is complicated by the large variability of material properties within any particular wood species (even among similar wood specimens specifically selected for tests), and by the highly complex indeterminate structural action that occurs between various elements of the floor system. Although the limited theoretical studies of the composite floor behavior, such as that presented in Ref. 23 to model the slip in nailed plate-rib joints, have been correlated with specific test data, the unknowns involved in the evaluation of wood-joist floors in existing buildings do not warrant the development of a sophisticated mathematical model. Instead, the approach in this study was to examine sufficient analytical and experimental information to

permit the development of a relatively simplified model that would adequately reflect the complex composite action of the floor system.

A wood beam, or joist, composed of perfectly clear wood without defects, and subjected to pure bending forces as a result of an increasing uniform static load, goes through two distinct phases prior to collapse. The first phase is elastic, where a plane section remains plane, and a linear relationship exists between stress and strain throughout the beam cross section. As the stress level is increased, the extreme fibers on the compression side reach their proportional limit. The second phase is therefore characterized by inelastic behavior on the compression side, and a linear elastic behavior on the tension side. Typical stress-strain curves for wood in tension and compression are shown on Figure 11; note that the tension portion of the stress-strain relationship remains essentially linear up to failure. Since the ultimate tensile strength of clear wood is much greater than its ultimate compressive strength, a redistribution of stress occurs across the beam section as the bending moment increases beyond the proportional limit in compression. To satisfy the conditions of equilibrium of internal forces at a section, the neutral axis shifts towards the tension side (Refs. 24 and 25). Test data also indicate that a plane section of a wood beam in pure bending remains approximately plane up to tensile failure.

As noted in Ref. 25, the second degree parabola has been found to be the best approximation to the compressive stress-strain distribution above the proportional limit. The theoretical stress distribution in a wood beam near failure would therefore appear as shown in Figure 12.

Resistance Function

As discussed above, a wood-joist floor system is a complex structural system because of both the effects of interaction between the floor elements, and the wide variability in the properties of wood. In addition,

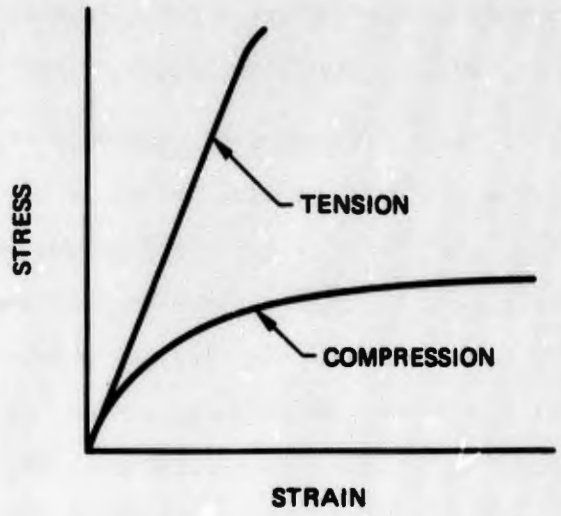

FIGURE 11 STRESS-STRAIN CURVES FOR AXIAL TENSION AND COMPRESSION IN WOOD

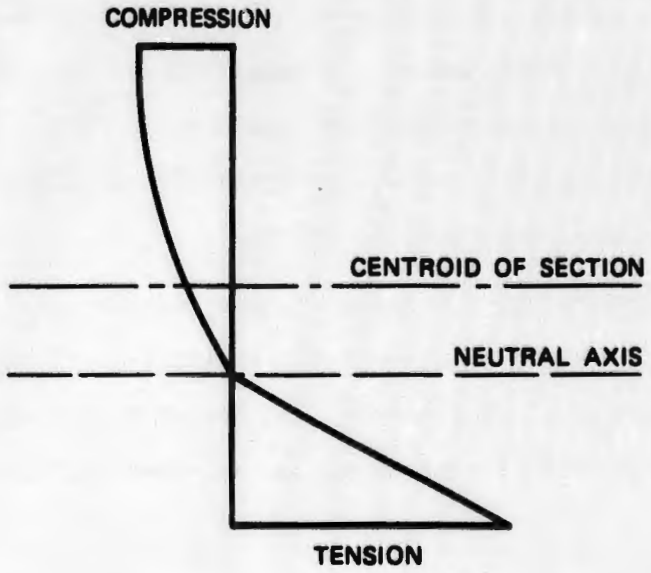

FIGURE 12 STRESS DISTRIBUTION NEAR FAILURE FOR RECTANGULAR WOOD BEAMS IN FLEXURE

predicting the collapse of existing floor systems under blast loading is further complicated by the variability in construction techniques, especially in the relatively unsupervised home construction industry, and by the fact that the properties of the wood used in any analysis are usually published average values for a wood species rather than actual values based on knowledge of the specific wood used. The differences between the published properties of wood and those in a specific existing floor system would be expected to show a much greater variation than for structural steel, or even for concrete. However, the use of published average property values for wood may be adequate because of the averaging effect resulting from the interaction among the elements of a floor system.

In any event, as stated, the unknowns involved in calculating the dynamic response and collapse of wood-joist floor systems do not justify the development of a complex mathematical model. The approach therefore was to use established theoretical procedures, and, where feasible, to modify the procedures to reflect the results of tests of actual floor systems. The method adopted was similar to that used for wall elements (Refs. 1 and 4), and for reinforced concrete floor systems (Ref. 7). That is, the resistance function was established for wood-joist floor systems by assuming that the deflected shape of the member under dynamic load is identical to that under a uniform static load and that the distribution of the restoring force and dynamic load is the same. The member is then transformed into an equivalent single-degree-of-freedom dynamic system by the use of transformation factors for the load, resistance, and mass. The equation of motion is solved on a computer using a numerical integration procedure.

The resistance function for wood-joist floor systems was assumed to consist of elastic and inelastic phases as shown on Figure 13, and was determined only for the case of a simply supported, uniformly loaded floor.

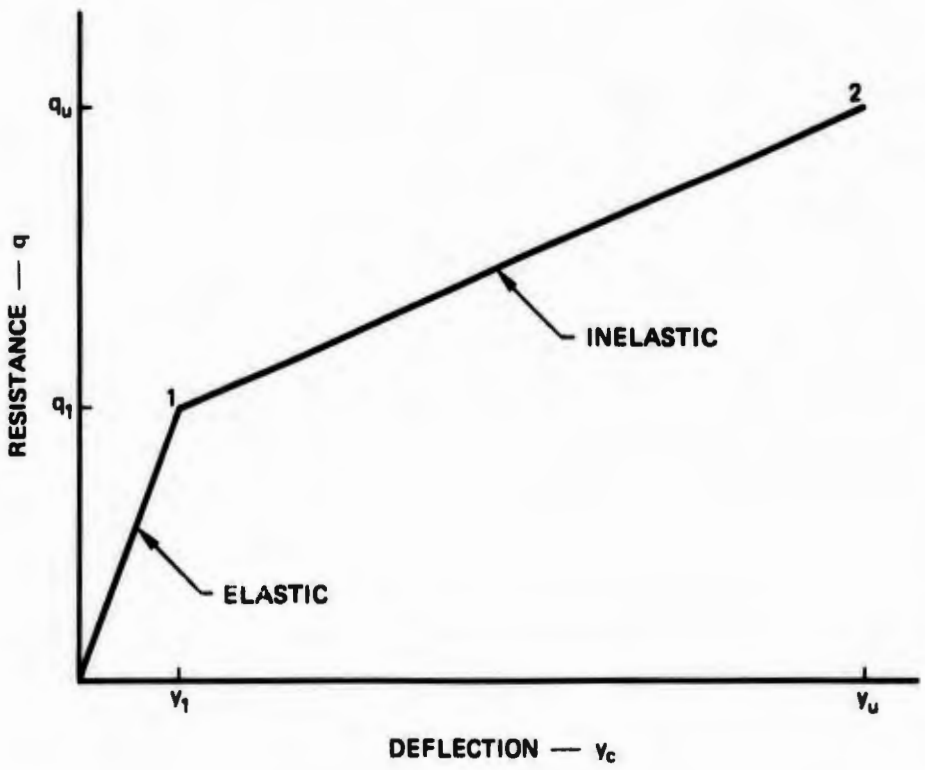

FIGURE 13 RESISTANCE FUNCTION FOR A SIMPLY SUPPORTED WOOD-JOIST FLOOR SYSTEM

Although scabs are sometimes used to reinforce wood joists at interior supports (e.g., Ref. 26), joists are not generally continuous over the support, and the scab cannot be expected to develop the bending strength of the joist. Also, although tests indicate that a ceiling on the bottom of a wood-joist floor has a stiffening effect (Refs. 26 and 27), a ceiling was not included in the mathematical model since the primary interest was in floors over basement areas where ceilings are usually not used.

Elastic Phase

The maximum elastic resistance, q_1, of a simply supported wood-joist floor with a uniformly distributed load is developed when the moment at the center section is a maximum, or

$$M_e = \frac{q_1 s L^2}{8} \quad , \tag{54}$$

where s is the joist spacing.

Since a linear relationship is assumed to exist between the stress and strain during the initial elastic phase, the extreme fiber stress is equal to

$$f_w = \frac{M h_j / 2}{I_e} \quad . \tag{55}$$

Test data (e.g., Ref. 28) have indicated that the effective moment of inertia, I_e, of a wood-joist floor system is greater than the moment of inertia of the joists, I_j, but less than that obtained from a T-section (Figure 14) if full composite action between the joist and flooring is assumed. For this study, the effect of the composite action is accounted for in the elastic phase by assuming that the effective moment of inertia is equal to the moment of inertia of the joist times a coefficient that

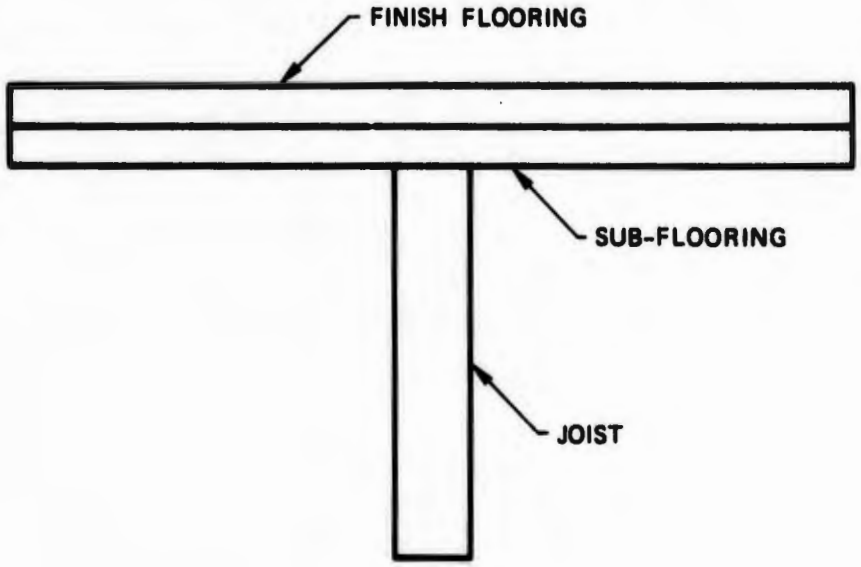

FIGURE 14 CROSS SECTION OF TYPICAL WOOD-JOIST FLOOR SYSTEM

is determined from the published test data on the response of wood-joist floors in the elastic range, or

$$I_e = c_f I_j \quad , \tag{56}$$

or, for a rectangular joist,

$$I_e = c_f \frac{bh_j^3}{12} \quad . \tag{57}$$

Substituting Eqs. 55 and 57 into Eq. 54, and rearranging terms, the maximum elastic resistance for a wood-joist floor system is

$$q_1 = \frac{4f_w c_f bh_j^2}{3sL^2} \quad . \tag{58}$$

The maximum deflection for the elastic phase is

$$y_1 = \frac{5q_1 sL^4}{32E_j c_f bh_j^3} \quad . \tag{59}$$

The problem, of course, is to determine the point in the response of the floor system where it is no longer linearly elastic; this is primarily a problem of determining a value for the extreme fiber stress, f_w, for use in Eq. 58 that reflects the upper limit of the elastic phase. Initially, in this study it was assumed that the elastic phase existed until the extreme fiber stress in compression reached the proportional limit, that is where $f_w = f_{wcp}$ in Eq. 58. However, comparisons of the analytical predictions with experimental data (Refs. 21 and 29) indicated that a better correlation could be obtained by estimating the failure strength of the weakest joist (first break), and using this value as the maximum elastic resistance of the floor system. In fact, test data in

Ref. 21 show this to be the case, at least for the lower grades of wood-joists.*

As a result of load sharing, the deflected shape of a floor system, which consists of a number of joists connected by flooring, is about the same throughout the floor when uniformly loaded (Refs. 28 and 30). The deflected shape of the weakest joist will approximate that of its stronger neighbors, even though it may have much less bending stiffness, and therefore carry less load. For any specific wood species, the strength of a joist in bending is influenced by a number of factors, such as size and location of knots, shakes and splits, moisture content, density, and slope of the grain (Refs. 16, 31, and 32). To determine the maximum elastic resistance, it was assumed that the bending strength of the weakest joist was limited by a defect resulting from the largest permissible knot† located at the bottom edge of the wide face in the middle third of the joist span as specified in the appropriate standard grading rules for the wood grade and species used (e.g., Refs. 32 and 33).

The maximum elastic resistance at first break is calculated by using Eq. 58, and substituting $f_w = f_r$ and $c_f = 1.0$, or

$$q_1 = \frac{4 f_r b h_j^2}{3 s L^2} \quad . \tag{58a}$$

The modulus of rupture, f_r, is that obtained from standard sources for small clear specimens (Ref. 34), and adjusted by the appropriate factors for knots, seasoning or moisture content, and size effect from Ref. 31.

---

*Limited data on the collapse of floors constructed of a higher grade Douglas fir in Refs. 18 through 20 also indicate that first break is a good measure of the maximum elastic resistance.

†As noted in Ref. 16, for design purposes the reduction in strength for various defects is not considered as cumulative. Because of the distribution of defects, this is also a reasonable assumption for the calculation of the floor resistance at first break.

Inelastic Phase

To develop the equation for the resistance function during the inelastic or plastic phase of the response of wood-joist floor systems, it was assumed that point 2 on Figure 13 represented the maximum theoretical resistance for a clear wood specimen. The resistance was assumed to vary linearly between the maximum elastic and inelastic resistances, and therefore, it was only necessary to determine the value of the maximum inelastic resistance.

Studies have shown that as the load on a wood beam is increased, a local failure first occurs in the compression zone, and is accompanied by a shifting of the neutral axis towards the tension side (e.g., Refs. 24, 25, and 35). For clear specimens without defects, the collapse of the beam results from a tensile fracture. Although several theories have been postulated to describe the stress distribution across a wood beam at failure, the second degree parabola as presented in Ref. 25, and shown on Figure 15, was adopted in this study.

In the development of the equation for the ultimate plastic moment at failure of a wood beam, the following assumptions were made in Ref. 25:

- Cross sections of the beam remain plane up to failure.
- The tensile stress-strain relationship is linear.
- The compressive stress-strain relationship is linear up to the proportional limit, and thereafter is approximated by a second degree parabola.
- The downward shift in the neutral axis at failure can be described by the relationship of the ultimate compressive and tensile stress distributions.

The ultimate internal resisting moment for a rectangular wood beam in pure bending can be formulated from the stress-strain relationship of wood in tension and compression and the general equations of static equilibrium across a section, where the sum of the normal stresses is equal to zero, or

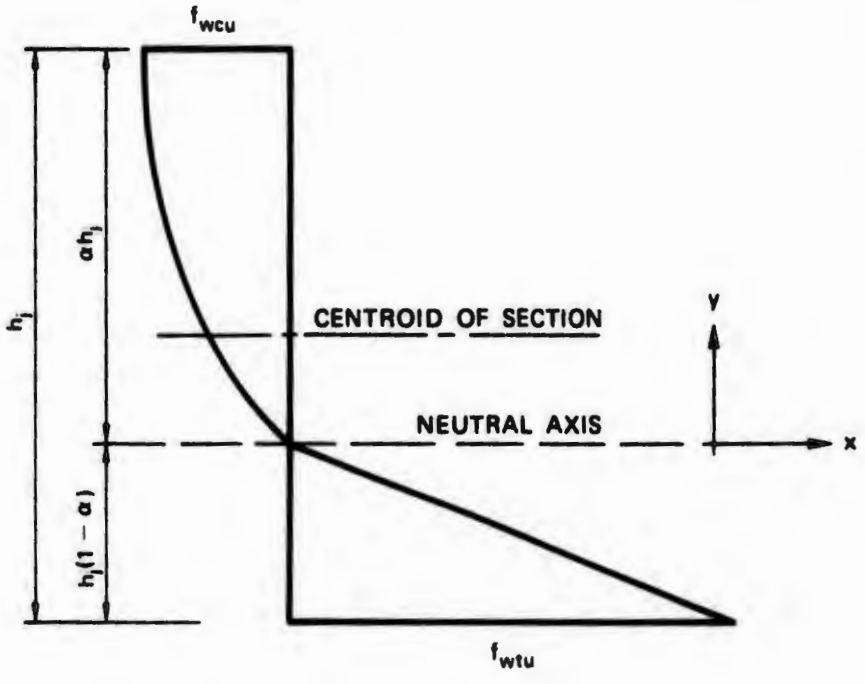

FIGURE 15 THEORETICAL STRESS DISTRIBUTION IN CLEAR WOOD BEAM SPECIMEN AT TENSILE FRACTURE

$$\int_A f_x \, dA = 0 \quad ,$$

and the moment of the normal stress about the neutral axis is equal to the bending moment M, or

$$\int_A f_x \, y \, dA = M \quad .$$

For the assumed case of a rectangular beam with the compression zone described by a second degree parabola and the tension zone by a straight line as shown in Figure 15, the equations of static equilibrium become

$$b \int_{-h_j(1-\alpha)}^{\alpha h_j} f_x \, dy = 0 \tag{60}$$

and

$$b \int_{-h_j(1-\alpha)}^{\alpha h_j} f_x \, dy = M \quad . \tag{61}$$

At the development of the ultimate bending resistance of the beam, the best fit to the test data for the distribution of the stress in the compressive zone, from Ref. 25, is a second degree parabola of the form

$$x = \frac{f_{weu}}{\alpha^2 h_j^2} y^2 - \frac{2 f_{weu}}{\alpha h_j} y \quad , \tag{62}$$

and the distribution of the tensile stress is a straight line of the form

$$x = -\frac{f_{wtu}}{h_j(1-\alpha)}\, y \quad . \tag{63}$$

Since, from Eq. 60, the sum of the areas of the tensile and compressive stresses across a section are equal to zero, then

$$F = b\int_0^{\alpha h_j}\left(\frac{f_{wcu}}{\alpha^2 h_j^2}\, y^2 - \frac{2f_{wcu}}{\alpha h_j}\, y\right) dy$$

$$+ b\int_{-h_j(1-\alpha)}^{0} -\frac{f_{wtu}}{h_j(1-\alpha)}\, y\, dy = 0 \quad ,$$

and by integrating and collecting terms,

$$\alpha = \frac{3f_{wtu}}{3f_{wtu} + 4f_{wcu}} \quad .$$

For $n = f_{wtu}/f_{wcu}$,

$$\alpha = \frac{3n}{3n + 4} \quad . \tag{64}$$

The ultimate internal resisting moment of the stress diagram in Figure 15 by Eq. 61 is

$$M_u = -b\int_0^{\alpha h_j}\left(\frac{f_{wcu}}{\alpha^2 h_j^2}\, y^2 - \frac{2f_{wcu}}{\alpha h_j}\, y\right) y\, dy$$

$$- b\int_{-h_j(1-\alpha)}^{0} -\frac{f_{wtu}}{h_j(1-\alpha)}\, y^2\, dy \quad ,$$

and by integrating and collecting terms

$$M_u = bh_j^2 \left[\frac{5}{12}\alpha^2 f_{wcu} + \frac{f_{wtu}}{3}(1 - \alpha)^2\right] \quad . \tag{65}$$

Since $f_{wtu} = nf_{wcu}$, and $\alpha = 3n/(3n + 4)$, then

$$M_u = \frac{nbh_j^2 f_{wcu}}{12(3n + 4)^2}(45n + 64) \quad . \tag{66}$$

To determine the ultimate resistance of a wood-joist floor system, it was assumed that the effect of the flooring on the resistance of the floor system was negligible at collapse of the joists. Therefore, the ultimate plastic resistance of a wood-joist floor system with joist spacing s is

$$q_u = \frac{8M_u}{sL^2} \quad . \tag{67}$$

By substituting Eq. 66 into Eq. 67, the ultimate resistance becomes

$$q_u = \frac{2nbh_j^2 f_{wcu}}{3sL^2(3n + 4)^2}(45n + 64) \quad . \tag{68}$$

The ultimate deflection, y_u, at the development of the ultimate bending resistance of a wood-joist floor is found from the usual equation for the deflection of a beam

$$y_u = \frac{5q_u sL^4}{384(EI)_{avg}} \quad . \tag{69}$$

However, since the quantity $(EI)_{avg}$ at large inelastic deflections of a wood beam is not equal to the flexural rigidity, $E_j I_j$, it is necessary to develop a rational basis for calculating $(EI)_{avg}$.

For a beam subjected to pure bending in the elastic region, the relationship between the radius of curvature, ρ, and the moment is

$$M = \frac{EI}{\rho} \quad ,$$

and in the inelastic region can be described (Ref. 36) as

$$M = \frac{(EI)'}{\rho} \quad . \tag{70}$$

It can also be determined that the radius of curvature

$$\rho = \frac{h_j(1 - \alpha)}{\epsilon} \quad , \tag{71}$$

and the strain

$$\epsilon = \frac{f_{wt}}{E} \quad . \tag{72}$$

By substituting Eqs. 71 and 72 into Eq. 70, and rearranging terms

$$(EI)' = \frac{h_j(1 - \alpha)EM}{f_{wt}} \quad .$$

At the development of the ultimate moment at the center section of a wood beam, $f_{wt} = f_{wtu} = nf_{wcu}$, $M = M_u$, and since $E = E_j$ then

$$(EI)' = \frac{bh_j^3E_j}{3(3n + 4)^3}(45n + 64) \quad . \tag{73}$$

For a simply supported wood beam at ultimate deflection, the quantity $(EI)'$ applies for the center section only, while the elastic E_jI_j applies at the supports. In this study, the quantity $(EI)_{avg}$ used to determine

the deflection at development of the ultimate resistance in a wood beam is assumed to be the average EI at the center and supports, or

$$(EI)_{avg} = \frac{E_j I_j + (EI)'}{2} \quad . \tag{74}$$

Since, for a rectangular section

$$I_j = \frac{bh_j^3}{12} \quad , \tag{75}$$

then by substituting Eqs. 73 and 75 into Eq. 74

$$(EI)_{avg} = \frac{bh_j^3 E_j}{24}\left[1 + \frac{4(45n + 64)}{(3n + 4)^3}\right] \quad . \tag{76}$$

The use of Eq. 69 to determine the deflection of a wood beam at the development of the ultimate plastic resistance of the beam tacitly assumes that the shape of the elastic curve for simply supported beams is valid up to collapse. This assumption is necessary, since none of the publications reviewed presented information on the deflected shape of wood beams at or near collapse. In any event, since Eq. 69 is used only to estimate the ultimate deflection and not to predict collapse (as noted in the next subsection), the difference in the assumed and actual deflected shapes is not felt to be of great importance.

Also, the above equations consider only the bending resistance of a wood-joist floor system, although a horizontal shear failure can limit or modify the resistance function. Studies of the effect of the span-to-depth ratio indicate that failure in horizontal shear is not likely to occur prior to a tensile failure in bending for the span-to-depth ratios usually found in actual wood-joist floor systems (Ref. 37). For example, the test results for full-scale floors in Refs. 17 through 20 show that all 12 of the floors tested failed in tension, or rupture, of the joists

(frequently influenced by knots), and only a few joists experienced a horizontal shear failure in addition to tension failure.

Failure Criterion

As mentioned in the introduction, wood-joist floor systems are constructed of joists with large differences in strength and stiffness characteristics, even when the joists are specifically selected for uniformity as test specimens. For example, compression and tensile strength values obtained from tests of a number of small, clear specimens of a single wood species exhibit a wide variation, and generally conform to a typical normal type of frequency distribution (e.g., Ref. 25). However, regardless of their individual stiffnesses, when joists are part of a floor system, test results indicate that the deflection of the joists are approximately the same under uniform load conditions (e.g., Refs. 21 and 30); the effect of load sharing is an effective reduction in the variability among individual joists. When tested as individual beams, many commercially available wood joists apparently fail as a result of a local defect while still within the elastic range (Ref. 14); therefore, load sharing also has the effect of increasing the strength of a floor system over that of the weakest joist. However, because of local defects and the variability of strength among joists, the ultimate strength of a floor system would represent some average value rather than approach either the strength of the weakest joist or the theoretical strength of clear specimens. That is, although the validity of Eq. 68 for predicting the ultimate static resistance has been experimentally verified for clear wood specimens, the ultimate resistance of clear specimens is not expected to represent the strength of wood-joist floors in actual buildings, especially for home construction where utility or standard grade lumber is generally used.

The development of a rational failure criterion for wood-joist floors is complicated by a number of factors, some of which are mentioned above. Also, because of the large number of variables involved in the response and collapse of a floor system, the available test data are insufficient to establish a statistical basis for developing a failure criterion. Instead, for this study it was necessary to rather arbitrarily establish a failure criterion without the benefit of adequate analytical or experimental information.

Therefore, to predict the collapse of wood-joist floor systems in the program for evaluation of existing structures, it was assumed that the resistance at collapse would occur between the maximum elastic and inelastic resistances (Points 1 and 2 in Figure 13, respectively). Since no rational method was available for calculating deterministically the maximum resistance developed in a floor system at collapse, the collapse resistance between Points 1 and 2 was described in the form of a probability distribution. An examination of the experimental data indicated that the maximum resistance developed by a floor system at failure would be closer to the maximum elastic resistance (Eq. 58a) than it would be to the ultimate plastic resistance (Eq. 68); this suggests that the probability distribution for the failure resistance would tend to be skewed towards the maximum elastic resistance. Although the β-distribution is well suited for describing a skewed distribution with finite end points (Ref. 38), only the normally distributed probability function was readily available for use in this study. Therefore, it was assumed that the probability of occurrence of the failure resistance for wood-joist floor systems was normally distributed between Points 1 and 2 on Figure 13, and the skewness was accounted for indirectly as follows.

The possibility is negligible that the maximum resistance at failure for an actual floor system would be greater than or equal to the theoretical ultimate plastic resistance for clear wood specimens as expressed

by Eq. 68; therefore, the probability that the maximum resistance would equal the ultimate resistance was set very high, say 0.999. On the other hand, the possibility that the maximum resistance of a floor would be less than the elastic resistance at the theoretical first break of the weakest joist, as expressed by Eq. 58a, would be relatively low; therefore, for this case, the probability of occurrence was set at 0.05 or 0.10. Furthermore, in the dynamic analysis of a specific floor system, values of the floor resistance above or below the limits selected were discarded. The truncated normal density function used for estimating the maximum resistance at failure of wood-joist floor systems is shown on Figure 16.

To determine the probability distribution for the incipient collapse overpressure for wood-joist floor systems, Monte Carlo, or simulation techniques as described in Ref. 4 for wall elements was used. Briefly, the technique uses a set of mathematically simulated floors, each of which possesses the characteristics of some real floor to determine an approximate distribution of the incipient collapse overpressure. The set of simulated floors is prepared by selecting the parameters to be varied, such as the maximum resistance at collapse, and determining the values of these parameters by randomly sampling their corresponding probability distribution functions. Each simulated floor is then analyzed dynamically using the randomly selected values and the deterministic equations developed previously. The results of the analyses of the set of floors provide a probability distribution of the incipient collapse overpressure.

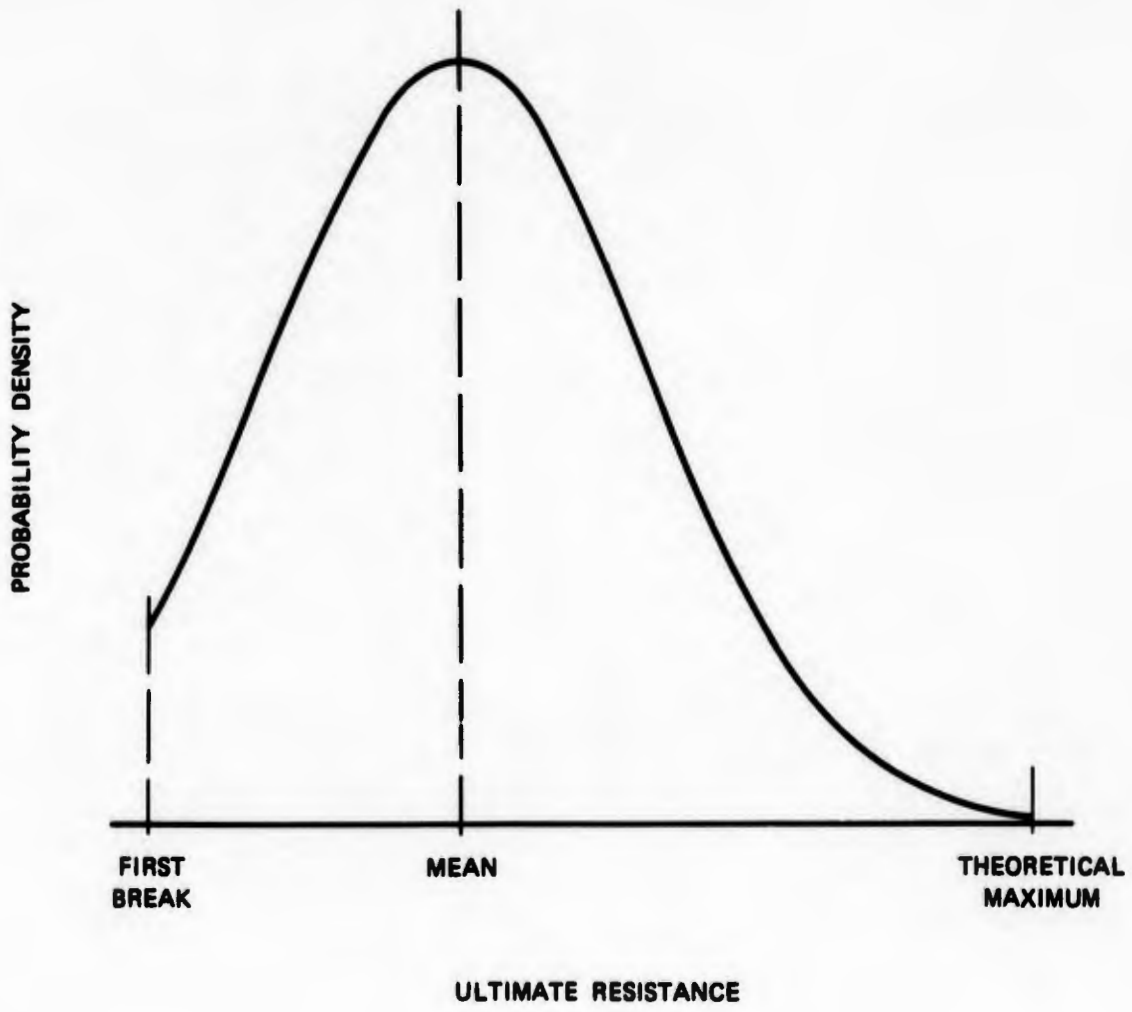

FIGURE 16 TRUNCATED NORMAL DENSITY FUNCTION FOR ESTIMATING THE ULTIMATE RESISTANCE AT FAILURE OF WOOD-JOIST FLOORS

IV DYNAMIC ANALYSIS OF NORTH CAROLINA NATIONAL BANK BUILDING

Introduction

As noted in Section I, a continuing concern in evaluating the collapse overpressure of existing buildings has been the relative blast strength of the exterior walls and frames of multistory buildings. To predict the collapse overpressure of the exterior walls for the existing NFSS buildings analyzed in this program (Refs. 5 and 6), it was assumed that the structural frame did not collapse at a lower overpressure than that predicted for the exterior wall. For weak-walled buildings, such an assumption is reasonable. In fact, it is often assumed for the analysis of blast-loaded frame buildings that the exterior walls can be considered as frangible, and therefore, that the wall loading transferred to the frame can be approximated by an impulse loading. However, for many of the actual buildings analyzed, the strength of the exterior walls under blast loading was sufficiently high to make it doubtful that the frame could survive at the overpressure level required to collapse the walls. For example, at the present time SRI has analyzed a total of 137 exterior wall cases for 59 NFSS buildings. As shown on Figure 17, the predicted incipient collapse overpressure for these walls ranged from less than 1 psi to over 40 psi, with 50 percent of the walls predicted to collapse at an incident overpressure level greater than 6 psi. The strength of the exterior walls is important in calculating the collapse of the frame, since for a given overpressure level, the blast loading on the total area of a nonfailing wall can be much more severe than the blast loading on the frame alone plus an impulse loading from a frangible-type wall.

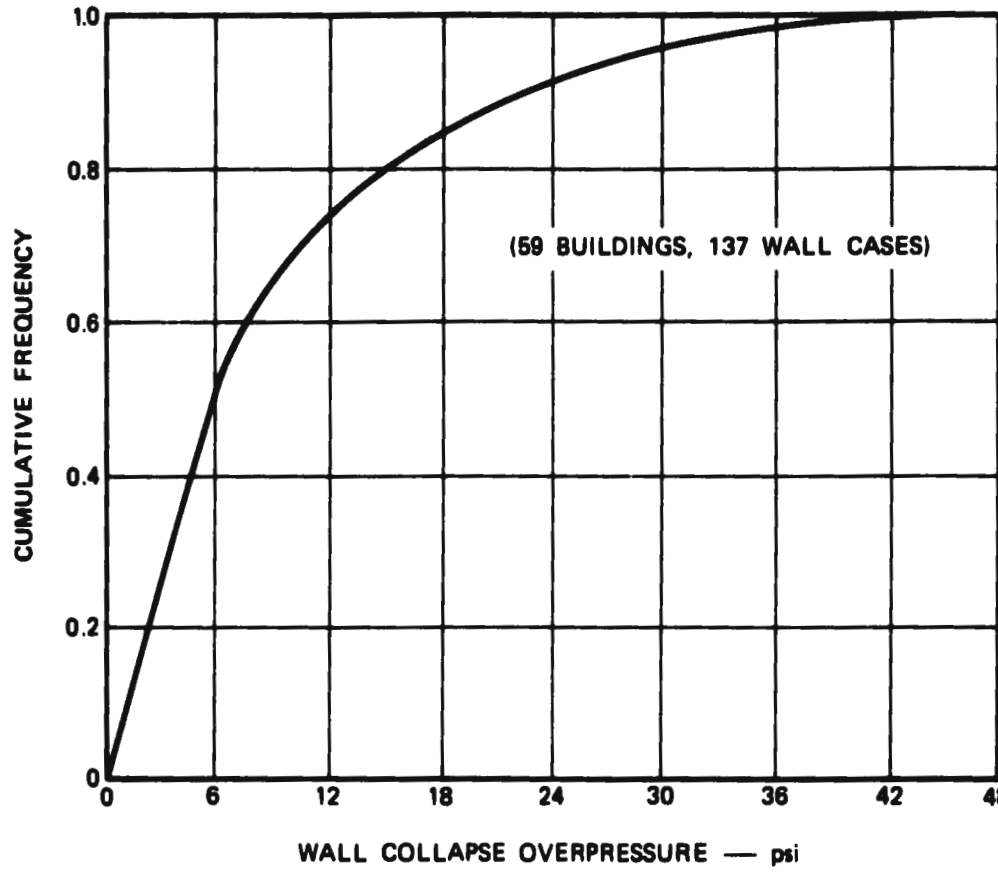

FIGURE 17 CUMULATIVE FREQUENCY DISTRIBUTION OF THE MEAN VALUES OF THE COLLAPSE OVERPRESSURES FOR THE EXTERIOR WALLS OF 59 BUILDINGS

To investigate the relative strength of the exterior walls and frame of a building would require a comprehensive computer program that included inelastic response of the frame under dynamic loading and realistic frame collapse mechanisms. Since such a program was not available for this study, an existing computer program for analyzing the elastic and inelastic dynamic response of two-dimensional structural frames (Ref. 8) was used to analyze the frame of the North Carolina National Bank Building. This building was selected for study since a previous analysis of the exterior walls (Ref. 6) had indicated that it was a strong-walled building.

Building Description

The North Carolina National Bank, constructed in 1922, is located on South Main Street, High Point, North Carolina. The building consists of eight stories and an unexposed basement; there is a mezzanine between the first and second stories. The overall height of the building is about 110 ft and plan dimensions of 50 ft by 115 ft provide an area of 5,750 sq ft on each floor level. Figure 18 shows the exterior walls and general window layout of the bank. Note that many of the windows on the first story of sides B and C have been bricked in.

The building has a structural steel frame with riveted and bolted column and beam connections. The ribbed floor system has a 4-in. thick concrete slab and 4- or 6-in. thick clay tile fillers.

The exterior walls on sides A and B of the first story are 17-in. thick and are constructed with a granite veneer and a brick backing. On sides C and D of the first story, the walls are generally 17-in. thick solid brick. On the upper stories, the walls are constructed with a 4-in. thick brick veneer and an 8-in. thick terra cotta backing. As can be noted in Figure 18, the exterior column lines on the upper stories of sides A and B are faced with a granite veneer. For all exterior walls, the facing is continuous over the frame members and the backing is inset

SIDES A AND B

SIDES B AND C

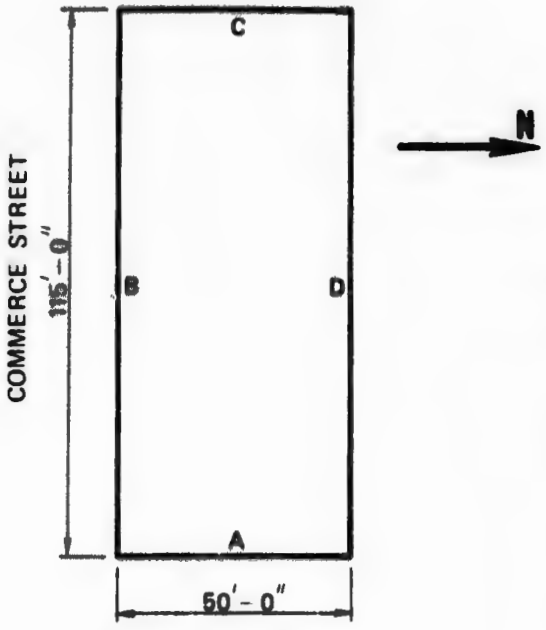

PLAN VIEW

SIDE D

SOURCE: RTI.

FIGURE 18 PHOTOGRAPHS AND PLOT PLAN OF NORTH CAROLINA NATIONAL BANK

in the frame. The interior partitions on the first story and mezzanine are constructed with unreinforced terra cotta, either 3- or 6-in. thick. On the upper stories the interior partitions are mostly 3-in. unreinforced terra cotta. The partitions are nonload bearing and have numerous openings that have been filled-in with light wood paneling.

Wall Analysis

The exterior walls on all sides were analyzed as unreinforced masonry unit walls with either one- or two-way arching. For Side A of the first story it was assumed that, because of the many openings, only one-way arching could develop between floor beams on the first and mezzanine stories. On Side B it was assumed that one-way arching would develop in the walls between windows. Furthermore, it was assumed that the bricked-in windows would not contribute to the arching strength of the walls but would remain in place for a sufficient length of time to influence the blast loading and room filling.

The specific walls analyzed were as follows:

- VP1: Side A, wall on first story; one-way arching wall.
- VP2: Side B, wall on first story; one-way arching wall.
- VP3: All sides, walls on upper stories; two-way arching wall.

The results of the dynamic analysis of the exterior walls of the Bank were:

	Predicted Collapse Overpressure, psi			
Case	Mean	Standard Deviation	10 Percent Probability Value	90 Percent Probability Value
VP1	16.4	4.2	11.0	21.8
VP2	5.4	0.7	4.6	6.3
VP3	15.7	4.0	10.5	20.8

Since the analysis indicated that the incipient collapse overpressure of the upper story walls was 15.7 psi, the building was considered as a strong-walled building, and was therefore a good candidate for examining the dynamic response of the structural frame.

Frame Analysis

Discussion

The blast loading on the building was calculated for a box-type building with openings (Type 2, Ref. 8), and the collapse overpressure of the exterior walls was assumed to be greater than that of the frame; i.e., to determine the frame loading, the exterior walls were assumed as nonfailing. The blast wave was assumed to strike the building at normal incidence to Side B, the Commerce Street side. The computer program determines the air blast loading on the basis of a specified peak incident overpressure level between 2 and 30 psi for a 10-Mt-yield nuclear weapon. Although the exterior walls had been analyzed for an air blast loading from a 1-Mt-yield weapon, there would be negligible difference in the predicted collapse overpressure of the walls for a 10-Mt yield.

Three different types of frame analyses were performed. The first was an elastic analysis to determine the magnitude of the base shear as a function of the blast overpressure level. For this analysis, the inset exterior walls on end frame lines A and H in Figure 19 were assumed to act as shear walls.

The second and third types of frame analyses were performed to determine the elastic and inelastic response, respectively, of the frame acting alone; for these analyses the effect of the shear wall action of the exterior walls on the frame response was assumed to be negligible. Such

an analysis should approximate the behavior of the building after failure of the shear walls (i.e., inset exterior end walls).

The elastic frame analysis was conducted at various incident overpressure levels and provided information on the possible collapse strength of the frame. Also, the elastic analysis assisted in the selection of the overpressure levels for running the more complex inelastic frame program.

The following input data, required for the various analyses, were obtained directly from the architectural and structural plans:

- Percentage of openings (front face)
- Clearing distance (front face)
- Floor weight
- Beam and column properties
  - Moment of inertia
  - Cross-sectional area
  - Plastic moment capacity
- Shear wall properties
  - Moment of inertia
  - Cross-sectional area
  - Plastic moment capacity
  - Shear area
  - Shear capacity

Figure 19 shows a simplified framing plan and Figure 20 shows the beam and column sizes for frame line A.

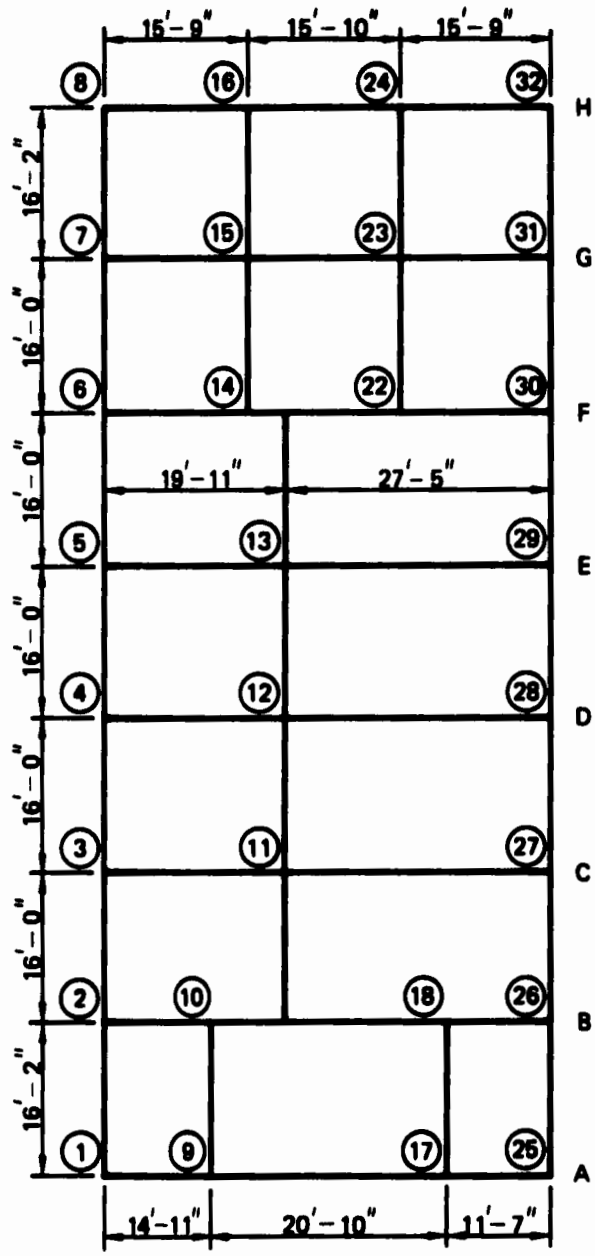

FIGURE 19 TYPICAL FRAMING PLAN (SIMPLIFIED)

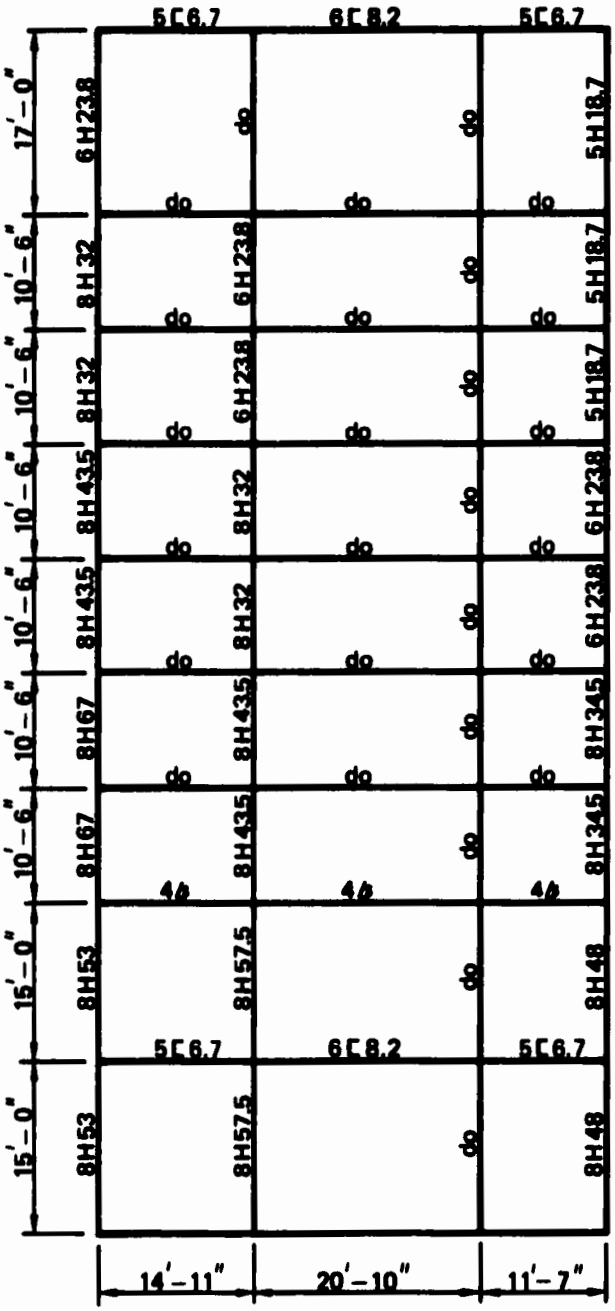

FIGURE 20 BEAM AND COLUMN SIZES FOR FRAME LINE A

Results

The results of the following frame analyses are summarized in Tables 1 and 2:

- Elastic shear wall, 2 psi overpressure
- Elastic frame
  - 16 psi overpressure
  - 5 psi overpressure
  - 4 psi overpressure
  - 3 psi overpressure
- Inelastic frame
  - 5 psi overpressure
  - 4 psi overpressure
  - 3 psi overpressure

The maximum stress ratio for the beams and columns, shown in Table 1, is the ratio of computed moment/yield moment and for the shear walls is the computed shear/ultimate shear capacity. The ductility ratio listed in Table 2 is the maximum rotation/yield rotation for the member. It should be noted, so as to avoid a condition of singularity in the plastic matrix for the inelastic frame program, in Ref. 8, "...it is assumed that each member in the structure is composed of two parallel elements--one remains linearly elastic under all loading conditions and one remains ideally elastoplastic.... For the computer program presented in this report it is assumed that linearly elastic elements represent five percent of the initial stiffness of the structure. Also, this makes it possible to account for some of the 'strain hardening' effects which are neglected in the normal ideally plastic idealization."

The results of the first analysis, for the shear wall building, indicated that the cracking of the exterior walls on the ends of the building acting as shear walls occurred at an incident overpressure of less than

Table 1

SUMMARY OF RESULTS OF ELASTIC FRAME ANALYSIS

Frame Line	Maximum Stress Ratio: Beam Moment	Maximum Stress Ratio: Column Moment	Maximum Stress Ratio: Shear Wall Shear	Axial Force (kips)
Elastic, Shear Wall, 2 psi	(Maximum Deflection = 2.2 in.)			
A	-	37.5	1.35	0
	<1	<1		2.9
CDE	<1	<1		6.2
F	<1	<1		9.0
G	<1	<1		5.3
H	-	35.9	2.55	0
Elastic, Frame, 16 psi	(y_{max} = 670.2 in.)			
A	45.5	23.9		584.4
B	50.8	20.5		886.9
CDE	31.5	20.2		846.8
F	45.6	20.2		1396.6
G	45.6	18.6		968.9
H	35.6	21.7		375.6
Elastic, Frame, 5 psi	(y_{max} = 135.5 in.)			
A	9.8	4.7		120.4
B	11.1	4.0		181.3
CDE	6.7	3.7		178.9
F	9.8	3.7		292.7
G	9.7	3.7		211.2
H	7.8	4.3		77.2
Elastic, Frame, 4 psi	(y_{max} = 98.8 in.)			
A	7.2	3.5		87.7
B	8.1	3.0		131.9
CDE	4.9	3.1		130.8
F	7.1	3.1		213.9
G	7.1	2.7		155.1
H	5.6	3.2		56.3
Elastic, Frame, 3 psi	(y_{max} = 65.4 in.)			
A	4.4	2.3		57.7
B	5.3	1.6		86.7
CDE	3.2	2.1		86.4
F	4.6	2.1		141.3
G	4.6	1.9		102.8
H	3.7	2.2		37.2

Table 2

SUMMARY OF RESULTS OF INELASTIC FRAME ANALYSIS

Story Level	Moment Ratio		Ductility Ratio		Axial Force (kips)
	Beam	Column	Beam	Column	
Inelastic, Frame 5 psi	(Maximum Deflection = 677.6 in.)				
Roof	1.91	2.01	27.0	29.4	3.7
8	2.51	1.08	29.4	3.0	8.9
7	2.51	1.37	30.9	10.7	14.1
6	2.69	1.19	35.2	6.1	19.7
5	2.72	1.35	35.0	8.5	25.3
4	2.63	1.58	32.6	18.2	30.7
3	2.31	2.19	26.4	55.7	35.5
2	0.12	1.26	<1	5.5	100.6
Mezz.	-	1.23	-	7.1	100.6
Inelastic, Frame 4 psi	(Maximum Deflection = 563.7 in.)				
Roof	1.81	1.91	23.2	26.7	3.5
8	2.25	0.95	25.7	<1	8.2
7	2.31	1.32	26.7	9.0	13.0
6	2.43	1.03	29.5	1.7	18.1
5	2.45	1.28	29.3	8.4	23.2
4	2.31	1.50	26.4	15.9	28.1
3	2.03	2.09	21.1	42.2	32.4
2	0.09	1.09	<1	3.0	72.6
Mezz.	-	1.17	-	3.1	72.6
Inelastic, Frame 3 psi	(Maximum Deflection = 249.0 in.)				
Roof	1.30	1.31	8.4	10.1	2.6
8	1.54	0.98	11.8	<1	6.0
7	1.60	1.12	12.6	2.6	9.6
6	1.62	0.94	13.4	<1	13.2
5	1.64	1.15	13.2	4.1	16.8
4	1.55	1.16	11.5	5.8	20.3
3	1.45	1.62	9.4	20.6	23.5
2	0.07	1.01	<1	1.1	59.3
Mezz.	-	1.03	-	1.9	59.3

2 psi, since the moment ratios for the shear walls are above 35 for the 2-psi-overpressure level. Therefore, it was assumed for the frame analyses that the inset end walls contributed negligible resistance to the building, and that the analysis of the frame acting alone should adequately model the building behavior under lateral load.*

An elastic analysis of the frame for 16 psi, which approximates the incipient collapse overpressure of the exterior walls, indicated a maximum stress ratio of about 24 for the columns and 51 for the beams. Since the elastic analysis was much simpler than the inelastic analysis, the frames were then analyzed for elastic behavior at 5-, 4-, and 3-psi overpressures to obtain an estimate of the frame strength. The results of the elastic analyses, summarized in Table 1, indicate that the strength of the frames was probably in the range of the lower overpressures examined, and therefore the inelastic frame analyses were run at 5-, 4-, and 3-psi incident overpressure levels.

The inelastic analyses, summarized in Table 2, indicated maximum ductility ratios at 3 psi of 13.4 for the beams and 20.6 for the columns, and maximum moment ratios of about 1.6 for the beams and columns. At the 4-psi level, the maximum ductility ratios were 29.5 in the beams and 42.2 in the columns, and the maximum moment ratios were in excess of 2. A simplified hand calculation indicated that the P-Δ effect, which is not included in the computer program, would increase some of the moment

---

*Ref. 39, which was a study of the effect of masonry filler walls on frame response, indicated that inset walls do have a significant effect on the frame resistance, even after cracking of the walls. The available frame program (Ref. 8) used could not model the effect of a cracked inset wall on the frame resistance without considerable modification. However, since the moment ratios were quite high for the 2-psi overpressure level, and since only two of eight frame lines had inset walls, it was felt that neglecting the inset walls did not significantly affect the estimate of frame collapse.

ratios by over 50 percent. As noted on Figure 21, the calculated lateral deflection of the top story, for the inelastic frame analysis, was about 21 ft for the 3-psi overpressure level, and 47 ft for the 4-psi level.

Summary

The results of the analyses provide an estimate of the collapse strength of the structural steel frame of the bank building under blast loading, even though the computer program used cannot predict frame collapse. If it is assumed that the frame would collapse at a ductility ratio of about 50,* then the estimated collapse overpressure is between 3- and 4-psi incident overpressure level. The actual blast strength could be much less, since the effect of the axial column load (P-Δ effect) and frame collapse mechanisms, such as column buckling and instability, are not accounted for in the computer program.

It should be mentioned that the frame of the North Carolina National Bank building appears to be constructed of relatively light structural shapes that may not necessarily be typical of most NFSS structures. In any event, however, the analysis indicated that the blast resistance of the frame of the building was much less than (possibly only one-fourth) that of the exterior walls. This, of course, is an important consideration in predicting either the magnitude of building damage or the number of casualties that might occur in buildings subjected to nuclear air blast.

---

*The selection of a ductility ratio of 50 as indicating a possible frame collapse is arbitrary, but is felt to be conservative for estimating a frame collapse from the results of an inelastic analysis. Other investigators, e.g., Ref. 40, have used a frame ductility ratio of 20 to indicate collapse. However, the actual ductility ratio used to estimate collapse is not too important, since, as noted on Table 2, for an increase in incident overpressure level from 3 to 4 psi increases the maximum column ductility ratio at story level three from 20.6 to 42.2.

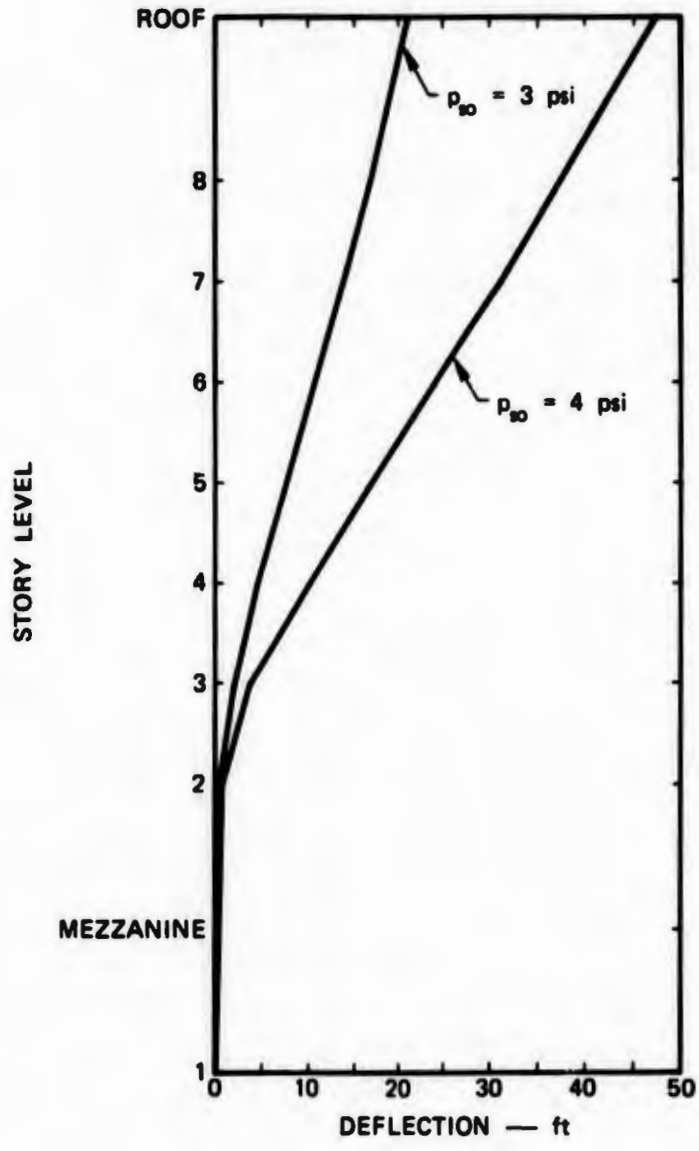

FIGURE 21 DEFLECTION OF FRAME FOR INELASTIC ANALYSIS AT 3 AND 4 PSI BLAST OVERPRESSURE LEVELS

Appendix A

CORRELATION OF ANALYTICAL AND EXPERIMENTAL RESULTS FOR LONGITUDINALLY RESTRAINED REINFORCED CONCRETE SLABS

Appendix A

CORRELATION OF ANALYTICAL AND EXPERIMENTAL RESULTS FOR LONGITUDINALLY RESTRAINED REINFORCED CONCRETE SLABS

Introduction

This appendix compares the analytical predictions obtained using the theoretical procedures developed in the main body of the report to experimental results from several tests of reinforced concrete slabs with longitudinally restrained edges. The experimental results are primarily for statically loaded slabs, although results for a few dynamically loaded slabs are included. All slabs were uniformly loaded.

Results from the following tests are included in the comparison.

- NCEL (Ref. 10)--Static and dynamic tests of 72-in. square slabs, 3-in. to 6-in. thick (L_s/h_s = 12 to 24), are reinforcement ratios from 0 to 1.33 percent.
- WES (Ref. 11)--Static and dynamic tests of 29-in. square slabs, 0.89-in. thick (L_s/h_s = 32.6), and reinforcement ratios from 0.55 to 1.02 percent.
- MIT (Ref. 12)--Static tests of 15-in. square slabs, 0.75-in. to 1.50-in. thick (L_s/h_s = 10 to 20), and reinforcement ratios from 0 to 2.0 percent.
- Wood (From Ref. 10)--Static tests of 68-in. square slabs, 2.25-in. thick (L_s/h_s = 30.2), and reinforcement ratios from 0 to 0.26 percent.
- Park (Ref. 9)--Static tests of 40-in. by 60-in. slabs (L_l/L_s = 1.50), 0.98-in. to 2.0-in. thick (L_s/h_s = 20.0 to 40.8), and reinforcement ratios from 0 to 1.21 percent. Edge restraints include: (1) all edges fully restrained; (2) one short edge simply supported on rollers, with remaining edges fully restrained; and (3) one long edge simply supported on rollers, with remaining edges fully restrained.

- Powell (From Ref. 9)--Static tests of 20.57-in. by 36.0-in. slabs (L_L/L_s = 1.75), 1.286-in. thick, (L_s/h_s = 16.0), and reinforcement ratios from 0 to 1.53 percent.

The results of these comparisons are presented in the following subsections.

Statically Loaded Slabs

The theoretical resistance functions outlined in a previous section are compared to results obtained from static load tests on longitudinally restrained reinforced concrete slabs. These comparisons are divided into two groups: (1) slabs with all edges fully restrained, and (2) slabs with one edge simply supported and the remaining edges fully restrained.

Slabs with All Edges Fully Restrained

Dimensions, reinforcement data, and concrete and steel strengths for the slabs with all edges fully restrained are summarized in Table A-1. Predicted resistance and deflection values for the stages of behavior shown in Figure 1 in Section II are compared with the test values in Table A-2. Average values of predicted-to-test results are given for each group of test slabs, as well as for the total number of slabs. In general, the predicted results compare favorably with the test results.

The ultimate flexural resistance computed from Eq. 42 is on the average 13 percent higher than the test results. The greatest disparity occurs for the slabs tested by Wood (Ref. 10), Park (Ref. 9), and Powell (Ref. 9). One reason for this may be that the concrete strength for these slabs is based on the cube strength, with the corresponding cylinder strength, f'_c assumed to be 80 percent of the cube strength. This percentage may be on the high side. The predicted ultimate flexural resistance is also seen to be better for the square slabs than for the

Table A-1

DETAILS FOR SLABS WITH ALL EDGES FULLY RESTRAINED

Slab Number	Slab Dimensions L_x (in.)	L_y (in.)	h_s (in.)	L_x/h_s	Strength f'_c (psi)	f_y (ksi)	Reinforcement Properties: Section 1 p (%)	d (in.)	p′ (%)	d′ (in.)	Section 2 p (%)	d (in.)	p′ (%)	d′ (in.)	Section 3 p (%)	d (in.)	p′ (%)	d′ (in.)	Section 4 p (%)	d (in.)	p′ (%)	d′ (in.)
WEL																						
3S1	72	72	3.00	24.0	3550	49.6	0.815	2.25	0.815	0.75	0.815	2.25	0.815	0.75	0.815	2.25	0.815	0.75	0.815	2.25	0.815	0.75
3S2	72	72	3.00	24.0	4140	-	NO REINFORCEMENT															
3S3	72	72	3.00	24.0	4120	49.6	0.815	2.25	0.815	0.75	0.815	2.25	0.815	0.75	0.815	2.25	0.815	0.75	0.815	2.25	0.815	0.75
3S4	72	72	3.00	24.0	3295	49.6	0.815	2.25	0.0	-	0.815	2.25	0.0	-	0.815	2.25	0.0	-	0.815	2.25	0.0	-
4.75S1	72	72	4.75	15.2	3165	47.4	0.889	3.75	0.889	1.00	0.889	3.75	0.889	1.00	0.889	3.75	0.889	1.00	0.889	3.75	0.889	1.00
6S1	72	72	6.00	12.0	3615	47.4	1.33	5.00	1.33	1.00	1.33	5.00	1.33	1.00	1.33	5.00	1.33	1.00	1.33	5.00	1.33	1.00
WES																						
IS1																						
IS2	29	29	0.89	32.6	3683	43.6	0.662	0.795	0.0	-	0.817	0.715	0.0	-	0.331	0.795	0.331	0.095	0.408	0.715	0.408	0.175 †
IS3							0.550	0.795	0.0	-	0.611	0.715	0.0	-	0.236	0.795	0.236	0.095	0.305	0.715	0.305	0.175
IIS1	29	29	0.89	32.6	3810	43.6	1.02	0.795	0.0	-	1.27	0.715	0.0	-	0.509	0.795	0.509	0.095	0.634	0.715	0.634	0.175 †
							0.663	0.795	0.0	-	0.922	0.715	0.0	-	0.331	0.795	0.331	0.795	0.460	0.715	0.460	0.175
MIT																						
42	15	15	0.75	20.0	5057	-	NO REINFORCEMENT															
44	15	15	0.75	20.0	4321	-	NO REINFORCEMENT															
45	15	15	1.50	10.0	4273	-	NO REINFORCEMENT															
46	15	15	0.75	20.0	5491	60.0	1.0	0.56	0.0	-	1.0	0.56	0.0	-	1.0	0.19	0.0	-	1.0	0.19	0.0	-
47	15	15	1.50	10.0	4565	55.0	1.0	1.22	0.0	-	1.0	1.22	0.0	-	1.0	0.28	0.0	-	1.0	0.28	0.0	-
48	15	15	0.75	20.0	4870	60.0	2.0	0.56	0.0	-	2.0	0.56	0.0	-	2.0	0.19	0.0	-	2.0	0.19	0.0	-
49	15	15	1.50	10.0	4619	55.0	2.0	1.22	0.0	-	2.0	1.22	0.0	-	2.0	0.28	0.0	-	2.0	0.28	0.0	-
WOOD																						
FS12	68	68	2.25	30.2	4720	33.8	0.26	1.81	0.0	-	0.26	1.81	0.0	-	0.26	0.44	0.0	-	0.26	0.44	0.0	-
FS13	68	68	2.25	30.2	3840	33.8	0.26	1.81	0.0	-	0.26	1.81	0.0	-	0.26	0.44	0.0	-	0.26	0.44	0.0	-
FS14	68	68	2.25	30.2	4144	-	NO REINFORCEMENT															

Table A-1 (Concluded)

Slab Number	Slab Dimensions L_2 (in.)	L_1 (in.)	h_s (in.)	L_2/h_s	Strength f'_c* (psi)	f_y (ksi)	Reinforcement Properties Section 1 p (%)	d (in.)	p′ (%)	d′ (in.)	Section 2 p (%)	d (in.)	p′ (%)	d′ (in.)	Section 3 p (%)	d (in.)	p′ (%)	d′ (in.)	Section 4 p (%)	d (in.)	p′ (%)	d′ (in.)
PARK																						
A1	40	60	2.00	20.0	4776	50.0	0.19	1.69	0.0	-	0.20	1.56	0.0	-	0.38	1.69	0.19	0.31	0.41	1.56	0.20	0.44
A2	40	60	2.00	20.0	4280	50.0	0.42	1.66	0.0	-	0.21	1.50	0.0	-	0.84	1.66	0.42	0.34	0.43	1.50	0.21	0.50
A3	40	60	2.00	20.0	5000	50.0	0.72	1.63	0.0	-	0.22	1.44	0.0	-	1.44	1.63	0.72	0.37	0.45	1.44	0.22	0.56
A4	40	60	2.00	20.0	4016	50.0	1.21	1.59	0.0	-	0.23	1.37	0.0	-	2.42	1.59	1.21	0.41	0.47	1.37	0.23	0.63
D1	40	60	2.00	20.0	5024	-	NO REINFORCEMENT															
D2	40	60	1.50	26.7	4960	-	NO REINFORCEMENT															
D3	40	60	0.98	40.8	5144	-	NO REINFORCEMENT															
D4	40	60	1.01	39.6	4440	-	NO REINFORCEMENT															
D5	40	60	0.99	40.4	3552	-	NO REINFORCEMENT															
POWELL																						
S46	20.57	36	1.286	16.0	5808	30.6	0.25	1.029	0.25	0.257	0.25	1.029	0.25	0.257	0.25	1.029	0.25	0.257	0.25	1.029	0.25	0.257
S47	20.57	36	1.286	16.0	6504	30.6	0.25	1.029	0.25	0.257	0.25	1.029	0.25	0.257	0.25	1.029	0.25	0.257	0.25	1.029	0.25	0.257
S48	20.57	36	1.286	16.0	5952	-	NO REINFORCEMENT															
S50	20.57	36	1.286	16.0	5400	30.6	0.45	1.029	0.45	0.257	0.45	1.209	0.45	0.257	0.45	1.029	0.45	0.257	0.45	1.029	0.45	0.257
S53	20.57	36	1.286	16.0	5448	-	NO REINFORCEMENT															
S54	20.57	36	1.286	16.0	5944	30.6	0.71	1.029	0.71	0.257	0.71	1.029	0.71	0.257	0.71	1.029	0.71	0.257	0.71	1.029	0.71	0.257
S55	20.57	36	1.286	16.0	5344	30.6	0.71	1.029	0.71	0.257	0.71	1.029	0.71	0.257	0.71	1.029	0.71	0.257	0.71	1.029	0.71	0.257
S56	20.57	36	1.286	16.0	5540	-	NO REINFORCEMENT															
S57	20.57	36	1.286	16.0	5744	-	NO REINFORCEMENT															
S58	20.57	36	1.286	16.0	5800	37.0	0.97	1.029	0.97	0.257	0.97	1.029	0.97	0.257	0.97	1.029	0.97	0.257	0.97	1.029	0.97	0.257
S59	20.57	36	1.286	16.0	5696	37.0	0.97	1.029	0.97	0.257	0.97	1.029	0.97	0.257	0.97	1.029	0.97	0.257	0.97	1.029	0.97	0.257
S60	20.57	36	1.286	16.0	5752	-	NO REINFORCEMENT															
S62	20.57	36	1.286	16.0	5962	37.0	1.53	1.029	1.53	0.257	1.53	1.029	1.53	0.257	1.53	1.029	1.53	0.257	1.53	1.029	1.53	0.257
S63	20.57	36	1.286	16.0	5272	37.0	1.53	1.029	1.53	0.257	1.53	1.029	1.53	0.257	1.53	1.029	1.53	0.257	1.53	1.029	1.53	0.257
S64	20.57	36	1.286	16.0	5760	-	NO REINFORCEMENT															

* f'_c (cylinder strength) for Wood, Park and Powell slabs based on 80% of cube strength.

† The upper values represent the slab middle strip reinforcement and the lower values the edge strip reinforcement.

Table A-2

THEORETICAL VERSUS TEST RESULTS FOR SLABS WITH ALL EDGES FULLY RESTRAINED

Slab Number	q_y (psi)			y_a (in.)			q_a (psi)			y_a (in.)			q_{ℓ_1} (psi)			y_{ℓ_1} (in.)			q_{ℓ_1}/y_{ℓ_1} (lb/in.^{3})		
	Theory	Test	Theory / Test	Theory	Test	Theory / Test	Theory	Test	Theory / Test	Theory	Test	Theory / Test	Theory	Test	Theory / Test	Theory	Test	Theory / Test	Theory	Test	Theory / Test
NCEL																					
3S1	31.9	32.2	0.99	1.26	1.52	0.83	19.6	20.1	0.98	2.75	3.75	0.73	76.8	43.0	1.76	10.8	5.5	1.96	7.11	7.82	0.91
3S2	22.3	23.5	0.95	1.26	1.00	1.26	-	-	-	-	-	-	-	-	-	-	-	-	-	-	-
3S3	34.4	34.6	0.99	1.26	1.36	0.93	20.3	16.6	1.22	2.85	3.25	0.88	76.8	42.5	1.81	10.8	8.5	1.27	7.11	8.00	0.89
3S4	27.5	32.1	0.86	1.26	1.35	0.93	17.5	21.0	0.83	3.78	4.00	0.95	38.5	30.5	1.26	10.8	8.0	1.35	3.56	3.81	0.93
4.75S1	93.0	85	1.09	1.24	0.92	1.35	52.2	50	1.04	3.72	3.60	1.03	133.9	74.0	1.81	10.8	6.9	1.57	12.4	10.7	1.16
6S1	221.0	182	1.21	0.92	1.10	0.84	129.8	143.0	0.91	2.77	-	-	266.4	-	-	10.8	-	-	-	-	-
Average			(1.02)			(1.02)			(1.00)			(0.90)			(1.66)			(1.54)			(0.97)
WES																					
'S1	14.9	13.1	1.14	0.37	0.63	0.59	6.7	5.1	1.31	1.12	1.60	0.70	22.1	20.3	1.09	4.35	4.47	0.97	5.08	4.54	1.12
IS2	14.9	15.5	0.96	0.37	0.45	0.82	6.7	7.8	0.86	1.12	1.50	0.75	22.1	22.4	0.99	4.35	4.10	1.06	5.08	5.46	0.93
IS3	14.9	13.8	1.08	0.37	0.60	0.62	6.7	8.8	0.76	1.12	1.55	0.72	22.1	27.0	0.82	4.35	4.60	0.95	5.08	5.87	0.86
IIS1	17.4	18.2	0.96	0.37	0.30	1.23	9.9	11.7	0.85	1.12	0.95	1.18	33.3	36.5	0.91	4.35	4.10	1.06	7.66	8.90	0.86
Average			(1.03)			(0.81)			(0.95)			(0.84)			(0.95)			(1.01)			(0.94)
MIT																					
42	37.9	35.6	1.06	0.315	0.366	0.86	-	-	-	-	-	-	-	-	-	-	-	-	-	-	-
44	33.3	25.9	1.29	0.315	0.272	1.16	-	-	-	-	-	-	-	-	-	-	-	-	-	-	-
45	185.0	144.0	1.28	0.156	0.167	0.93	-	-	-	-	-	-	-	-	-	-	-	-	-	-	-
46	48.6	59.5	0.82	0.315	0.325	0.97	24.1	20.0	1.20	0.79	0.88	0.90	68.4	60	1.14	2.25	2.50	0.90	30.4	24.0	1.27
47	226.0	209.0	1.08	0.155	0.160	0.97	93.7	93	1.01	0.47	1.40	0.34	136.6	120	1.14	2.25	2.40	0.94	60.7	50.0	1.21
48	50.0	55.0	0.91	0.315	0.425	0.74	40.3	38.5	1.05	0.66	0.90	0.73	136.9	98	1.40	2.25	2.20	1.02	60.8	44.5	1.37
49	234.4	220.0	1.07	0.155	0.155	1.00	162.6	128	1.27	0.47	0.95	0.49	273.3	204	1.34	2.25	2.20	1.02	121.5	92.7	1.31
Average			(1.07)			(0.95)			(1.13)			(0.62)			(1.25)			(0.97)			(1.29)
WOOD																					
FS12	16.74	16.88	0.99	0.945	0.90	1.05	1.82	-	-	-	-	-	-	-	-	-	-	-	-	-	-
FS13	15.08	12.27	1.23	0.945	0.90	1.05	3.25	-	-	-	-	-	-	-	-	-	-	-	-	-	-
FS14	14.08	9.31	1.51	0.945	-	-	-	-	-	-	-	-	-	-	-	-	-	-	-	-	-
Average			(1.24)			(1.05)															

Table A-2 (Concluded)

Slab Number	q_s (psi)			y_s (in.)			q_s (psi)			y_s (in.)			q_{ft} (psi)			y_{ft} (in.)			q_{ft}/y_{ft} (lb/in.^{3})		
	Theory	Test	Theory / Test	Theory	Test	Theory / Test	Theory	Test	Theory / Test	Theory	Test	Theory / Test	Theory	Test	Theory / Test	Theory	Test	Theory / Test	Theory	Test	Theory / Test
PARK																					
A1	29.2	30.8	0.95	0.84	1.0	0.84	8.8	7.2	1.22	2.52	2.5	1.01	9.1	10.0	0.91	6.0	4.0	1.50	1.52	2.50	0.61
A2	28.7	31.3	0.92	0.84	0.95	0.88	11.8	11.5	1.03	2.52	2.3	1.10	13.8	15.5	0.89	6.0	4.0	1.50	2.30	3.88	0.59
A3	37.3	37.8	0.99	0.84	0.90	0.93	20.3	14.0	1.45	2.52	2.2	1.15	27.7	21.0	1.32	6.0	4.0	1.50	4.62	5.25	0.88
A4	38.7	37.3	1.04	0.84	0.75	1.12	25.5	17.0	1.50	2.52	2.2	1.15	39.5	25.0	1.58	6.0	4.0	1.50	6.58	6.25	1.05
D1	25.1	24.6	1.02	0.84	0.86	0.98	-	-	-	-	-	-	-	-	-	-	-	-	-	-	-
D2	14.0	12.9	1.09	0.63	0.71	0.89	-	-	-	-	-	-	-	-	-	-	-	-	-	-	-
D3	6.17	4.61	1.34	0.41	0.34	1.21	-	-	-	-	-	-	-	-	-	-	-	-	-	-	-
D4	5.77	4.14	1.39	0.42	0.50	0.90	-	-	-	-	-	-	-	-	-	-	-	-	-	-	-
D5	4.62	3.84	1.20	0.42	0.40	1.05	-	-	-	-	-	-	-	-	-	-	-	-	-	-	-
Average			(1.10)			(0.98)			(1.30)			(1.10)			(1.17)			(1.50)			(0.78)
POWELL																					
S46	50.2	45.0	1.12	0.38	-	-	7.0	-	-	-	-	-	-	-	-	-	-	-	-	-	-
S47	54.9	38.6	1.42	0.38	-	-	7.0	-	-	-	-	-	-	-	-	-	-	-	-	-	-
S48	47.1	36.9	1.28	0.38	-	-	-	-	-	-	-	-	-	-	-	-	-	-	-	-	-
S50	50.6	48.1	1.05	0.38	-	-	12.2	-	-	-	-	-	-	-	-	-	-	-	-	-	-
S53	43.7	42.0	1.04	0.38	-	-	-	-	-	-	-	-	-	-	-	-	-	-	-	-	-
S54	58.5	52.9	1.11	0.38	-	-	18.8	-	-	-	-	-	-	-	-	-	-	-	-	-	-
S55	54.5	55.0	0.99	0.38	-	-	18.7	-	-	-	-	-	-	-	-	-	-	-	-	-	-
S56	44.3	37.5	1.18	0.38	-	-	-	-	-	-	-	-	-	-	-	-	-	-	-	-	-
S57	45.7	30.2	1.51	0.38	-	-	-	-	-	-	-	-	-	-	-	-	-	-	-	-	-
S58	65.3	49.6	1.32	0.38	-	-	29.4	-	-	-	-	-	-	-	-	-	-	-	-	-	-
S59	64.6	50.8	1.27	0.38	-	-	29.3	-	-	-	-	-	-	-	-	-	-	-	-	-	-
S60	45.7	32.5	1.41	0.38	-	-	-	-	-	-	-	-	-	-	-	-	-	-	-	-	-
S62	77.3	61.8	1.25	0.38	-	-	41.9	-	-	-	-	-	-	-	-	-	-	-	-	-	-
S63	72.8	67.3	1.08	0.38	-	-	41.0	-	-	-	-	-	-	-	-	-	-	-	-	-	-
S64	45.8	35.0	1.31	0.38	-	-	-	-	-	-	-	-	-	-	-	-	-	-	-	-	-
Average			(1.22)																		
Grand Average			(1.13)			(0.96)			(1.09)			(0.91)			(1.26)			(1.25)			(1.00)

rectangular slabs. This may be due to the deflection required to develop the crushing strain of the concrete along the hinge lines being different for the x- and z-direction strips. Since the resistance predicted by Eq. 42 is based upon the ultimate deflection for the z-direction strips, this results in a slightly erroneous value for the x-direction strips, and thus for the predicted ultimate resistance. The predicted ultimate deflection for the compressive membrane region is slightly lower than the measured values. This also contributes to the higher predicted strengths. As discussed previously, the ultimate deflection given by Eq. 28 is bounded by an empirical upper limit of 0.42 times the slab thickness.

The predicted secondary resistance is on the average 9 percent higher than the measured resistance. The corresponding predicted deflection is on the average 9 percent lower than the test results. As was the case for the ultimate deflection in the compressive membrane region, the secondary deflection is bounded by an empirical upper limit, the limit for this deflection taken as three times the slab thickness. As shown in subsequent plots of the load-deflection curves, the secondary resistance region is generally not well defined. This is particularly true for the deflection. The predicted values are meant to be approximate only. In general, it is felt the difference in predicted and test resistance during this region has a minor effect on the total predicted behavior of the slab.

The predicted values for the ultimate tensile membrane resistance and deflection are both on the average approximately 25 percent higher than the measured values. These percentages may be somewhat misleading, however, as the test values do not correspond to failure values for all the test slabs. This is the case for the NCEL slabs, where at the deflections indicated for y_{ft}, the slabs, though badly damaged, are still

intact. The deflections for the slabs tested by Park similarly do not indicate collapse. The values for the slabs tested at WES and MIT, however, correspond to significant rupture of the steel reinforcement and partial collapse of the slabs. The agreement between the predicted and test results is quite good for these slabs, particularly for the collapse deflection. A better value for comparison purposes may be the slope of the tensile membrane resistance curve (q_{ft}/y_{ft}). The agreement between the predicted and measured slopes of the tensile membrane resistance is, on the average, quite good.

Variation of the static resistance with the center deflection is shown for several of the test slabs in Figures A-1 through A-4. Both predicted and measured results are given. A brief discussion of the results for each group of tests is also presented in the following paragraphs.

NCEL. As can be seen from Table A-2 and Figure A-1, the predicted resistance functions for the NCEL slabs agree quite well with the test results. This is particularly true for the compressive membrane region, which is the primary region of interest for this study. In general, good agreement is also found for the secondary resistance. However, comparison of the maximum tensile membrane resistance values given in Table A-2 show the predicted results to be considerably higher than the test results. As can be seen from Figure A-1, the slope of the predicted resistance curve during this region is only slightly less than the slope of the measured resistance. Thus, the discrepancy in the maximum resistance is due primarily to the difference between the predicted and measured values of the collapse deflection, y_{ft}. The test values of y_{ft} for the NCEL slabs correspond to rupture of the steel reinforcement at the supports. A review of the photographs given in Ref. 10 for the slabs after the static tests shows that although the slabs are severely cracked, they are

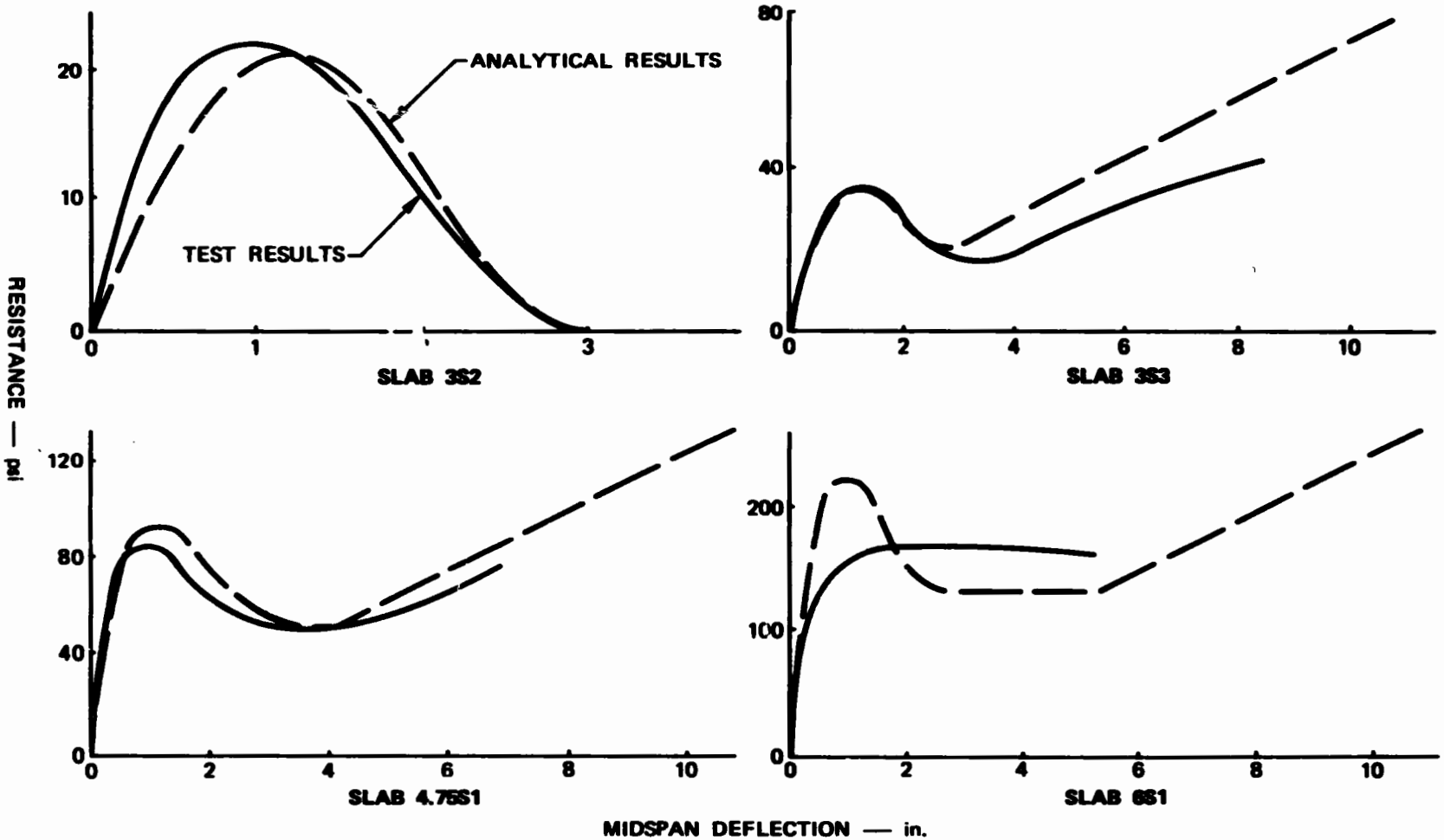

FIGURE A-1 STATIC RESISTANCE DIAGRAMS FOR NCEL SLABS

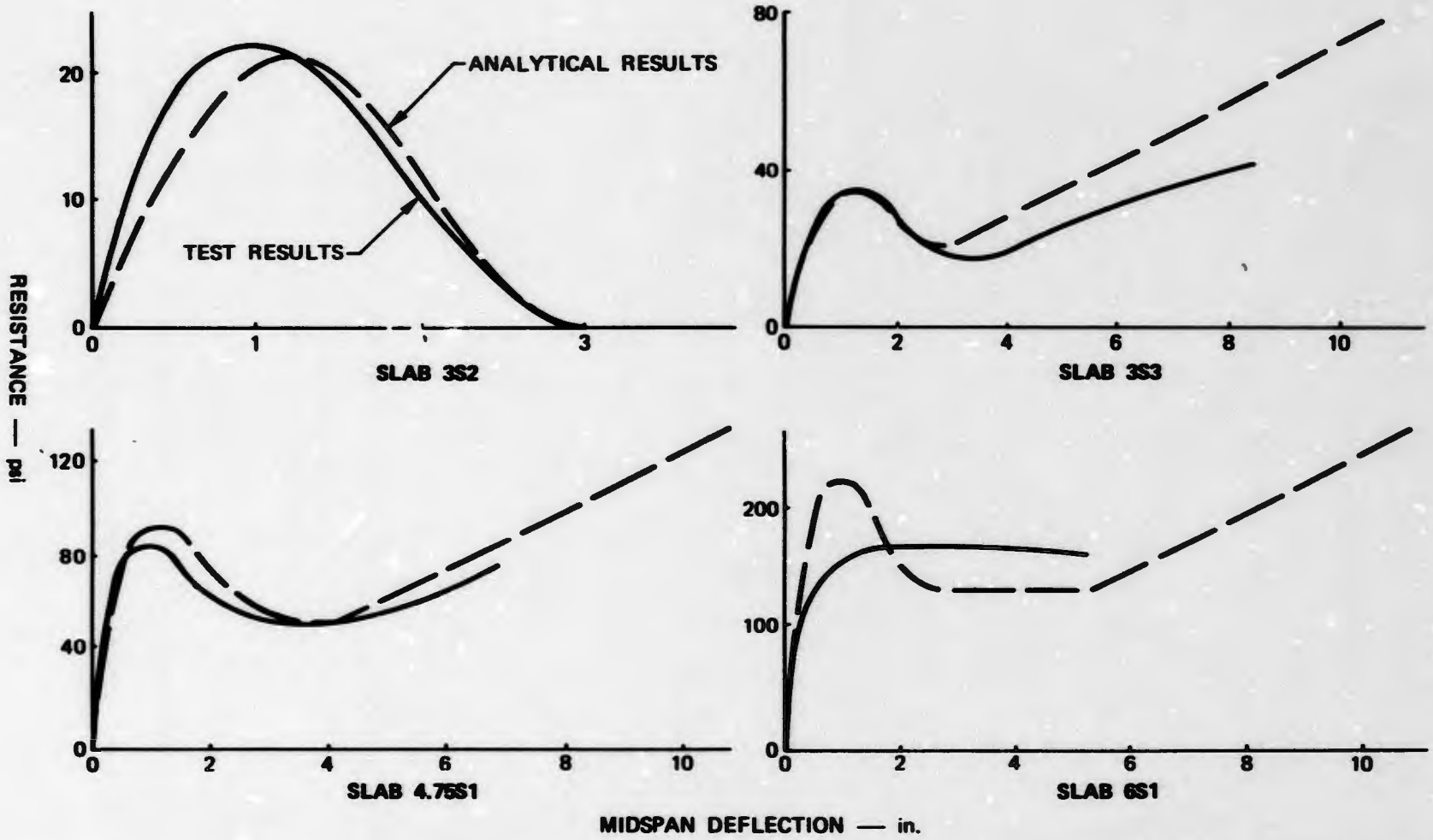

FIGURE A-1 STATIC RESISTANCE DIAGRAMS FOR NCEL SLABS

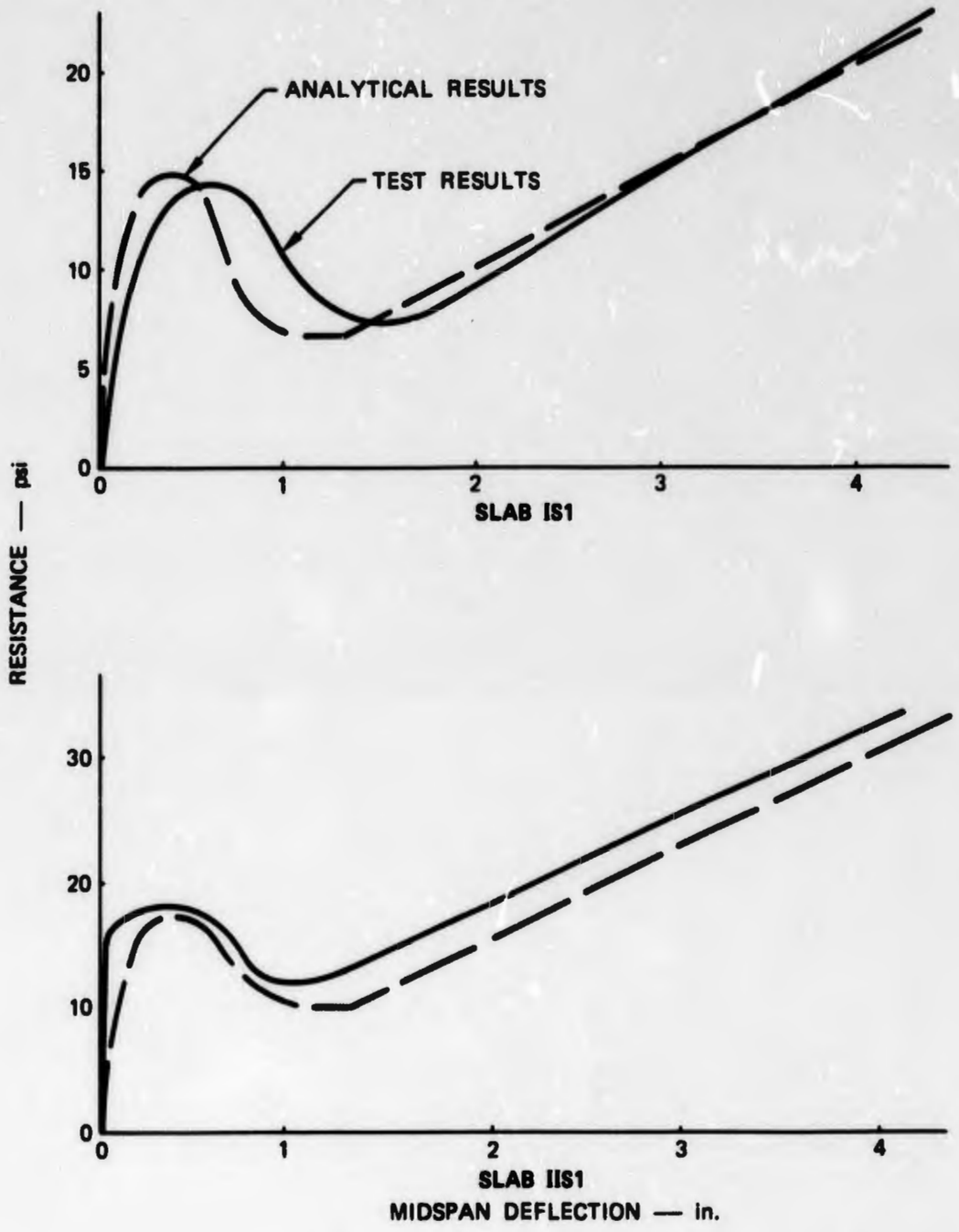

FIGURE A-2 STATIC RESISTANCE DIAGRAMS FOR WES SLABS

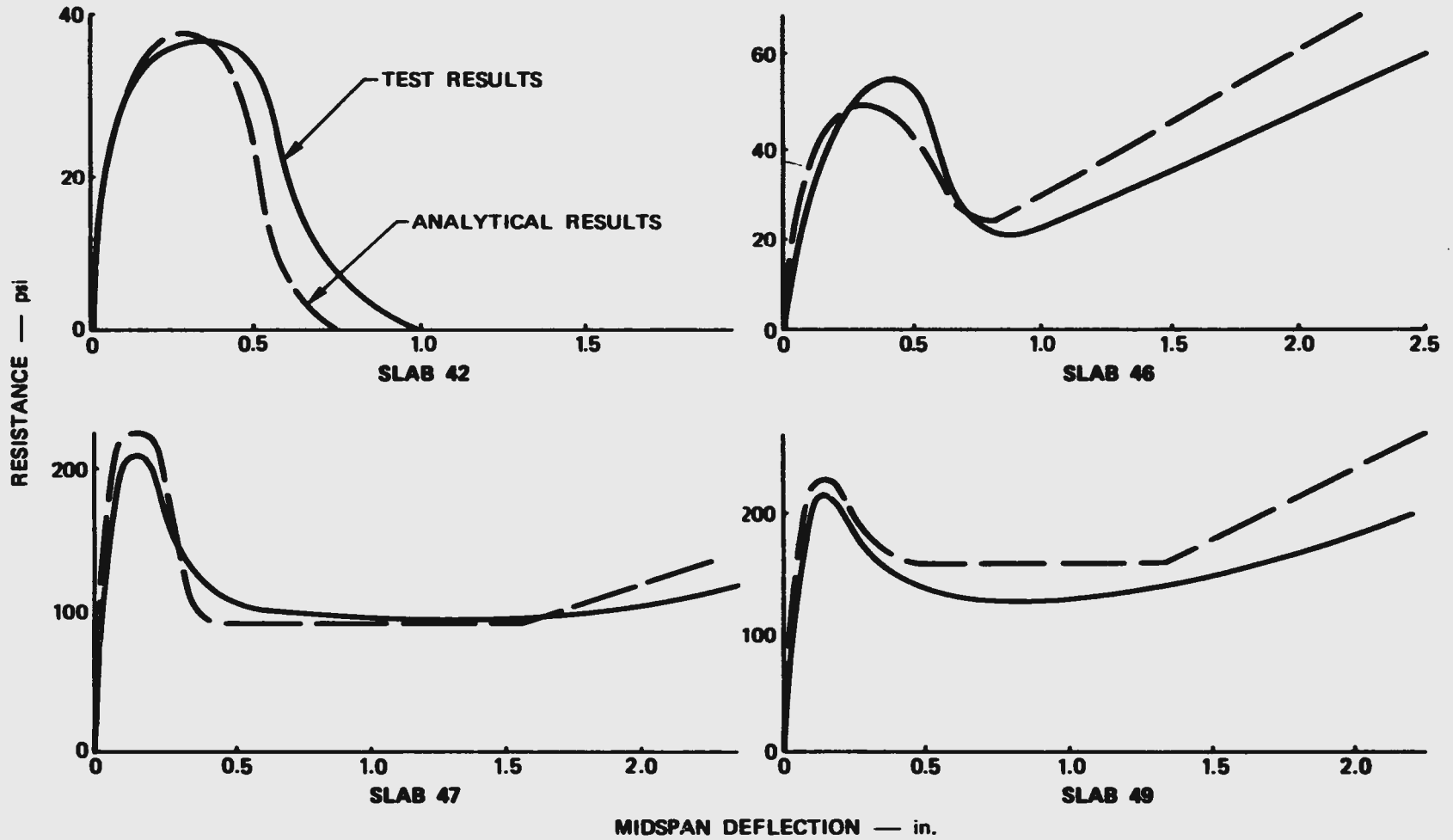

FIGURE A-3 STATIC RESISTANCE DIAGRAMS FOR MIT SLABS

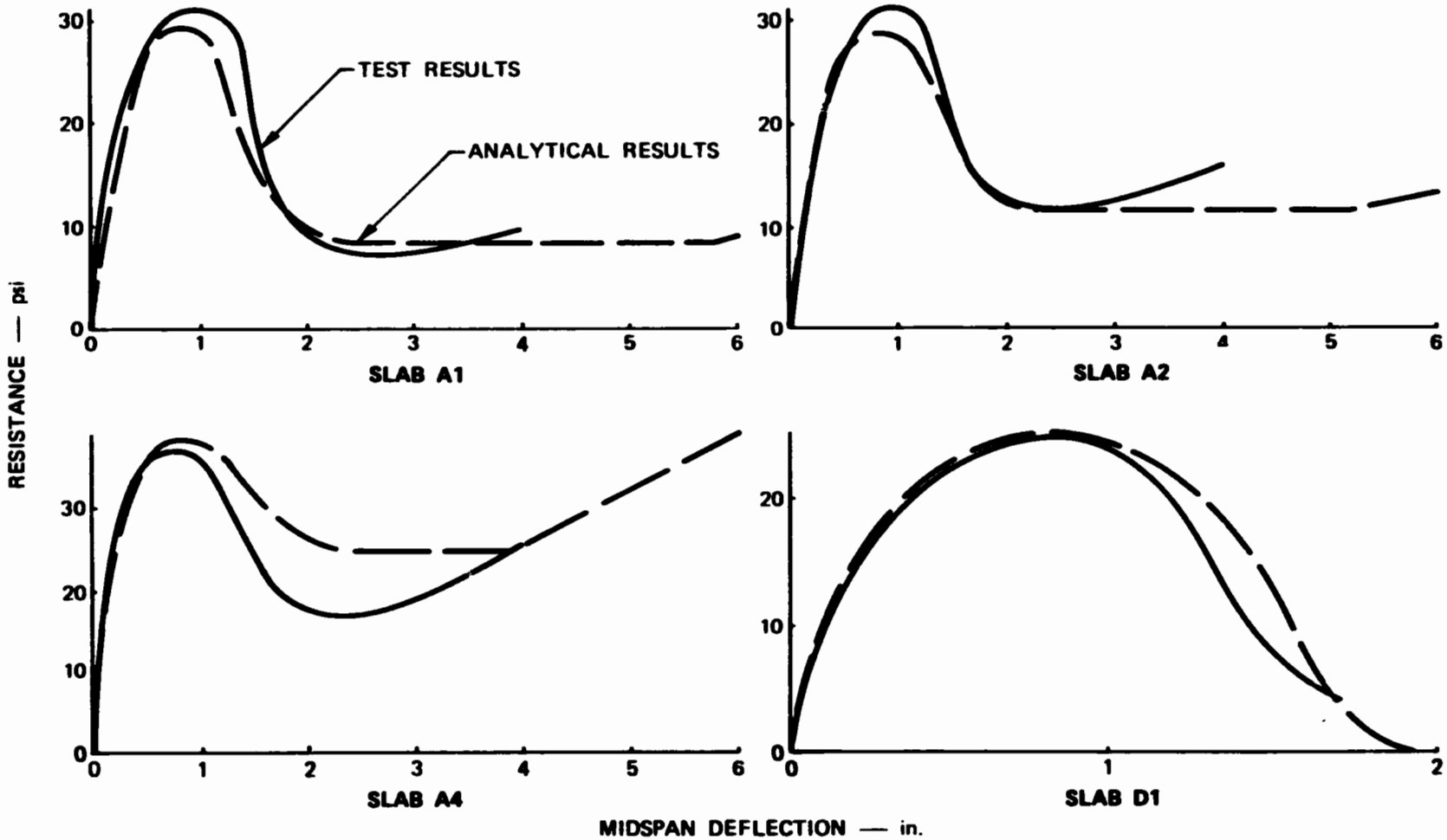

FIGURE A-4 STATIC RESISTANCE DIAGRAMS FOR PARK SLABS WITH ALL EDGES FULLY RESTRAINED

still intact and would still provide protection. How much reserve strength, if any, the slabs still have is unknown. Thus, comparison of the maximum tensile membrane resistance is felt to be somewhat questionable for these slabs.

WES. The predicted and test results for the WES slabs are presented in Figure A-2. These results indicate that the predicted ultimate strength in the compressive membrane region agree quite well with the test results, although the corresponding predicted ultimate deflection is about 80 percent of the test values on the average. As indicated in Table A-1 the steel reinforcement percentage for the edge strips of the slabs was different than for the middle strips. Since the procedures developed in this study assume a uniform distribution of steel reinforcement in each slab direction (not necessarily the same in both directions), an average value of the reinforcement in the middle and edge strips was used in the analysis. Agreement between the predicted and measured results for the secondary and tensile membrane regions is also quite good.

MIT. The predicted resistance functions are compared to the load-deflection behavior obtained from tests of longitudinally restrained slabs conducted at MIT in Figure A-3. The predicted resistance compares fairly well to the test results in the compressive membrane region, but is somewhat high in the tensile membrane region. The predicted deflection at collapse compares very well with the test results, however.

Wood. No resistance functions were plotted for the slabs tested by Wood (From Ref. 10). Also, results are presented in Table A-2 for the compressive membrane region only. For this region, the predicted resistance is approximately 25 percent higher than the test results. One possible reason for this discrepancy may be the factor used in converting the cube strength of the concrete to a corresponding cylinder strength.

The cylinder strength was assumed to be 80 percent of the cube strength. This assumed percentage may be somewhat higher than is actually the case.

Park. Table A-2 compares predicted resistance functions values to the results presented in Ref. 9 for tests on rectangular slabs (length-to-width ratio of 1.5). Representative plots of the predicted and actual load-deflection curves are also given in Figure A-4. The predicted results compare fairly well with the test results for the compressive membrane region. However, for the secondary region the predicted resistance is approximately 30 percent higher than the test results. The predicted slope for tensile membrane region is considerably below the test results. It should be noted that test results are available only for slab deflections up to 4.0 in., rather than up to failure. Comparisons of predicted and test results for the tensile membrane region are thus questionable for these slabs.

Powell. Results are presented in Ref. 9 only for the ultimate compressive membrane strength of the rectangular slabs (length-to-width ratio of 1.75) tested by Powell. The predicted ultimate resistance for this region is on the average 22 percent higher than the test results.

Slabs with One Edge Simply Supported

Park (Ref. 9), in addition to his tests on rectangular slabs with all edges fully restrained, also conducted tests on two additional series of slabs with one of their edges simply supported on rollers, the remaining edges of both series being fully restrained. The series B slabs were tested with one of the short edges simply supported, while the series C slabs were tested with one of the long edges simply supported. The steel content of these series of slabs was the same as the corresponding series A slab listed in Table A-1 (i.e., steel contents of slabs A1, B1, and C1

were identical), except that there was no top steel at the simply supported edge and that the length of the other top steel was such as to suit the particular slab. The remaining dimensions and properties were also the same except for the concrete strengths, which are listed in Table A-3.

Predicted resistance and deflection values for the various stages of behavior are compared with the test results in Table A-3. Variation of the static resistance with the center deflection is shown for both predicted and test results of the slabs in Figure A-5. Due to restrictions of the computer program, the predicted results for the compressive membrane region are based upon all edges restrained against rotation rather than the actual case of one of the edges simply supported. The predicted results reflect the actual condition of no longitudinal restraint in the direction perpendicular to the simply supported edge, however.

Because of the necessity of treating all edges as restrained against rotation for the calculation of the ultimate flexural resistance, the predicted results would be expected to be slightly higher than the test results. This is found to be the case for the slabs with one of the long edges simply supported: the predicted ultimate flexural resistance is 37 percent higher on the average than the test results. For the slabs with one of the short edges simply supported, however, the predicted ultimate flexural resistance is 13 percent less than the test results. However, the analytical predictions neglected to consider the compressive membrane forces in the direction at right angles to the simply supported edges. Some membrane forces are bound to develop in this direction because the fully restrained edges adjacent to the simply supported edge are unable to increase in length. This effect is felt to be greater for the slabs with one of the short edges simply supported due to the greater length of the fully restrained long edges.

Table A-3

THEORETICAL VERSUS TEST RESULTS FOR SLABS WITH ONE EDGE ON ROLLERS, OTHER EDGES FULLY RESTRAINED

Slab Number	f_c' (psi)	q_s (psi)			y_s (in.)			q_p (psi)			y_p (in.)			q_s (psi)			y_s (in.)			q_s/y_s (lb/in.^{3})		
		Theory	Test	Theory / Test	Theory	Test	Theory / Test	Theory	Test	Theory / Test	Theory	Test	Theory / Test	Theory	Test	Theory / Test	Theory	Test	Theory / Test	Theory	Test	Theory / Test
PARK																						
B1	3560	18.0	20.2	0.89	0.84	0.60	1.40	8.5	-	-	2.52	1.4	1.80	(7.2)	-	-	(6.0)	-	-	(1.20)	-	-
B2	3616	19.6	24.1	0.81	0.84	0.60	1.40	12.7	10.4	1.22	2.52	1.65	1.53	14.1	13.0	1.08	6.0	2.8	2.14	2.35	4.64	0.51
B3	3744	24.5	25.6	0.96	0.84	0.60	1.40	19.9	11.8	1.69	2.52	1.65	1.53	27.1	17.0	1.59	6.0	3.1	1.94	4.52	5.48	0.83
B4	3776	27.2	32.9	0.83	0.84	0.60	1.40	24.1	18.5	1.30	2.52	1.45	1.74	38.0	38.0	1.00	6.0	4.0	1.50	6.33	9.50	0.67
Average				(0.87)			(1.40)			(1.40)			(1.65)			(1.23)			(1.86)			(0.67)
C1	5000	16.5	16.7	0.99	0.84	1.05	0.80	8.2	-	-	2.52	-	-	(4.5)	-	-	(6.0)	-	-		-	-
C2	4384	21.5	18.8	1.14	0.84	0.90	0.93	12.9	-	-	2.52	-	-	(4.5)	-	-	(6.0)	-	-		-	-
C3	4064	31.3	18.1	1.73	0.50	0.68	0.74	19.7	-	-	1.51	-	-	(4.5)	-	-	(6.0)	-	-		-	-
C4	5088	43.3	26.6	1.63	0.34	0.80	0.42	25.6	-	-	1.03	-	-	(4.5)	-	-	(6.0)	-	-		-	-
Average				(1.37)			(0.72)															

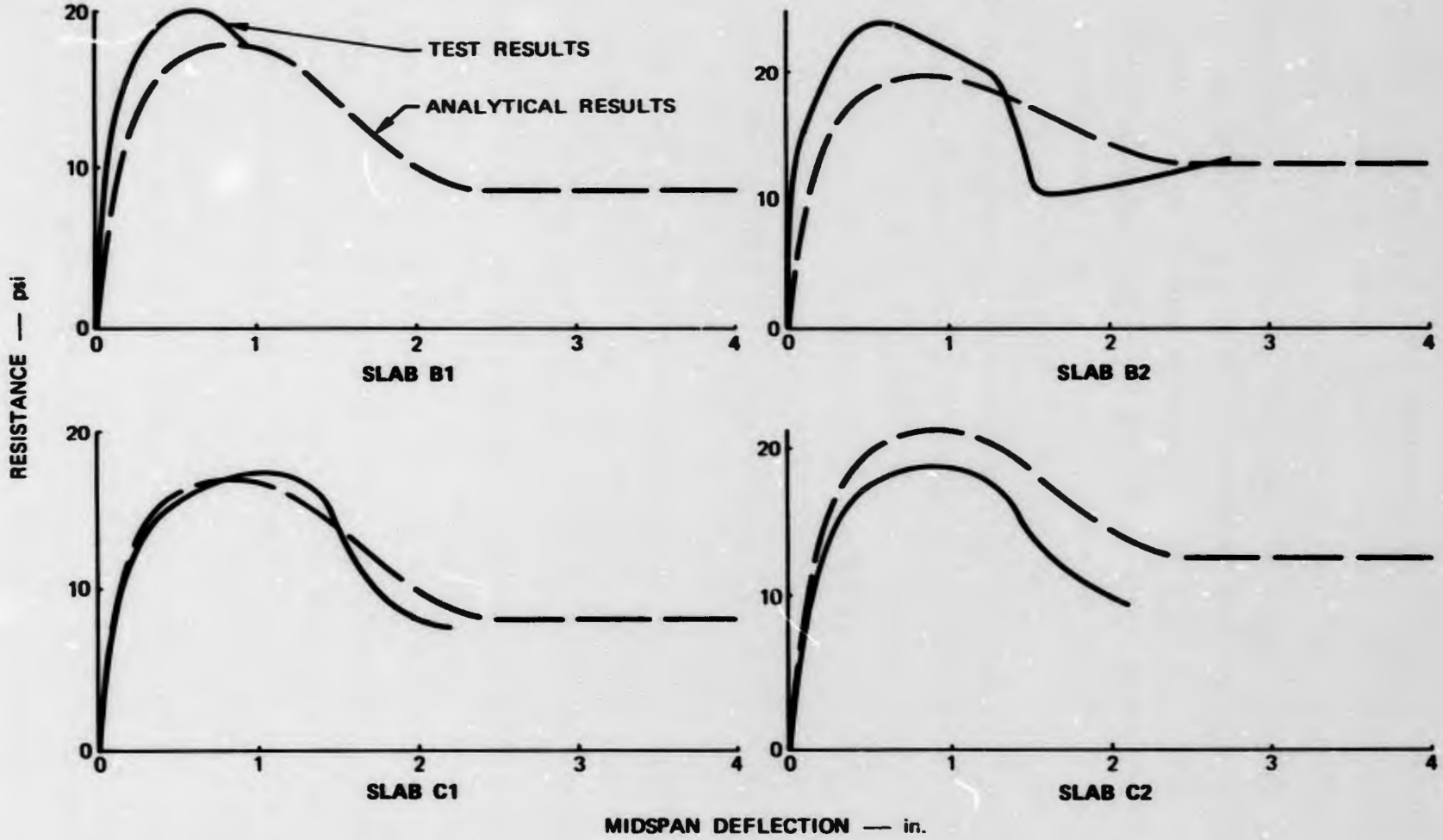

FIGURE A-5 STATIC RESISTANCE DIAGRAMS FOR PARK SLABS WITH ONE EDGE SIMPLY SUPPORTED

An additional factor in the comparison of the predicted and actual ultimate flexural resistance is the difference in the corresponding ultimate deflections. The predicted ultimate deflection for the slabs with one of the short edges simply supported in 0.84 in., equal to upper bound empirical limit of 0.42 times the slab thickness. The corresponding ultimate deflection was only 0.30 times the slab thickness, however. Since q_u decreases with increasing y_u, the 40 percent higher deflection contributes greatly to the 13 percent lower predicted ultimate flexural resistance. The opposite effect exists for the slabs with one of the long edges simply supported. The predicted ultimate deflection, which for this case is calculated using Eq. 29, is on the average 28 percent lower than the experimental deflection. This is a large contributor to the 37 percent higher predicted ultimate flexural resistance, particularly for slabs C3 and C4. Due to the increasing percentage of steel reinforcement in the short direction as compared to the long direction, the value of β defining the location of the yield lines is reduced, thus resulting in reduced values of the predicted ultimate deflection. The predicted ultimate flexural resistance for these two slabs is approximately 70 percent greater than the corresponding test results.

Test results for the secondary resistance are available only for the slabs with one short edge simply supported. For these slabs, the predicted secondary resistance is on the average 40 percent higher than the test values. One reason for this is again the treating of the simply supported edge as being rotationally restrained for computational purposes. The predicted secondary deflection is on the average 65 percent higher than the corresponding experimental deflections.

The slope of the predicted tensile membrane resistance curve (q_{ft}/y_{ft}) for the slabs with one edge simply supported is approximately two-thirds of the measured results. This discrepancy again, no doubt, results from neglecting any tensile membrane forces in the long direction

perpendicular to the simply supported edge. The tensile membrane resistance for slab B1 is less than the secondary resistance (flexural resistance with no compressive membrane forces). This is also true for the slabs with one of the long edges simply supported. As was the case for the slabs tested by Park with all edges fully restrained, the measured deflections for y_{f_t} do not correspond to collapse of the slab.

Overall, the predicted results for the slabs with one edge simply supported and the remaining edges fully restrained are seen to only approximate the actual results. This is due, no doubt, to the many assumptions required for the analysis.

Dynamically-Loaded Slabs

This section compares the predicted dynamic behavior of longitudinally restrained slabs to the time-deflection response of dynamically loaded slabs tested at NCEL and WES (Refs. 10 and 11). For all the slabs, the edges were fully restrained. Dimensions, reinforcement data, and steel strengths are the same as the corresponding statically loaded slabs, except for the concrete strengths, which are given in Table A-4. A comparison of the predicted and measured results for the dynamic tests is also given in Table A-4. Typical deflection-time histories, both actual and predicted, are shown for several of the slab tests in Figures A-6 to A-9. A discussion of the results for the two series of tests is presented in the following paragraphs.

NCEL. Three slabs were subjected to dynamic loads. Except for the concrete strengths, which are listed in Table A-4, the slabs were the same as the corresponding statically loaded slabs listed in Table A-1. The dynamic loads consisted of an approximately rectangular load impulse with a short rise time (1 to 2 msec). For the final loading on each slab, sudden decreases in the pressure occurred as the air leaked through the slab.

Table A-4

THEORETICAL VERSUS TEST RESULTS FOR DYNAMICALLY LOADED SLABS

Test	Peak Load (psi)	f'_c (psi)	DIF (%)	Maximum Dynamic Deflection (in.) Theory	Test	Theory / Test	Time to Maximum Deflection (msec) Theory	Test	Theory / Test
NCEL									
3D1-1	3.5	3795	40	0.024	0.05	0.48	5.2	5.2	1.00
3D1-2	10.5	3795	40	0.10	0.09	1.11	7.5	7.1	1.06
			40	1.07			29		
3D1-3	39.0	3795	30	5.36	10+	-	55	>100	-
			20	7.20			42		
Incipient	59.9	3795	40				20		
Collapsed	56.2	3795	30	10.8+	-	-	25		
Load	50.6	3795	20				25		
4.75D1	10.5	3320	-	-	0.03	-	-	4.0	-
4.75D2	18.0	3320	40	0.05	0.05	1.00	4.0	4.2	0.95
4.75D1-3	50.0	3320	40	0.26	0.37	0.70	6.0	7.0	0.86
4.75D1-4	62.0	3320	40	0.38	0.46	0.83	7.0	7.5	0.93
4.75D1-5	77.0	3320	40	-	0.60	-	-	7.0	-
4.75D1-6	87.0	3320	40	0.76	0.76	1.00	8.0	9.4	0.85
			40	1.29			30		
4.75D1-7	98.0	3320	30	1.75	12+		13	>30	-
			20	9.64			10		
Incipient	124.4	3320	40				25		
Collapse	117.0	3320	30	10.8+	-	-	25	-	-
Load	109.3	3320	20				25		
4.75D2-1	11.0	3595	40	0.016	0.04	0.40	3.0	4.2	0.71
4.75D2-2	91.0	3595	40	0.84	0.77	1.09	8.0	7.1	1.13
4.75D2-3	55.0	3595	40	0.32	0.50	0.64	6.0	6.0	1.00
4.75D2-4	91.0	3595	40	0.84	0.96	0.88	8.0	7.7	1.04
			40	1.72			12		
4.75D2-5	110.0	3595	30	9.66	9.2+	-	30	>25	-
			20	10.8			25		
Incipient	123.5	3595	40				25		
Collapse	116.3	3595	30	10.8+	-	-	25	-	-
Load	109.4	3595	20				25		

Table A-4 (Concluded)

Test	Peak Load (psi)	f_c' (psi)	DIF (%)	Maximum Dynamic Deflection (in.)			Time to Maximum Deflection (msec)		
				Theory	Test	Theory / Test	Theory	Test	Theory / Test
WES									
ID1	15.0	3683	25	0.48	0.25	1.92	7	-	-
ID1B	34.7	3683	25	4.35+	13+	-	9	24	-
ID2	26.5	3485	25	4.35+	7.5+	0.58	12	31	0.39
ID3	27.8	3485	25	4.35+	13+	-	12	31	0.39
ID4	27.0	3485	25	4.35+	7.0	0.62	12	34	-
ID5	27.4	3485	25	4.35+	13+	-	12	15	-
Incipient Collapse Load	18.2	3683	25	4.35+	-	-	20	-	-
	26.4*	3683	25	7.25+	-	-	16	-	-
IID1	56.8	3810	25	4.35+	13+	-	7	15	-
IID2	36.6	3810	25	4.35+	8.1	0.54	10	28	0.36
IID3	43.1	3810	25	4.35+	13+	-	9	28	-
Incipient Collapse Load	25.6	3810	25	4.35+	-	-	14	-	-
	38.8*	3810	25	7.25+	-	-	14	-	-

* Based on collapse deflection of 0.25 of the slab length.

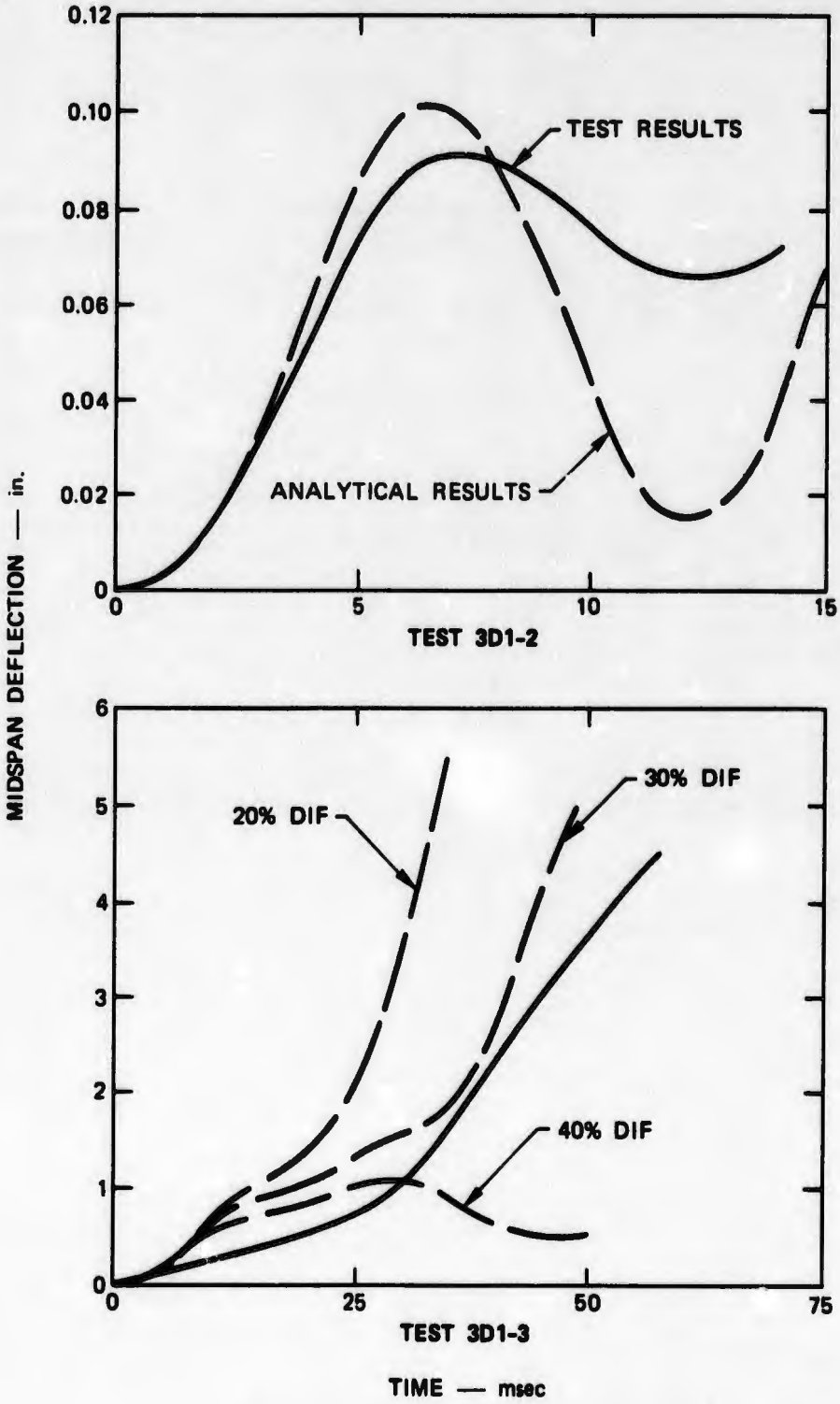

FIGURE A-6 DYNAMIC DEFLECTION-TIME HISTORIES FOR NCEL SLAB 3D1

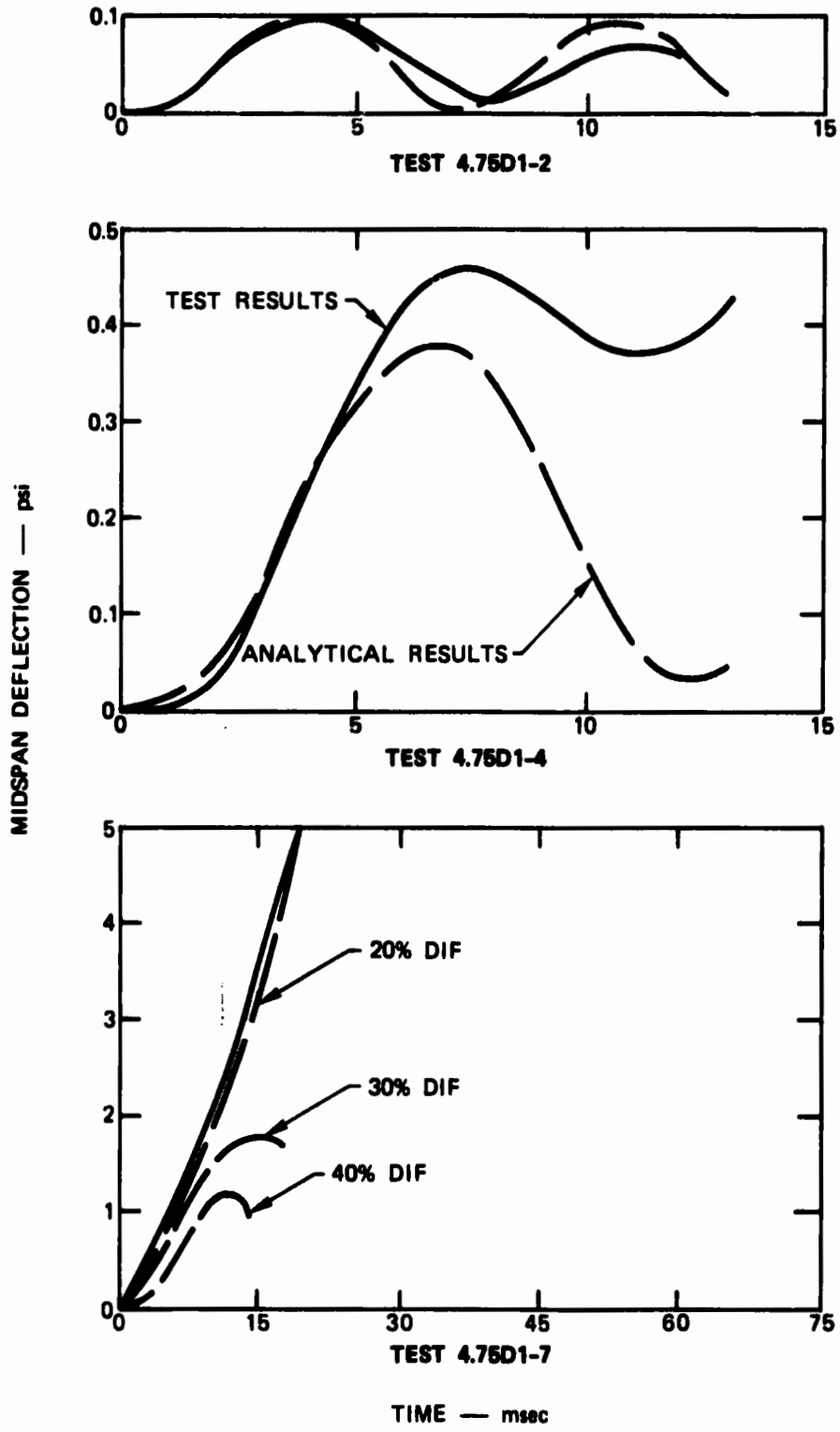

FIGURE A-7 DYNAMIC DEFLECTION-TIME HISTORIES FOR NCEL SLAB 4.75D1

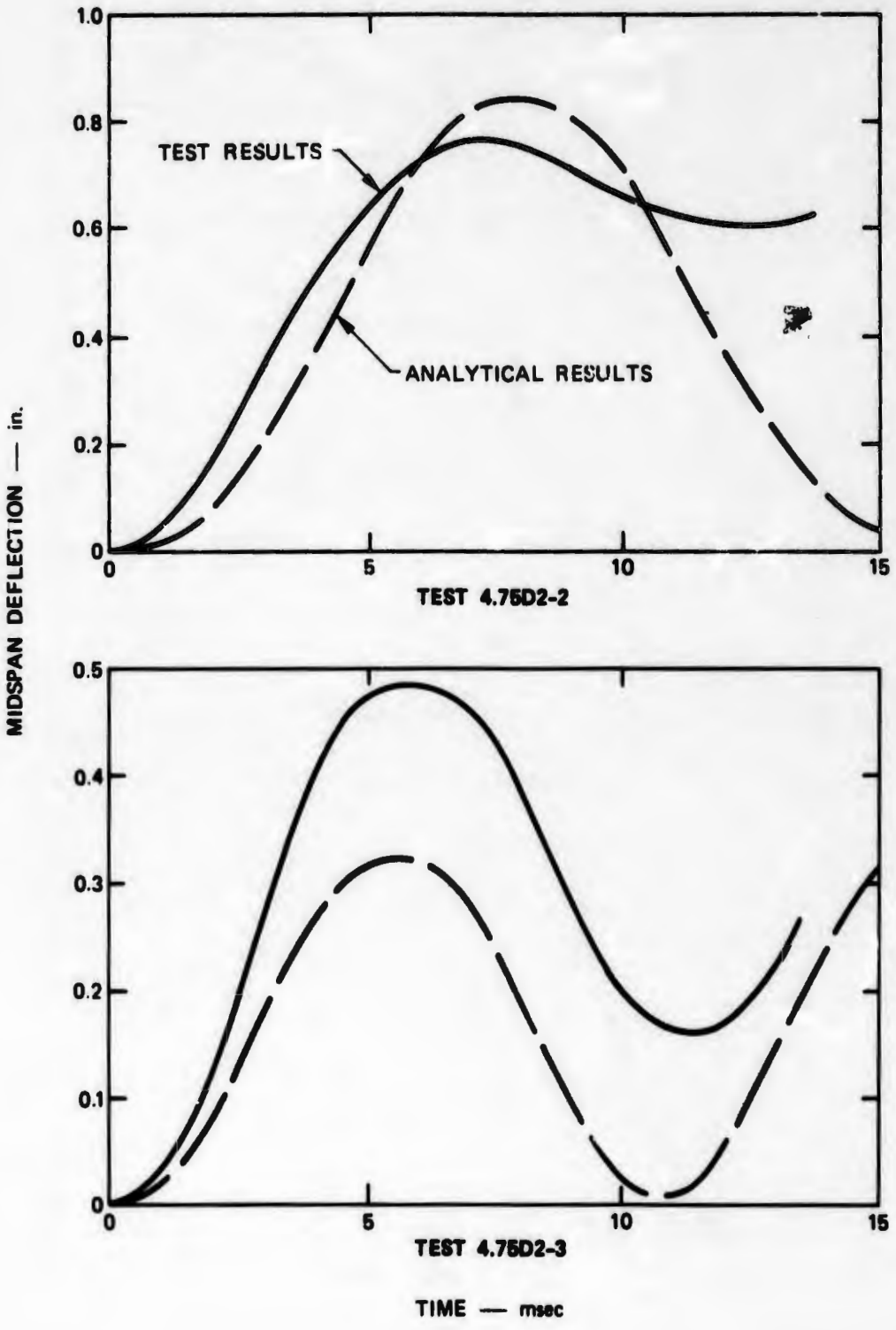

FIGURE A-8 DYNAMIC DEFLECTION-TIME HISTORIES FOR NCEL SLAB 4.75D2

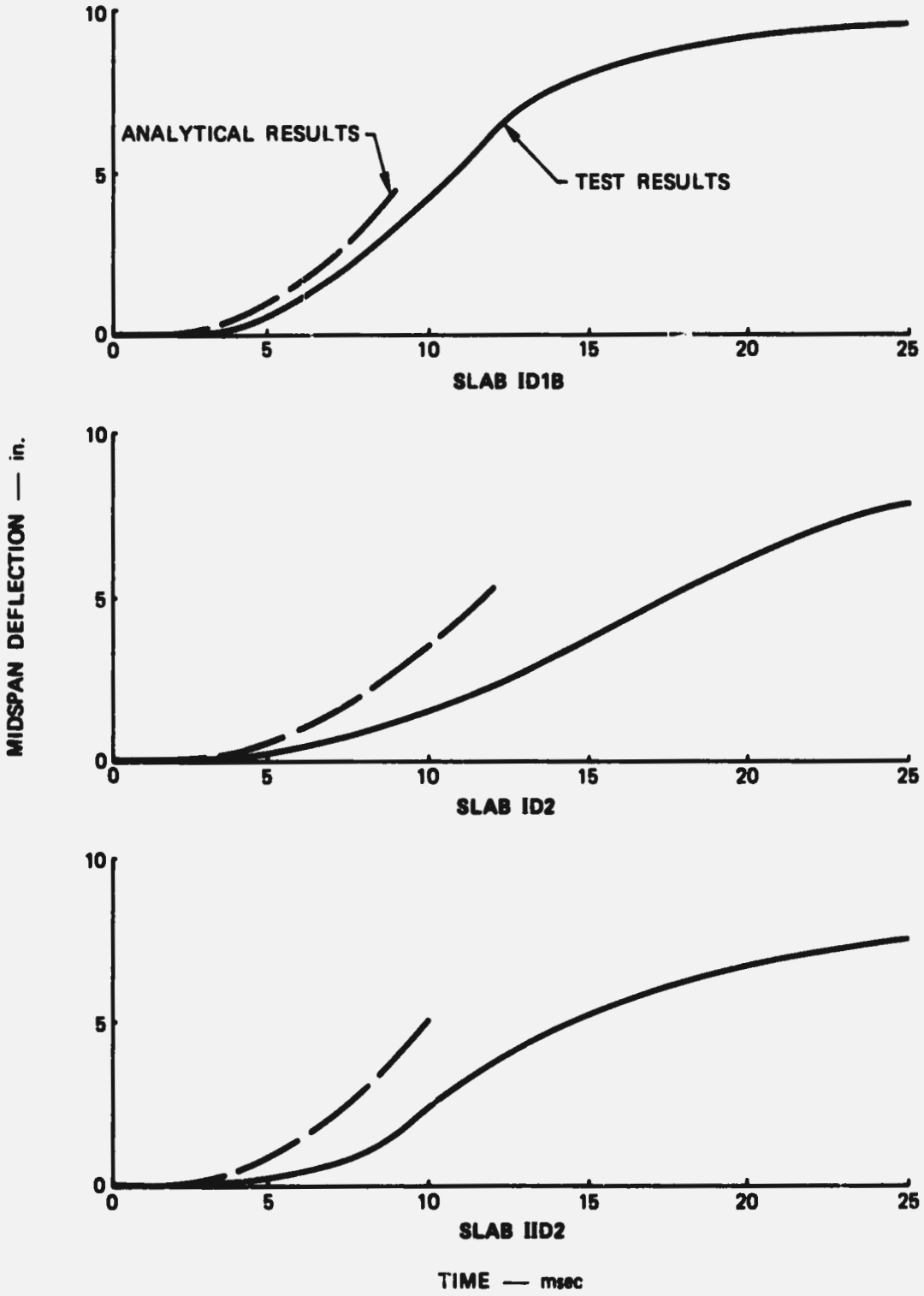

FIGURE A-9 DYNAMIC DEFLECTION-TIME HISTORIES FOR WES SLABS

Slab 3D1 required three cycles of loading to failure, while slabs 4.75D1 and 4.75D2 were subjected to seven and five cycles of loading, respectively. All slabs received very little damage prior to the last cycle of loading. The last cycle of loading caused a local failure of slab 3D1 and total destruction of the 4.75-in. thick slabs.

Results in Ref. 10 indicate a dynamic increase factor (DIF) of 30 to 60 percent for the dynamically loaded slabs. A value of 40 percent was used for the predicted results given in Table A-4. Except for the last cycle of loading for each slab, the predicted maximum deflection and corresponding time of occurrence are in good agreement with the test results. For the last cycle of loading, however, the predicted results do not indicate failure, as occurred during the tests. Therefore, additional predictions were made for 20- and 30-percent dynamic increase factors. Predicted time-deflection histories are compared with test results for several of these tests in Figures A-6 to A-8. Results are discussed for each of the slabs in the following paragraphs.

The predicted deflection time-histories shown for test 3D1-3 in Figure A-6 indicate that the best agreement with test results occurs for a dynamic increase factor of 30 percent. As indicated in Table A-4, however, the best agreement for maximum deflection occurs for a DIF of 20 percent. This discrepancy may be due, at least in part, to the local failure experienced by slab 3D1.

Predicted deflection-time histories are compared to the results from tests 4.75D1-2, 4.75D1-4, and 4.75D1-7 in Figure A-7. The predicted deflection-time curve for test 4.75D1-2 agrees quite well with the test results. For test 4.75D1-4, the predicted maximum deflection is somewhat less than that experienced during the test. After the maximum deflection occurs, the predicted deflection-time curve deviates considerably from the test results. This large deviation results from neglecting damping

in the dynamic analysis. For test 4.75D1-7, the best agreement between predicted and actual results occurs for a dynamic increase factor of 20 percent.

Predicted deflection-time histories are compared to results from tests 4.75D2-2 and 4.75D2-3 in Figure A-8. The predicted deflections are in fairly good agreement with the actual results up to maximum deflection. After this, again because damping was neglected in the dynamic analysis, the predicted deflections deviate widely from the actual results. No results were plotted for test 4.75D2-5. The results from Table A-4, however, indicate the best agreement between predicted and test results occurs for a dynamic increase factor of 30 percent.

Incipient collapse pressures were also predicted for the three test slabs, using dynamic increase factor factors of 20, 30, and 40 percent. These values are shown in Table A-4. Comparison of these values with the measured peak loads for the last cycle of loading for each slab indicates that the best agreement occurs for a 20-percent dynamic increase factor. Even these values are slightly higher than the actual test results. Possible reasons for this may be inaccuracies in the predicted resistance function, particularly for the tensile membrane region, and possible damage experienced by the slabs during the prior test load cycles.

WES. Dynamic tests were conducted on eight slabs. Properties for these slabs were the same as listed for the corresponding series I and II slabs in Table A-1, except for the concrete strengths, which are listed in Table A-4. A comparison of the predicted and test results is also given in Table A-4. The dynamic loads consisted of an approximate triangular impulse with a rise time of about 4 msec, followed by a fairly rapid decay until about 20 msec, and a slower decrease to zero at about 100 to 120 msec. Except for test ID1, the pressures were such that collapse occurred on the first cycle of loading. Due to bad primacord, a

low pressure of 15 psi resulted for test ID1, with only hairline cracks, occurring around the periphery of the slab. A second test load, ID1B, collapsed the slabs.

Based on results from Ref. 11, a dynamic increase factor of 25 percent was used for the predicted results given in Table A-4. A comparison of these results with the test results at first glance indicates a wide disparity. It should be noted, however, that the values given for the maximum test deflections include behavior after collapse of the slab has occurred, while the predicted results are only concerned with behavior up to the predicted collapse deflection. Since so many of the test slabs experienced total collapse, comparisons between the predicted and test results are inconclusive. However, disregarding deflections of the slabs that totally collapsed (and also test ID1), the maximum deflections averaged 7.25 in. (25 percent of the slab span) for the series I slabs and 8.1 in. (28 percent of the slab span) for the series II slabs. The predicted results, however, indicate collapse to occur at 4.35 in., or 50 to 60 percent of the actual deflections. The reason for this discrepancy may be due to the fact that statically-loaded slabs (on which the predicted resistance is based) start to fail in one area, subsequently unloading the rest of the slab. Thus, failure is concentrated in one area of a statically loaded slab. Dynamically loaded slabs, however, tend to fail more uniformly, with the quicker response of the slab evening out the local defects. This may result in a larger deflection since local effects are minimized.

Predicted and actual deflection-time histories are shown for several of the slabs in Figure A-9. These results indicate that, for the periods of comparison, the predicted response is quicker than actually occurred. One reason for this difference is the use of the load-mass factor (used in simplifying the actual slab to an equivalent single degree-of-freedom system) corresponding to the plastic region for the entire range of

behavior. During the initial stages of behavior, the actual slab is somewhat stiffer than indicated by use of this factor. While having a minor effect on the maximum response, the effect on the time to maximum response is less than actually occurred. This effect is also observed in comparing the predicted and actual time to maximum deflection in Table A-4. This effect is felt to be minor as far as the incipient collapse overpressure is concerned.

Predicted incipient collapse overpressures for the series I and II slabs were calculated as 18.2 psi and 25.6 psi, respectively. These values correspond to the upper bound average values of 28.7 psi and 45.5 psi, respectively, obtained from the tests. Modifying the resistance functions to reflect the collapse deflections observed in the test (0.25 of the slab length) increases the predicted incipient collapse overpressures to 26.4 psi and 38.8 psi for the series I and II slabs, respectively. These correspond quite favorably to the actual results.

Summary

In general, the analytical predictions for the static resistance of longitudinally restrained, reinforced concrete slabs were found to compare favorably with experimental results from several tests of statically and dynamically loaded slabs. This correlation was extremely good for the compressive membrane region for the square slabs fully restrained on all four edges. The predicted ultimate compressive membrane resistance for rectangular slabs fully restrained on all edges was found to be slightly on the high side. Predicted secondary resistance and deflection values were also found to compare favorably with experimental results. Although predicted values for both the ultimate tensile membrane resistance and deflection were about 25 percent higher than the measured results, these comparisons are somewhat misleading, since not all of the slabs were

tested to collapse. Agreement between predicted and measured results for the slope of the tensile membrane resistance was quite good.

A limited number of comparisons were also made for rectangular slabs with one edge simply supported on rollers and the remaining edges fully restrained. In general, correlation between the predicted and measured resistance function values was only fair. These results would tend to indicate that for such slabs the predicted resistance function should be considered as approximate only.

Predicted dynamic response was also compared with the time-deflection behavior of several dynamically loaded square slabs with all edges longitudinally restrained. The slab response model generally provided an adequate prediction of the experimental behavior. Dynamic increase factors of 20 to 40 percent were used in calculating the predicted response. Best correlations were obtained for a dynamic increase factor of about 25 percent. Experimental results also indicated dynamic collapse deflections on the order of 25 percent of the slab length, as compared to values of approximately 15 percent of the slab length obtained from the static tests used in most of the analyses. This increase is felt to be due to the minimizing of the effect of local failures as a result of the rapid response of the dynamically loaded slabs as compared to the statically loaded slabs.

REFERENCES

1. Wiehle, C. K., and J. L. Bockholt, "Existing Structures Evaluation, Part I: Walls," Stanford Research Institute (for Office of Civil Defense), Menlo Park, California, November 1968 (AD-687 293).

2. Iverson, J. H., "Existing Structures Evaluation, Part II: Window Glass and Applications," Stanford Research Institute (for Office of Civil Defense), Menlo Park, California, December 1968 (AD-687 294).

3. Jensen, G. F., "Existing Structures Evaluation, Part III: Structural Steel Connections," Stanford Research Institute (for Office of Civil Defense), Menlo Park, California, December 1969 (AD-701 088).

4. Wiehle, C. K., and J. L. Bockholt, "Existing Structures Evaluation, Part IV: Two-Way Action Walls," Stanford Research Institute (for Office of Civil Defense), Menlo Park, California, September 1970 (AD-719 306).

5. Wiehle, C. K., and J. L. Bockholt, "Existing Structures Evaluation, Part V: Applications," Stanford Research Institute (for Office of Civil Defense), Menlo Park, California, July 1971 (AD-733 343).

6. Wiehle, C. K., and J. L. Bockholt, "Blast Response of Five NFSS Buildings," Stanford Research Institute (for Office of Civil Defense), Menlo Park, California, October 1971 (AD-738 547).

7. Wiehle, C. K., and J. L. Bockholt, "Dynamic Analysis of Reinforced Concrete Floor Systems," Stanford Research Institute (for Defense Civil Preparedness Agency), Menlo Park, California, May 1973 (AD-768 206).

8. T. Y. Lin & Associates, "A Computer Program to Analyze the Dynamic Response of High Rise Buildings to Nuclear Blast Loading," Vols. I and II, PG 80-18-1 & 2, Office of Civil Defense, Washington, D.C., February 1964.

9. Park, R., "Ultimate Strength of Rectangular Concrete Slabs Under Short-Term Uniform Loading with Edges Restrained Against Lateral Movement," Proceedings of the Institution of Civil Engineers, Vol. 28, June 1964.

10. Keenan, W. A., "Strength and Behavior of Restrained Reinforced Concrete Slabs Under Static and Dynamic Loadings," Technical Report R621, U.S. Naval Civil Engineering Laboratory, Port Hueneme, California, April 1969 (AD-688 421).

11. Brown, W. M., and M. S. Black, "Dynamic Strength Study of Small, Fixed-Edge, Longitudinally Restrained, Two-Way-Reinforced Concrete Slabs," Draft Report, U.S. Army Engineer Waterways Experiment Station, May 1973.

12. Brotchie, J. F., A. Jacobson, and S. Okugo, "Effect of Membrane Action on Slab Behavior," Technical Report R-65-25, School of Engineering, Massachusetts Institute of Technology, Cambridge, Massachusetts, August 1965 (AD-470 747).

13. Park, R., "Tensile Membrane Behavior of Unformly Loaded Rectangular Reinforced Concrete Slabs with Fully Restrained Edges," Magazine of Concrete Research, Vol. 16, No. 46, March 1964.

14. Zahn, J. J., "Strength of Multiple-Member Structures," Research Paper FPL 139, U.S. Department of Agriculture, Forest Products Laboratory, Madison, Wisconsin, July 1970.

15. Uniform Building Code, International Conference of Building Officials, Pasadena, California, 1967.

16. Wood Handbook, Agricultural Handbook No. 72, U.S. Department of Agriculture, Forest Products Laboratory, 1955.

17. Heck, G. E., "Structural Properties of Conventional Wood-Frame Construction for Walls, Partitions, Floors, and Roofs," Report BMS25, National Bureau of Standards, U.S. Department of Commerce, Washington, D.C., September 1939.

18. Whittemore, H. L., and A. H. Stang, "Structural Properties of Wood-Frame Wall, Partition, Floor, and Roof Constructions with 'Red Stripe' Lath Sponsored by the Weston Paper and Manufacturing Co.," Report BMS36, National Bureau of Standards, U.S. Department of Commerce, Washington, D.C., January 1940.

19. Whittemore, H. L., and A. H. Stang, "Structural Properties of 'Palisade Homes' Constructions for Walls, Partitions, and Floors Sponsored by Palisade Homes," Report BMS37, National Bureau of Standards, U.S. Department of Commerce, Washington, D.C., February 1940.

20. Whittemore, H. L., and A. H. Stang, "Structural Properties of Prefabricated Wood-Frame Constructions for Walls, Partitions, and Floors Sponsored by American Houses, Inc.," Report BMS47, National Bureau of Standards, U.S. Department of Commerce, Washington, D.C., June 1940.

21. Polensek, A., et al., "Response of Nailed Wood-Joist Floors to Static Loads," Reprint from Forest Products Journal, Vol. 22, No. 9, September 1972, pp. 52-61.

22. Vanderbilt, M. D., J. R. Goodman, and M. E. Criswell, "Service and Overload Behavior of Wood Joist Floor Systems," ASCE Journal of the Structural Division, Vol. 100, No. ST1, January 1974, pp. 11-30.

23. Amana, E. J., and L. G. Booth, "Theoretical and Experimental Studies of Nailed and Glued Plywood Stressed-Skin Components: Part I - Theoretical Study," The Institute of Wood Science Journal, Vol. 4, No. 1, September 1967, pp. 43-69.

24. Ramos, A. N., "Stress-Strain Distribution in Douglas-Fir Beams Within the Plastic Range," No. 2231, U.S. Department of Agriculture, Forest Products Laboratory, Madison, Wisconsin, December 1961.

25. Zakic, B. D., "Inelastic Bending of Wood Beams," ASCE Journal of the Structural Division, Vol. 99, No. ST10, October 1973, pp. 2079-2095.

26. Hurst, H. T., "The Wood Frame House as a Structural Unit; Part I - Floor Deflection as Influenced by Various Stages of Construction," Technical Bulletin 179, Virginia Polytechnic Institute, Virginia Agricultural Experiment Station, Blacksburg, Virginia, June 1965.

27. Russell, W. A., "Deflection Characteristics of Residential Wood-Joist Floor Systems," Housing Research Paper 30, Housing and Home Finance Agency, Washington, D.C., April 1954.

28. Polensek, A., and G. H. Atherton, "Performance of Wood-Joist Floor Systems Under Static and Dynamic Loads," Proceedings of the Symposium on Research to Improve Design of Light-Frame Structures, U.S. Department of Agriculture, Forest Products Laboratory, Madison, Wisconsin, February 1970.

29. Polensek, A., "Static and Dynamic Properties of Glued Wood-Joist Floors," Reprint from Forest Products Journal, Vol. 21, No. 12, December 1971, pp. 31-39.

30. Williston, E. M., and T. L. Abner, "Design Criteria for Wood Floor Systems," Forest Products Journal, Vol. 12, No. 9, September 1962, pp. 403-409.

31. "Standard Methods for Establishing Structural Grades and Related Allowable Properties for Visually Graded Lumber," D 245 - 70, 1973 Annual Book of ASTM Standards, Part 16, American Society for Testing and Materials, Philadelphia, Pennsylvania, 1973, pp. 150-173.

32. Standard Grading Rules for West Coast Lumber, Douglas Fir, Western Hemlock, Western Red Cedar, White Fir, Sitka Spruce, No. 16, West Coast Lumber Inspection Bureau, Portland, Oregon, September 1970. (Revised January 1, 1973).

33. Standard Grading Rules for Southern Pine Lumber, Southern Pine Inspection Bureau, Pensacola, Florida, 1970.

34. "Standard Methods for Establishing Clear Wood Strength Values," D 2555 - 73, 1973 Annual Book of ASTM Standards, Part 16, American Society for Testing and Materials, Philadelphia, Pennsylvania, 1973, pp. 761-782.

35. Dietz, A. G., "Stress-Strain Relationships in Wooden Beams Subjected to Pure Bending," Ph.D. Thesis, Massachusetts Institute of Technology, 1941.

36. Timoshenko, Stephen P., and James M. Gere, Theory of Elastic Stability, McGraw-Hill Book Company, New York, 1961.

37. Beghtel, S. C., and C. B. Norris, "Strength of Wood Beams of Rectangular Cross Section as Affected by Span-Depth Ratio," No. 1910, U.S. Department of Agriculture, Forest Products Laboratory, Madison, Wisconsin, January 1959. (Reaffirmed 1965).

38. Pickering, E. E., and J. L. Bockholt, "Probabilistic Air Blast Failure Criteria for Urban Structures," Stanford Research Institute (for Office of Civil Defense), Menlo Park, California, November 1971 (AD-738 558).

39. Fiorato, A. E., M. A. Sozen, and W. L. Gamble, "An Investigation of the Interaction of Reinforced Concrete Frames with Masonry Filler Walls," SRS No. 370, University of Illinois (for Office of Civil Defense), Urbana, Illinois, November 1970 (AD-719 267).

40. Edmunds, J. E., and P. M. Sears, "Debris Model Research and Five-City Study Applications," URS 686-4, URS Research Company (for Office of Civil Defense, Burlingame, California, June 1968 (AD-857 239L).

40. Edmunds, J. E., and P. M. Sears, "Debris Model Research and Five-City Study Applications," URS 686-4, URS Research Company (for Office of Civil Defense, Burlingame, California, June 1968 (AD-857 239L).

BIBLIOGRAPHY

WOOD TECHNOLOGY

Amana, E. J., and L. G. Booth, "Theoretical and Experimental Studies of Nailed and Glued Plywood Stressed-Skin Components: Part I. Theoretical Study," The Institute of Wood Science Journal, Vol. 4, No. 1, September 1967, pp. 43-69.

Amana, E. J., and L. G. Booth, "Theoretical and Experimental Studies of Nailed and Glued Plywood Stressed-Skin Components: Part II. Experimental Study," The Institute of Wood Science Journal, Vol. 4, No. 2, 1967, pp. 19-34.

American Softwood Lumber Standard, NBS Voluntary Product Standard PS 20-70, National Bureau of Standards, Washington, D. C., January 1970.

Beghtel, S. C., and Charles B. Norris, "Strength of Wood Beams of Rectangular Cross Section as Affected by Span-Depth Ratio," No. 1910, Forest Products Laboratory, Madison, Wisconsin, January 1959. (Reaffirmed 1965)

Bohannan, Billy, "Effect of Size on Bending Strength of Wood Members," Research Paper FPL 56, Forest Products Laboratory, Madison, Wisconsin, May 1966.

Bohannan, Billy, "Structural Engineering Research in Wood," ASCE Journal of the Structural Division, Vol. 94, No. ST2, February 1968, pp. 403-416.

Dietz, Albert George, "Stress-Strain Relationships in Wooden Beams Subjected to Pure Bending," Ph.D. Thesis, Massachusetts Institute of Technology, 1941.

Heck, G. E., "Structural Properties of Conventional Wood-Frame Construction for Walls, Partitions, Floors, and Roofs," Report BMS25, National Bureau of Standards, Washington, D. C., September 1939.

Hurst, H. T., "Performance of the House as a Structural Unit," Proceedings of the Symposium on Research to Improve Design of Light-Frame Structures, Forest Products Laboratory, Madison, Wisconsin, February 1970.

Hurst, H. T., "The Wood Frame House as a Structural Unit; Part I - Floor Deflection as Influenced by Various Stages of Construction," Technical Bulletin 179, Virginia Polytechnic Institute, Virginia Agricultural Experiment Station, Blacksburg, Virginia, June 1965.

Ifju, Geza, and E. George Stern, "Wood in the Construction of Mass-Produced Houses," Virginia Polytechnic Institute, Blacksburg, Virginia, August 1971. (PB-207 812)

Keeton, John R., "Dynamic Properties of Small, Clear Specimens of Structural-Grade Timber," Technical Report R 573, Naval Civil Engineering Laboratory, Port Hueneme, California, April 1968.

Lew, H. S., et al., "Transient Vibration Tests on Wood-Joist Floors," National Bureau of Standards, Washington, D. C., June 30, 1970. (PB-211 854)

Littleford, T. W., "A Comparison of Flexural Strength-Stiffness Relationships for Clear Wood and Structural Grades of Lumber," Information Report VP-X-30, Forest Products Laboratory, Vancouver, British Columbia, December 1967.

Markwardt, L. J., and T. R. C. Wilson, "Strength and Related Properties of Woods Grown in the United States," U.S. Department of Agriculture Technical Bulletin, No. 479, September 1935.

Onysko, D. M., "Performance of Wood-Joist Floor Systems, a Literature Review," Information Report OP-X-24, Forest Products Laboratory, Ottawa, Ontario, January 1970.

Papers from the June, 1965 Structural Division Specialty Conference, in Chicago, Illinois, ASCE Journal of the Structural Division, Vol. 93, No. ST2, April 1967, pp. 1-140.

Patterson, David W., "Nailed Wood Joints under Lateral Loads," M. S. Thesis, Colorado State University, Fort Collins, Colorado, April 1973.

Penner, Bryan G., "Experimental Behavior of Wood Flooring Systems," M. S. Thesis, Colorado State University, Fort Collins, Colorado, December 1972.

Polensek, Anton, "Human Response to Vibration of Wood-Joist Floor Systems," Wood Science, Vol. 3, No. 2, October 1970, pp. 111-119.

Polensek, Anton, "Static and Dynamic Properties of Glued Wood-Joist Floors," Forest Products Journal, Vol. 21, No. 12, December 1971, pp. 31-39.

Polensek, Anton, "Static and Dynamic Analysis of Wood-Joist Floors by the Finite Element Method," Ph.D. Thesis, Oregon State University, June 1973.

Polensek, A., and G. H. Atherton, "Performance of Wood-Joist Floor Systems under Static and Dynamic Loads," Proceedings of the Symposium on Research to Improve Design of Light-Frame Structures, Forest Products Laboratory, Madison, Wisconsin, February 1970.

Polensek, Anton, et al., "Response of Nailed Wood-Joist Floors to Static Loads," Forest Products Journal, Vol. 22, No. 9, September 1972, pp. 52-61.

Proceedings of the Symposium on Research to Improve Design of Light-Frame Structures, February 25-26, 1970, Forest Products Laboratory, Madison, Wisconsin.

Ramos, Agustin N., "Stress-Strain Distribution in Douglas-Fir Beams Within the Plastic Range," No. 2231, Forest Products Laboratory, Madison, Wisconsin, December 1961.

Russell, William A., "Deflection Characteristics of Residential Wood-Joist Floor Systems," Housing Research Paper 30, Housing and Home Finance Agency, Washington, D.C., April 1954.

Standard Grading and Dressing Rules for Douglas Fir, West Coast Hemlock, Sitka Spruce, Western Red Cedar Lumber, No. 15, West Coast Lumber Inspection Bureau, Portland, Oregon, 1956.

Standard Grading Rules for Southern Pine Lumber 1970, Southern Pine Inspection Bureau, Pensacola, Florida, 1970.

Standard Grading Rules for West Coast Lumber, Douglas Fir, Western Hemlock, Western Red Cedar, White Fir, Sitka Spruce, No. 16, West Coast Lumber Inspection Bureau, Portland, Oregon, September 1970. (Revised January 1, 1973)

"Standard Methods for Establishing Clear Wood Strength Values," D 2555 - 73, 1973 Annual Book of ASTM Standards, Part 16, American Society for Testing and Materials, Philadelphia, Pennsylvania, 1973, pp. 761-782.

"Standard Methods for Establishing Structural Grades and Related Allowable Properties for Visually Graded Lumber," D 245 - 70, 1973 Annual Book of ASTM Standards, Part 16, American Society for Testing and Materials, Philadelphia, Pennsylvania, 1973, pp. 150-173.

Vafai, Abolhassan, and George Pincus, "Torsional and Bending Behavior of Wood Beams," ASCE Journal of the Structural Division, Vol. 99, No. ST6, June 1973, pp. 1205-1221.

Vanderbilt, M. Daniel, James R. Goodman, and Marvin E. Criswell, "Service and Overload Behavior of Wood Joist Floor Systems," ASCE Journal of the Structural Division, Vol. 100, No. ST1, January 1974, pp. 11-30.

Whittemore, H. L., and A. H. Stang, "Structural Properties of Wood-Frame Wall, Partition, Floor, and Roof Constructions with 'Red Stripe' Lath, Sponsored by The Weston Paper and Manufacturing Co.," Report BMS36, National Bureau of Standards, Washington, D.C., January 1940.

Whittemore, H. L., and A. H. Stang, "Structural Properties of 'Palisade Homes' Constructions for Walls, Partitions, and Floors, Sponsored by Palisade Homes," Report BMS37, National Bureau of Standards, Washington, D.C., February 1940.

Whittemore, H. L., and A. H. Stang, "Structural Properties of Prefabricated Wood-Frame Constructions for Walls, Partitions, and Floors, Sponsored by American Houses, Inc.," Report BMS47, National Bureau of Standards, Washington, D.C., June 1940.

Williston, E. M., and T. L. Abner, "Design Criteria for Wood Floor Systems," Forest Products Journal, Vol. 12, No. 9, September 1962, pp. 403-409.

Wood Handbook, Agricultural Handbook No. 72, Forest Products Laboratory, Madison, Wisconsin, 1955.

Yokel, Felix Y., "Report on Study of Evaluation Criteria for Floors under Concentrated Load," National Bureau of Standards, Washington, D.C., n.d. (PB-212 297)

Zahn, John J., "Strength of Multiple-Member Structures," Research Paper FPL 139, Forest Products Laboratory, Madison, Wisconsin, July 1970.

Zakic, Borislav D., "Inelastic Bending of Wood Beams," ASCE Journal of the Structural Division, Vol. 99, No. ST10, October 1973, pp. 2079-2095.

NOMENCLATURE

A	Area of section
A_s	Area of tension steel in reinforced concrete slab per unit width, sq in./in.
A_s'	Area of compression steel in reinforced concrete slab per unit width, sq in./in.
A_{tL}	Area of reinforcing steel per unit width continuous along the long span in reinforced concrete slab, sq in./in.
A_{tS}	Area of reinforcing steel per unit width continuous along short span in reinforced concrete slab, sq in./in.
b	Width of cross section, in.
c_f	Coefficient relating effective moment of inertia of wood-joist floor and moment of inertia of joist
d	Distance from compressive face of reinforced concrete slab to centroid of tension steel, in.
d'	Distance from compressive face of reinforced concrete slab to centroid of compressive steel, in.
E	Modulus of elasticity, psi
E_j	Modulus of elasticity of wood joist, psi
E_s	Modulus of elasticity of steel, psi
E_T	Total energy input of uniform load acting on slab, in.-lb
E_x, E_z	Energy input of uniform load for slab strips in the x-direction and z-direction, lb
$(EI)'$	Quantity defined by Eqs. 70 and 73
$(EI)_{avg}$	Quantity defined by Eq. 74
f_c'	Compressive strength of 6- by 12-in. concrete cylinder, psi
f_c''	Compressive strength of concrete in flexure, $(k_3 f_c')$, psi
f_{dc}'	Dynamic compressive strength of concrete, psi
f_{dy}	Dynamic yield strength of reinforcing steel, psi
f_r	Modulus of rupture, psi
f_s	Stress in tension steel,
f_s'	Stress in compression ste
f_w	Unit stress in wood, psi
f_{wcp}	Proportional limit in com
f_{wcu}	Ultimate unit compressive
f_{wt}	Unit tensile stress in wo
f_{wtu}	Ultimate unit tensile str
f_y	Static yield strength of
h_j	Height of wood joist, in.
h_s	Thickness of concrete sla
I	Moment of inertia, in.^{4}
I_e	Effective moment of inert floor, in.^{4}
I_j	Moment of inertia of wood
k_t, k_t'	Tensile membrane factors
k_u	Coefficient indicating po axis of reinforced concre strength
k_{ub}	Coefficient indicating po axis of reinforced concre taneous yielding of tensi of concrete (balanced con
k_1	Coefficient relating the compressive stress to the strength of concrete in f
k_3	Coefficient relating the strength of concrete in f pressive strength of 6- b
K_{LM}	Load-mass factor
L	Span length, in.
L_l	Length of slab in long di
L_s	Length of slab in short d
M	Bending moment, in.-lb
M_c	Bending moment at center
M_u	Ultimate moment capacity midthickness of slab, in. Ultimate moment capacity joist, in.-lb

f_s	Stress in tension steel, psi
f'_s	Stress in compression steel, psi
f_w	Unit stress in wood, psi
f_{wcp}	Proportional limit in compression in wood, psi
f_{wcu}	Ultimate unit compressive stress in wood, psi
f_{wt}	Unit tensile stress in wood, psi
f_{wtu}	Ultimate unit tensile stress in wood, psi
f_y	Static yield strength of reinforcing steel, psi
h_j	Height of wood joist, in.
h_s	Thickness of concrete slab, in.
I	Moment of inertia, in.^{4}
I_e	Effective moment of inertia of wood-joist floor, in.^{4}
I_j	Moment of inertia of wood joist, in.^{4}
k_t, k'_t	Tensile membrane factors
k_u	Coefficient indicating position of neutral axis of reinforced concrete slab at ultimate strength
k_{ub}	Coefficient indicating position of neutral axis of reinforced concrete slab at simultaneous yielding of tension steel and crushing of concrete (balanced condition)
k_1	Coefficient relating the average concrete compressive stress to the maximum compressive strength of concrete in flexure
k_3	Coefficient relating the maximum compressive strength of concrete in flexure to the compressive strength of 6- by 12-in. cylinders
K_{LM}	Load-mass factor
L	Span length, in.
L_l	Length of slab in long direction, in.
L_s	Length of slab in short direction, in.
M	Bending moment, in.-lb
M_c	Bending moment at center of span, in.-lb
M_u	Ultimate moment capacity per unit width about midthickness of slab, in.-lb/in. Ultimate moment capacity at center of wood joist, in.-lb

	Ultimate moment capacity per unit width about midthickness of section under the average thrust along the span, in.-lb/in.
	Thrust per unit width causing simultaneous yielding of tension steel and crushing of concrete at section, lb/in.
	Thrust per unit width at ultimate behavior (initial crushing of extreme fiber of concrete at hinge section), lb/in.
$,N_{u z}$	Thrust per unit width at ultimate behavior for slab strips in x-direction and z-direction, lb/in.
	Ratio of ultimate tensile stress and ultimate compressive stress of wood beam
	Steel ratio, tension steel
	Steel ratio, compression steel
	Peak incident overpressure, psi
	Unit resistance for uniformly loaded member, psi
	Tensile membrane resistance per unit area of slab corresponding to y_{ft}, psi
	Secondary resistance per unit width of longitudinally restrained reinforced concrete slab, psi
	Ultimate flexural resistance per unit area of longitudinally restrainded reinforced concrete slab, psi
	Ultimate resistance per unit area of wood-joist floor system, psi
	Maximum resistance per unit area for elastic phase, psi
	Reinforcing index, $d(p - p')f_y/f_c''$, in.
	Reinforcing index, $d(pf_s - p'f_s')/f_c''$, in.
	Joist spacing, in.
	Ratio of longitudinal movement of slab in x-direction to slab length in long direction resulting from partial restraint
	Ratio of longitudinal movement of slab in z-direction to slab length in short direction resulting from partial restraint

s_x', s_z'	Longitudinal movement per unit le strip in x-direction and z-direct from effect of partial restraint strain, in./in.
W_T	Total work done by the resisting thrust on the slab, in.-lb
W_x, W_z	Work done by the resisting moment on the slab strips in the x-direc direction, lb
x	Distance along slab in long direct
y	Deflection of slab along yield li
y_c	Deflection at center of beam or s
y_{ft}	Deflection at collapse of slab in membrane mode, in.
y_s	Deflection at development of seco tance of slab, in.
y_t	Deflection at intersection of seco tensile membrane phases, in.
y_u	Deflection at ultimate resistance beam, in.
y_1	Maximum deflection for elastic ph
z	Distance along slab in short direc
α	Coefficient relating the height o to the distance from the compressi the neutral axis
β	Coefficient defining location of y
γ_1, γ_2	Parameters defined by Eqs. 1a and
ϵ	Strain, in./in.
ϵ_a	Total axial strain along a slab st from the compressive membrane forc
ϵ_s	Strain in tension steel, in./in.
ϵ_s'	Strain in compression steel, in./i
ϵ_u	Ultimate concrete strain in flexur
θ_x	Angle of rotation of slab strip in radians
ρ	Radius of curvature of neutral axi beam
φ	Slope of end portion of slab strip

	pacity per unit width about ction under the average pan, in.-lb/in.
	dth causing simultaneous n steel and crushing of n, lb/in.
	dth at ultimate behavior of extreme fiber of concrete lb/in.
	dth at ultimate behavior x-direction and z-direction,
	tensile stress and ultimate of wood beam
	n steel
	ssion steel
	ressure, psi
	uniformly loaded member,
	sistance per urit area of to y_{ft}, psi
	per unit width of longi- reinforced concrete slab,
	sistance per unit area of rainded reinforced concrete
	per unit area of wood- psi
	er unit area for elastic
$(p - p')f_y/f_c''$	in.
$(pf_s - p'f_s')/f_c''$	in.
	movement of slab in x- gth in long direction l restraint
	movement of slab in z- gth in short direction l restraint
s_x', s_z'	Longitudinal movement per unit length of slab strip in x-direction and z-direction resulting from effect of partial restraint and axial strain, in./in.
W_T	Total work done by the resisting moment and thrust on the slab, in.-lb
W_x, W_z	Work done by the resisting moment and thrust on the slab strips in the x-direction and z-direction, lb
x	Distance along slab in long direction, in.
y	Deflection of slab along yield line, in.
y_c	Deflection at center of beam or slab, in.
y_{ft}	Deflection at collapse of slab in tensile membrane mode, in.
y_s	Deflection at development of secondary resistance of slab, in.
y_t	Deflection at intersection of secondary and tensile membrane phases, in.
y_u	Deflection at ultimate resistance of slab or beam, in.
y_1	Maximum deflection for elastic phase, in.
z	Distance along slab in short direction, in.
α	Coefficient relating the height of a wood beam to the distance from the compression face to the neutral axis
β	Coefficient defining location of yield lines
γ_1, γ_2	Parameters defined by Eqs. 1a and 1b
ϵ	Strain, in./in.
ϵ_a	Total axial strain along a slab strip resulting from the compressive membrane force, in./in.
ϵ_s	Strain in tension steel, in./in.
ϵ_s'	Strain in compression steel, in./in.
ϵ_u	Ultimate concrete strain in flexure, in./in.
θ_x	Angle of rotation of slab strip in x-direction, radians
ρ	Radius of curvature of neutral axis of bending beam
φ	Slope of end portion of slab strip, radians